

PÁZMÁNY PÉTER CATHOLIC UNIVERSITY
Faculty of Information Technology and Bionics
Roska Tamás Doctoral School of Sciences and Technology

**Investigation of cortical synchronous activity
of neuronal populations, *in vitro***

Ph.D. Dissertation

Author:

Katharina HOFER

Thesis Advisors:

Prof. Dr. István ULBERT, D.Sc

Dr. Lucia WITTNER, Ph.D



Budapest, 2017

Abstract

In vitro models of behaviourally relevant oscillations of the brain are useful tools to explore the generation mechanisms of synchronisation processes. This is especially valid for human studies, where the examination of *in vivo* mechanisms is obviously limited. This thesis makes an attempt to uncover the cellular and network properties of two behaviour-related cortical oscillations.

Hippocampal sharp-waves (SPWs) occur during slow wave sleep and behavioural immobility and are thought to play an important role in memory formation. Human neocortical interictal activity is a hallmark in epilepsy diagnosis and is considered to be a pathological synchronisation. The *in vitro* models of these two synchronies, however, share several similarities. 1) They consist of a recurring local field potential gradient (LFPg) transient superimposed with high frequency oscillations and increased cellular firing. 2) Two types of SPWs were distinguished in the rat CA3 region based on their different LFPg and current source density (CSD) patterns. Type 1 (T1) displayed a negative LFPg transient in the pyramidal cell layer, and the associated CSD sink was confined to the proximal dendrites. Type 2 (T2) SPWs were characterised by positive LFPg transients in the cell layer, and showed CSD sinks involving both the apical and basal dendrites. On the other hand, human neocortical slices also generated two types of synchronies: interictal-like discharges (IIDs, classified as epileptiform events) emerged only in epileptic samples, and were hypersynchronous bursts characterised by elevated levels of excitation. Synchronous population activity (SPA) was initiated in both epileptic and non-epileptic tissue, with a considerably lower degree of excitability and synchrony, and could not be linked to epilepsy. In several cases, the simultaneous emergence of two types of activity was observed in both the rat CA3 region and the human neocortex. 3) All examined synchronies depended on excitatory and inhibitory signalling, involving both principal cells and interneurons. However, the ratio of inhibited principal cells was different in the two models: only a small subset of CA3 pyramidal cells fired as most of them were hyperpolarised during the SPWs, while the majority of participating principal cells was depolarised and/or increased their firing rate during SPAs. 4) The role of inhibitory interneurons was crucial in the generation of both cortical synchronies. Reducing the activity of parvalbumin-positive interneurons resulted in a decreased recurrence frequency of SPWs and converted T1 into T2 SPWs. Further suppression of the remaining basket cell firing blocked the SPW activity completely. Interneuronal firing was also increased during SPAs in the human neocortex.

These results suggest that the rat hippocampal CA3 region and the human neocortical neuronal networks can generate multiple patterns of population activity *in vitro*. They indicate that both excitatory and inhibitory microcircuits participate in the generation of cortical synchronous events, showing that a complex interplay between principal cells and interneurons underlies the emergence of rat hippocampal as well as human neocortical physiological and pathological synchronies.

Acknowledgements

First and foremost, I would like to thank my two supervisors, Lucia Wittner and István Ulbert. I truly appreciate that they gave me this chance to work as a scientist in the field that captures my fascination so much. The two of them are amazingly supportive supervisors who gave me the freedom to try out my own ideas regarding data analysis while always offering an open door to get advice and feedback. I would also like to thank them for their financial support and that they provided me with the opportunity to attend and present my work at international and national conferences and seminars, which greatly expanded my horizon, provided ideas for my projects, boosted my knowledge of the scientific field and improved my mathematical understanding. Köszönöm szépen!

I would also like to thank the Pázmány Péter Catholic University for providing the financial support for my work as well as many of the conference attendances mentioned above. I would also like to thank them for providing the academic framework for my dissertation and many useful lectures. Without their programming courses getting me started, I would not have been able to analyse my data the way I did.

Moreover, I would like to thank my colleagues, who helped me on countless occasions with navigating the jungle that comes with living in a foreign country without speaking the local language well enough. I also truly enjoy the many nerdy conversations at lunch or on other occasions, animatedly discussing topics most people would not spend much thought about. Some of you have become very close friends and I am glad you became a part of my life.

I would like to highlight those colleagues who I collaborated with on the two presented projects. Both of my main projects were group efforts, but this particularly applies to the human neocortical project. Although I have tried to focus my dissertation on the work I have done personally, work of others is included as well. A project involving human brain tissue obtained during surgery would not be possible without the surgeons and clinicians providing the tissue samples. In this context, I would like to thank Loránd Erőss, Dániel Fabó, László Entz and Attila Bagó for their continued collaboration. Moreover, I would like to thank the many epilepsy and brain tumour patients who have consented to this study, making this kind of research possible. The electrophysiological *in vitro* experiments were performed by Lucia Wittner (rat and human), Kinga Tóth (human), Ágnes Kandrács (human) and myself (rat and human). In case of the rat project, Ildikó Pál helped with performing the experiments involving referential recordings. Lucia Wittner, Ágnes Kandrács, Kinga Tóth, Csilla Szabó and myself all participated in the arduous task of cell clustering as well as SPW, SPA and IID detection that form the basis of all analyses that were carried out for this dissertation. Lucia Wittner then categorised all of the clustered cells by cell type, Ágnes Kandrács performed the ripple analysis, Kinga Tóth performed immunohistochemical stainings, and Lucia

Wittner and Kinga Tóth analysed the human neocortical sections using electron microscopy. Although the ripples as well as the anatomical findings are not discussed in this dissertation, they are important parts of the publications that stem from these projects and I would like to take the opportunity to thank them for all the work they did.

Last but not least, I would like to show my gratitude to my family, who has helped me in so many ways and whose support I could not have done without. I would like to thank my parents Jutta and Andreas Hofer, who have always provided a safe haven throughout my life and have motivated me to push through rough patches when I hit them. They have had a huge impact in making me the person I am today in the best possible way and I am proud to be their daughter. I would also like to thank my sister Angelika and my brother Martin, who, in addition to being my siblings, are also some of my best friends in life. My sister's ability to cheer me up with pictures and stories of her little children or my brother's ability to kindle my interest in statistics have truly helped me in doing the work I did these past few years. Each one of these four very probably immensely underestimates the role they played in my achievements. Thank you.

Document structure

Table of Contents

1	General introduction	12
1.1	Background	12
1.2	Questions	13
1.2.1	Question group 1: Rat SPW study	13
1.2.2	Question group 2: Human SPA study	13
1.2.3	Question group 3: Data processing and algorithm development	14
2	Sharp-waves in the rat hippocampus	15
2.1	Introduction	15
2.2	Methods	16
2.2.1	Tissue preparation	16
2.2.2	Electrophysiological recordings	17
2.2.3	Pharmacology	18
2.2.4	Data analysis	18
2.3	Results	20
2.3.1	SPWs were locally generated in the CA3 region	20
2.3.2	Two types of SPW activity were identified	21
2.3.3	Simultaneous occurrence of T1 and T2	23
2.3.4	T1 and T2 are indistinguishable on referential recordings	25
2.3.5	T1 and T2 in different CA3 subregions	25
2.3.6	The role of glutamatergic and GABAergic signalling	27
2.3.7	The role of excitatory pathways in the generation of SPWs	30
2.3.8	Behaviour of pyramidal cells during SPWs	31
2.3.9	Behaviour of interneurons during SPWs	33
2.3.10	The role of perisomatic interneurons	36
2.4	Discussion	39
2.4.1	The rodent CA3 region can generate two types of SPWs <i>in vitro</i>	39
2.4.2	Cellular interactions during SPWs	40
2.4.3	Interaction and Competition between T1 and T2 SPWs	41
2.4.4	Differences between CA3 subregions	42

3	Synchronous population activity in the human neocortex	43
3.1	Introduction	43
3.2	Methods	44
3.2.1	Patients	44
3.2.2	Tissue preparation	45
3.2.3	Electrophysiological recordings	45
3.2.4	Data analysis	45
3.3	Results	55
3.3.1	SPA and IID in the human neocortical slice	55
3.3.2	Spatial subtypes of NSAs	59
3.3.3	Simultaneous occurrence of multiple NSAs	61
3.3.4	Regression on SPA properties	62
3.3.5	Characterisation of cellular activity	64
3.3.6	Cell-SPA interactions	71
3.4	Discussion	83
3.4.1	SPAs are not interictal spikes	83
3.4.2	The role of bursting behaviour in the generation of population activity	84
3.4.3	Simultaneous generation of SPAs and IIDs	84
3.4.4	SPAs and IIDs are mostly local events	85
3.4.5	Increased excitability in epilepsy modifies SPAs	86
3.4.6	The role of excitatory and inhibitory neuronal activity during SPAs	87
4	Conclusion and Thesis statements	88
4.1	Thesis statements	89
4.1.1	Thesis group 1: Rat SPW study findings	89
4.1.2	Thesis group 2: Human SPA study findings	89
4.1.3	Thesis group 3: Data processing and algorithm development	90
5	References	91
6	Appendices	101
6.1	NSA and AP waveform measurements	101
6.1.1	NSA waveform measurements	101
6.1.2	Action potential waveform measurements	103
6.2	Explanatory notes on multiple regression analysis	104
6.3	Additional findings	106
6.3.1	Multiple spots of NSAs within one slice	106
6.3.2	Regression on SPA recurrence properties	106
6.3.3	AP shapes across patient groups and cell types	107
6.4	Significant differences	107

List of Figures

1.1	Cortical population activity across species	13
2.1	Two types of SPW activity in the CA3 region	22
2.2	Simultaneous occurrence of T1 and T2 SPWs	24
2.3	Involvement of neurotransmitter receptors and excitatory pathways	28
2.4	Intracellular responses of putative pyramidal cells during SPWs	32
2.5	Interneuron firing patterns during and around SPWs	34
2.6	The role of perisomatic interneurons	38
3.1	Calculation of firing change quantiles	51
3.2	Time bins relative to the SPA shape	53
3.3	SPA and IID in neocortical tissue	56
3.4	NSA properties	57
3.5	Multiple spatial types of SPAs	60
3.6	NSA locations	61
3.7	Cell AP shapes and ISI histograms	65
3.8	Cell firing and AP shape properties	67
3.9	PETHs of cell firing around SPA events	73
3.10	Cell firing patterns during SPA	75
3.11	Properties of cell-SPA interactions	78
6.1	NSA and MUA waveform measurements	102
6.2	AP waveform measurements	104
6.3	Example graphical representation of p-values	108

List of Tables

2.1	Drugs used to modify neuronal activity	19
2.2	Features of T1 and T2 SPWs	23
2.3	T1 and T2 in different CA3 subregions	26
2.4	Correlated occurrence of T1 and T2 between neighbouring CA3 subregions	27
2.5	Pharmacological manipulation of SPWs	29
2.6	Intracellular responses of putative pyramidal cells during SPWs	31
2.7	Numbers of clustered interneurons	33
2.8	Interneuron firing patterns during and around SPWs	35
3.1	Case numbers for patients, slices and recordings	45
3.2	Patients	47
3.3	Detected NSAs	48
3.4	NSA properties	58
3.5	NSA locations	59
3.6	Regressions on SPA properties	63
3.7	Clustered neurons	64
3.8	Cell properties	66
3.9	Regressions on cell properties	70
3.10	Numbers of local and distant cells	71
3.11	Numbers of increased, unchanged and decreased PCs, INs and UCs	76
3.12	Properties of cell-SPA interactions	77
3.13	Regressions on cell-SPA relation properties	79
3.14	Numbers of increased, unchanged and decreased local and distant cells	81
3.15	Cell responses during multiple SPAs	83
6.1	Significant differences regarding NSA properties	109
6.2	Significant differences regarding the regression on SPA properties	110
6.3	Significant differences regarding cell properties	112
6.4	Significant differences regarding the regression on cell properties	114
6.5	Significant differences regarding cell-SPA interactions	116
6.6	Significant differences regarding the regression on cell-SPA interactions	117
6.7	Significances for the number of in- and decreased cells across patient groups	118
6.8	Significances for the number of in- and decreased PCs, INs and UCs	118
6.9	Significances for the number of in- and decreased local and distant cells	118
6.10	Significances for the cell responses during multiple SPAs across patient groups	119
6.11	Significances for the cell responses during multiple SPAs within patient groups	119

List of Abbreviations

ACh	acetylcholine
ACSF	artificial cerebrospinal fluid
AHP	afterhyperpolarisation (of an AP)
amp	amplitude
AMPA	a-amino-3-hydroxyl-5-methyl-4-isoxazole-propionate
AP	action potential
AP5	D,L-2-amino-5-phosphonovaleric acid (NMDAR antagonist)
asym	asymmetry
Bic	bicuculline methiodide (GABA _A R antagonist)
CA	cornu ammonis
CB1	cannabinoid receptor, type 1
CCh	Carbachol (AChR agonist)
CCK	cholecystokinin
CGP52432	3-[[[(3,4-Dichlorophenyl)methyl]amino]propyl] diethoxymethyl) phosphinic acid (GABA _B R antagonist)
CI	confidence interval
ContrEpi	patient group with controllable (pharmacoresponsive) epilepsy
CSD	current source density
DAMGO	[D-Ala 2,N-Me-Phe 4,Gly 5-ol] enkephalin acetate (μ -opioid receptor agonist)
DCG-IV	(2S,20R,30R)-2-(20,30-Dicarboxycyclopropyl) glycine (mGluR2 agonist)
DG	dentate gyrus
EEG	electroencephalogram
fMRI	functional magnetic resonance imaging
freq	frequency
GABA	γ -amino-butyric acid
GABA _A R	GABA _A receptor
GABA _B R	GABA _B receptor
gran	granular
hACSF	ACSF for human tissue
hc	hippocampus
IID	interictal discharge
IN	interneuron
infra	infragranular
ISI	interspike interval
KA	kainate
LFP	local field potential
LFPg	local field potential gradient
ln	natural logarithm

MF	mossy fibre
mGluR2	type II metabotropic glutamate receptor
MUA	multiple unit activity
NBQX	2,3-dihydroxy-6-nitro-7-sulfamoyl-benzo(f) quinoxaline (AMPA and KA receptor antagonist)
NMDA	N-methyl-d-aspartate
NoEpi	patient group without detectable epilepsy or seizures
NSA	neocortical synchronous activity (the umbrella term for SPA and IID)
O-LM cell	hippocampal interneuron with their soma in the oriens, projecting to str. lacunosum-moleculare
p2p delay	peak-to-peak delay (main AP peak to AHP peak time difference)
PC	principal cell (pyramidal neurons of the hc and neocortex as well as granule cells of the neocortex)
PDS	paroxysmal depolarising shift
PETH	peri-event time histogram
PV	parvalbumin
QCD	quartile coefficient of dispersion
rACSF	ACSF for rat tissue
recu	recurrence
ResEpi	patient group with pharmacoresistant epilepsy
RMP	resting membrane potential
SD	standard deviation
SOM	somatostatin
SPA	synchronous population activity
SPW	sharp-wave
str.	stratum
supra	supragranular
T1	type 1 SPW
T2	type 2 SPW
TFR plot	time-frequency plot
UC	unclear cell
varcoeff	variation coefficient, coefficient of variation

1. General introduction

1.1 Background

The need to link certain electrophysiological phenomena to different behaviours emerged with the birth of electrophysiology, and helps to understand brain functions and neurological diseases. A particularly remarkable characteristic of the mammalian cortices (both archi- and neocortex) is their capacity to generate physiological and pathological synchronies. Physiological synchronous events, so called sharp wave-ripple complexes were observed in the rodent hippocampus during sleep and behavioural immobility. They are short episodes of large amplitude synchronisations involving a large amount of hippocampal neurons, and are known to have an important role in learning and memory formation [1, 2]. However, if synchrony exceeds a certain level, and neuronal circuits show a hypersynchronous and wide spread activation, it results in the emergence of pathological activity: epileptic seizures and interictal spikes. Considerable effort has been made in the last decades to understand the cellular and network basis of both physiological and pathological synchronisation processes. Several recent studies, including ours, showed that hippocampal slices of rats [3–5] and mice [6, 7] exhibit spontaneous rhythmic population activity *in vitro*, similar to *in vivo* observed sharp wave-ripple complexes. On the other hand, surgically removed brain tissue from therapy resistant epileptic patients provides an excellent opportunity to examine human neuronal activity *in vitro* at network and single cell levels, as well as to study morphological modifications. Spontaneous interictal-like activity could be observed *in vitro* in human hippocampal [8–11] and neocortical [12–14] slice preparations, in a physiological perfusion solution. The similarity of *in vitro* sharp waves in control rodent slices and interictal-like events in human epileptic tissue is considerable in many aspects (see figure 1.1). The frequency (0.5 – 5 Hz), the waveform and the pharmacology of both types of synchronous events were similar, independently of the species examined and the investigator research group. These events consist of a 50 - 500 μV amplitude slow field potential transient with superimposed fast oscillations, with both glutamatergic excitatory and GABAergic inhibitory signalling involved [6–8, 12]. Principal cells, at resting membrane potential, show either hyperpolarising, depolarising or mixed responses to the synchronous population events, in control rodent [5–7] and epileptic human neocortical [12] and hippocampal slices [8, 10, 11].

Methods to examine brain activity have considerably developed in the last few decades. More extensive and probably more accurate data can be achieved with multiple channel electrodes to study the network properties of cortical synchronisations. During my doctoral period, I used a 24 contact linear electrode system combined with simultaneous intracellular recordings to describe

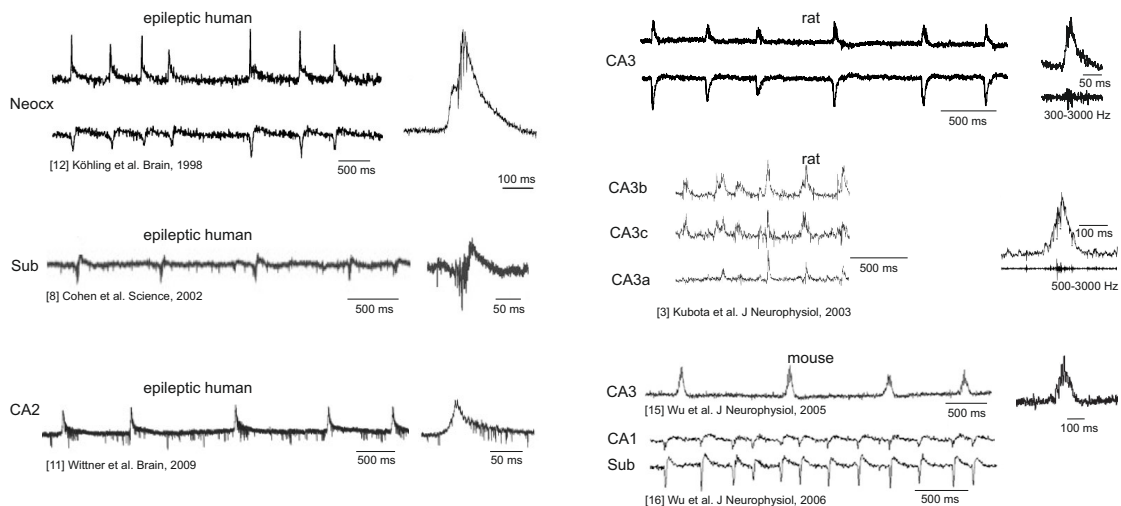


Figure 1.1: Cortical population activity across species Interictal-like events in vitro in hippocampal and neocortical slices derived from epileptic patients (left panel) feature a similar waveform to sharp waves observed in rodent hippocampal slices (right panel). The traces in the top right panel are recordings from our own study. All other traces were published previously by other groups as indicated [3, 8, 11, 12, 15, 16]. Abbreviations: Neocx, neocortex; Sub, subiculum.

the properties of rat hippocampal sharp waves and human neocortical synchronous activity. I made an attempt to describe the network and cellular features of these two functionally very different but phenomenologically very similar synchronies. By finding certain differences, I hope to elucidate certain aspects of the subtle border between physiological and pathological processes.

1.2 Questions

1.2.1 Question group 1: Rat SPW study

- Ia** What are the LFPg, CSD and MUA characteristics of rat hippocampal SPWs in vitro?
- Ib** In which hippocampal subregion do SPWs emerge in vitro?
- Ic** Do rat hippocampal slices generate different types of SPWs?
- Id** What are the generation mechanisms of rat hippocampal SPWs? Are excitatory and inhibitory circuits participating?
- Ie** How do hippocampal pyramidal cells and interneurons behave during SPWs?

1.2.2 Question group 2: Human SPA study

- IIa** What are the LFPg, CSD and MUA characteristics of human neocortical SPAs/IIDs?
- IIb** Which neocortical layers to human SPAs and IIDs occur in?
- IIc** Are SPAs affected by the changes in the neocortex that are associated with epilepsy (such as alterations in the neuronal network and/or hyperexcitability)?

II d What are the firing characteristics of human neocortical cells in epileptic and non-epileptic tissue, in general and during NSA?

II e How do excitatory principal cells and inhibitory interneurons behave during NSA?

1.2.3 Question group 3: Data processing and algorithm development

II a How can neuronal firing during SPAs be assessed in a systematic and automated manner?

II b What factors should be considered when developing a program to analyse the shape of SPAs?

II c How can the process of categorising cells into cell types (based on AP shape and autocorrelogram) be facilitated? Which factors should be shown, which should be hidden from the user to ensure unbiased sorting?

2. Sharp-waves in the rat hippocampus

This part of the thesis is based on the paper "The Hippocampal CA3 Region Can Generate Two Distinct Types of Sharp Wave-Ripple Complexes, *In Vitro*" by Hofer *et al.* [5].

2.1 Introduction

Sharp wave-ripple complexes have been observed in the hippocampus of rodents during slow wave sleep and behavioural immobility [1]. These synchronous population bursts are thought to have an important role in memory consolidation within the hippocampus and in conversion to longterm memory trace [2]. Hippocampal SPWs have been associated with large field potential deflections and high frequency oscillatory ripple activity [17, 18]. The generation of SPWs is thought to depend on synchronous firing in a small subset of CA3 pyramidal cells together with an enhanced discharge rate of interneurons [19].

In vitro models of SPW activity also consist of rhythmically recurring field potential transients accompanied by high frequency oscillations and increased neuronal firing, showing striking similarities with SPWs occurring *in vivo*. *In vitro* population events are typically initiated in the hippocampal CA3 region, and spread to the DG, the CA1 region and the subiculum [3, 6, 16, 20–22]. Different neural responses of CA3 pyramidal cells have been described during SPWs *in vitro*. In some models, hyperpolarising, depolarising or mixed responses were detected [4, 15, 23], while in other studies pyramidal cells either fired or received only excitatory synaptic currents during SPWs [7, 24].

The role of inhibitory cells in the generation of SPWs *in vitro* seems to be crucial [23, 25]. Hippocampal interneurons can be classified into partially overlapping morphological or functional groups. Perisomatic interneurons (PV⁺ axo-axonic and basket cells and CB1⁺ basket cells) innervate the axon initial segments and the somatic region of PCs, controlling their output, while dendritic inhibitory cells innervate the dendritic region of PCs to influence their inputs. The interneuron-selective interneurons specifically innervate inhibitory cells and are supposed to have a role in network synchronisations [26–28]. GABAergic signalling is generally agreed to regulate the generation of SPWs *in vitro* [6, 20, 22]. A different study which examined the firing behaviour of different interneuron types during SPWs in mouse hippocampal slices found that parvalbumin-containing basket cells were the most active during SPWs, whereas axo-axonic cells and CB1-positive basket interneurons were recruited to a lesser extent [25].

It has been demonstrated that a hippocampal SPW is spontaneously initiated when the summed activity of CA3 PCs coincidentally reaches a certain threshold. Subsequently, pyramidal cell

(PC) activity further increases exponentially until it drives the PV⁺ basket cells, which, due to their reciprocal inhibition, start firing at ripple frequency, which then phase locks PC activity to ripple frequency [29]. This phase locking mechanism has been termed FINO (fast inhibitory neuronal oscillation). The dependence on coincidental PC firing exponentially growing until a SPW is triggered explains the stochastic nature of SPW recurrence [29]. Another group has recently demonstrated that a hippocampal SPW can be triggered by inducing firing in a single PC. However, in contrast to what would be expected according to the stochastic model, the SPW was triggered at a delay that corresponds to the delay of a PC exciting an interneuron (IN), i.e. leaving no time for exponential growth of PC activity [30]. In an other *in vitro* model, firing of individual PV⁺ perisomatic inhibitory interneurons was shown to suppress and subsequently initiate SPWs [23]. Therefore, the exact cellular mechanisms involved in SPW generation are still disputed.

In this study, we aimed to reveal the cellular and network properties of spontaneously occurring SPWs in rat hippocampal slices. The use of laminar multielectrodes allowed detailed LFPg, MUA and CSD analyses of the SPW's spatio-temporal properties. We found that the DG, the CA3 region, and the CA1 region can generate spontaneous SPWs *in vitro*, in slices with intact intrahippocampal connections. In the CA3 region, two types of SPWs exhibited differences in recurrence frequency, LFPg pattern and amplitude, MUA increase and CSD pattern. Simultaneous intra- and extracellular recordings of CA3 pyramidal cells and interneurons, as well as pharmacological manipulations indicated that distinct interneuron populations (with the leading role of perisomatic interneurons) are activated during the different SPWs and recruit different ensembles of CA3 pyramidal cells.

2.2 Methods

2.2.1 Tissue preparation

The experiments were performed according to the EC Council Directive of November the 24th, 1986 (86/89/EEC). Moreover, all experimental procedures were reviewed and approved by the local ethical committee and the Hungarian Central Agricultural Office (license number 22.1/4228/003/2009).

Adult Wistar rats of both sexes of 200 – 500 g were anaesthetised intraperitoneally with urethane (1 g/kg) and intracardially perfused with sucrose solution (248 mM sucrose, 26 mM NaHCO₃, 1 mM KCl, 10 mM MgCl₂, 1 mM CaCl₂, 10 mM glucose and 1 mM phenol red, equilibrated with 5% CO₂ – 95% O₂ at 3 – 5 °C) after which the brain was dissected and transferred into the same ice cold sucrose solution. The ventral hippocampus and adjacent brain areas were cut into 500 μm thick slices using a vibratome. Directly after cutting, the slices were transferred to an interface chamber and perfused with a physiological solution (rACSF: 124 mM NaCl, 26 mM NaHCO₃, 4 mM KCl, 2 mM MgCl₂, 2 mM CaCl₂ and 10 mM glucose, equilibrated with 5% CO₂ – 95% O₂, note the slight difference to hACSF described in section 3.2.2) at 34 – 35 °C. The slices were left to recover for at least one hour before recording.

In a subset of experiments, the DG, the CA3 region or the CA1 region were isolated ("mini slices") by cutting at the border between the CA3 and CA1 regions and at the end of the two blades of the DG (resulting in a portion of the CA3c subregion being included in the DG slice).

These cuts were performed immediately after the slice cutting procedure, before transferring the tissue to the interface chamber.

2.2.2 Electrophysiological recordings

Cells were recorded intracellularly using microelectrode pipettes containing 2 M K-Acetate beveled to a resistance of 50 – 100 M Ω . Current-clamp recordings were performed within 10 – 20 minutes of cell penetration using BA-1S amplifier (NPI Electronic GmbH, Tamm, Germany). Minimal quality requirements were a membrane potential more negative than -50 mV, an input resistance higher than 20 M Ω and overshooting action potentials.

LFPg recordings were performed while the slices were kept in an interface chamber employing a gravity operated bathing system. The LFPg was recorded using a laminar multielectrode array with 24 channels and 50 μ m intercontact distance. Using a custom made gradient amplifier (band pass 0.01 Hz – 10 kHz; [31–34]) resulted in the recording of the voltage differences between neighbouring electrode contacts (i.e. the LFP gradient), which reflects the first spatial derivative of the LFP. The signal was digitised using a 32 channel, 16 bit resolution analogue-to-digital converter (National Instruments, Austin, TX) and recorded at 20 kHz sampling rate, using a home-written routine in LabView7 (National Instruments, Austin, TX). The multielectrode was placed onto the hippocampal slice perpendicularly to the pyramidal cell layer, so that its contacts covered the entire radial range of the dendritic trees of the pyramidal cells from the str. oriens to the str. lacunosum-moleculare. In some cases, subsequent recordings were performed from more than one CA3 subregion. Recordings from all three CA3 subregions of the same slice were performed in 14 slices, in the CA3a and CA3b subregions in 28 slices, in CA3b and CA3c subregions in 25 slices and in the CA3a and CA3c subregions in 16 slices. For the analysis of correlated SPW occurrences between the CA3 subregions, the latter 16 slices were excluded from the analysis, as the activity of the CA3b subregion was not recorded. SPW activity was considered to be correlated when the same type of SPW was observed in at least two neighbouring subregions. The SPW was regarded a local event when the same type of SPW was not detected in any neighbouring subregion. Thus, if a SPW type occurred in the CA3a and CA3c subregions, but not in CA3b region, it was considered as two local SPWs. In some cases T1 and T2 occurred in the same recording simultaneously (T1+T2). In the cases when simultaneous T1+T2 was observed in one subregion and T2 in the neighbouring subregion T1 was considered local, T2 was regarded correlated activity. Note that this analysis cannot determine whether or to which extent the SPW events occur in synchrony in the two CA3 subregions due to the consecutive (rather than simultaneous) manner of the recordings from the different CA3 subregions.

In a subset of experiments referential LFP recordings were performed in parallel to the LFP gradient recordings. In these cases, the slices were left to recover in an interface chamber in rACSF at 35 °C. Before recording, the slices were transferred to a dual superfusion submerged chamber ([35], also rACSF at 35 °C). Referential recordings were made with extracellular glass electrodes with a resistance of 2 – 5 M Ω and filled with rACSF. The multielectrode was placed on the slice as described before while the glass electrode was placed in the pyramidal layer 50 – 300 μ m away from the multielectrode with the reference electrode in the bathing medium. For the referential recording a two-channel Multiclamp 700A amplifier (Axon Instruments, Foster City, CA) was

used. The signal was low-pass filtered (2 kHz) and digitised at 10 kHz with a Digidata 1320A A/D board (Axon Instruments, Foster City, CA) controlled by the software pClamp8 (Axon Instruments, Foster City, CA). The LFPg was simultaneously recorded as described above.

In a different subset of experiments, stimulation experiments were performed using a tungsten bipolar electrode made from two electrodes (1 M Ω impedance, 100 μ m diameter, FHC Inc. Bowdoin, ME) with a tip distance of 80 – 100 μ m. A BioStim stimulator system (Supertech Pécs, Hungary) was used to generate stimuli of 0.02 – 0.05 mA intensity, 0.2 ms duration and 1 s interstimulus intervals. The bipolar electrode was placed either in the granule cell layer of the DG to stimulate mossy fibres or at the border of the str. pyramidale and str. oriens of the CA3a region to stimulate CA3 recurrent collaterals. The activation patterns of both types of stimuli were recorded and compared to spontaneous SPWs.

2.2.3 Pharmacology

The effects of pharmacological agents on SPW activity was investigated by adding the drug to the rACSF solution serving as the input to the interface chamber (dropping speed around 4 – 6 ml/min). Table 2.1 summarises the drugs used to modify neuronal activity in this study. The drug action was related to the amount of bathing solution that had flown through the recording chamber. The drug reached the slice after around 20 ml were used, as the tubing system and the recording chamber had to be filled with the drug cocktail before reaching the slice. Therefore, 100 ml of drug-containing rACSF were used for each experiment. As a control, spontaneous SPWs were recorded in untreated slices for at least 20 min before the application of the drug cocktail. If the SPW activity was stable, the last 3 min before the application of the drug were used as the control segment. The effect of the drug started to be visible after 5 – 8 min (\sim 30 ml of drug cocktail) and became stable after \sim 10 min (\sim 40 ml of drug cocktail). The last 3 min of recording before switching back to control rACSF was analysed as the drug affected period. In the cases where a washout period was analysed, a 3 min segment of recording after \sim 30 min of control rACSF was used, except in the case of bicuculline, which required a wash-out time of 1.5 – 2 hours.

2.2.4 Data analysis

Electrophysiological recordings were analysed using the Neuroscan Edit 4.5 software (Compumedics Neuroscan, Charlotte, NC, USA) and Matlab (The MathWorks, Natick, MA, USA).

SPWs were detected from the LFPg using an amplitude threshold of 3 times the SD (implemented in Matlab) after performing two Hamming-window spatial smoothing steps and applying a band-pass filter from 1 to 30 Hz. The events were centred around the peak of the SPW. The quality of the detection was visually assessed and the threshold adjusted if necessary. Event-triggered averages were calculated from the wideband LFPg and the multi unit activity (the 500 Hz high-pass filtered and full wave rectified LFPg). The current source density, which estimates population wide transmembrane currents, was calculated by taking one additional derivative across the spatial dimension of the LFPg as described previously [32–34]. All averages (LFPg, MUA and CSD) were baseline-corrected (-150 – -50 ms). In CSD plots, sinks are represented in red, sources in

Effect	Drug (Abbreviation)	Working Concentration
GABA _A R antagonist	bicuculline methiodide (Bic)	10 μ M
GABA _B R antagonist	3-[[[(3,4-Dichlorophenyl)methyl]amino]propyl]diethoxymethyl)phosphinic acid (CGP52432)	2 μ M
AMPA and KA receptor antagonist	2,3-dihydroxy-6-nitro-7-sulfamoyl-benzo(f)quinoxaline (NBQX)	5 μ M
NMDAR antagonist	D,L-2-amino-5-phosphonovaleric acid (AP5, also: D,L-APV)	50 μ M
μ -opioid receptor agonist	[D-Ala 2,N-Me-Phe 4,Gly 5-ol] enkephalin acetate (DAMGO)	1 μ M
AChR agonist	Carbachol (CCh)	5 μ M
mGluR2 agonist	(2S,20R,30R)-2-(20,30-Dicarboxycyclopropyl)glycine (DCG-IV)	1 μ M

Table 2.1: Drugs used to modify neuronal activity. CCh was purchased from Sigma-Aldrich, the other drugs were acquired from Tocris Bioscience (Izinta Kft., Hungary). CCh was used to reduce the activity of CCK/CB1-positive basket cells [36] whereas DAMGO was used to reduce the activity of PV-positive basket, somatostatin-positive O-LM cells (dendritic inhibitory interneurons) and hippocampo-septal cells [26, 37–39]. DCG-IV was applied to block mossy fibre activity [40].

blue, in MUA plots, red reflects increases in MUA activity, blue reflects decreases. Amplitudes were measured on the channel with the largest amplitude situated in the pyramidal layer.

Single unit activity was clustered from the band-pass filtered LFPg (500 Hz – 5 kHz, zero phase shift, 48dB/octave) using routines written in Matlab or with the program Klusters [41]. Clusters with a refractory period of 1.5 ms were considered to be single neurons. Cells located outside of the pyramidal layer were taken to be INs. To differentiate between principal cells and interneurons within the pyramidal layer, the averaged action potential (AP) waveform and the autocorrelogram were taken into account. If the AP width measured at the half-maximum amplitude was less than 0.25 ms, the cell was considered to be an IN, if it was larger than 0.5 ms, the cell was taken to be a PC. In cases where the half-maximum amplitude was not characteristic, the shape of the autocorrelogram was taken into account. If a cell could not be clearly attributed to be a PC or IN, it was excluded from the analysis. There were no cells with contradicting AP width and autocorrelogram shape. Peri-event time histograms were generated for each cell to determine its firing pattern around SPWs events. Overall, 71 INs, 17 PCs and 3 mossy cells were identified. Of all the clustered INs, 47 were identified due to their location (31 in str. oriens, 13 in str. lucidum + str. radiatum, 2 in str. lacunosum-moleculare and 1 in the hilus), 24 INs were identified due to their waveform and autocorrelogram within the str. pyramidale.

As almost none of the data were normally distributed, the non-parametric Mann-Whitney

U-test (also called Wilcoxon rank sum test), the Kruskal–Wallis test (in case of more than 2 groups) or the Wilcoxon signed rank tests (in case of paired data) were applied. In order to test for unequal proportions in contingency tables, the Chi-square test was applied. However, when over 20 % of the values expected under the null hypothesis were below five or at least one of the observed values was zero, the Fisher’s exact test was used instead. In case of significant outcomes, the standardised residuals $((observed - expected) / \sqrt{expected})$ were calculated post-hoc for each table cell to determine which cell or cells significantly deviate from their expected values.

2.3 Results

2.3.1 SPWs were locally generated in the CA3 region

Ventral hippocampal slices of the rat spontaneously generated population activity in a physiological bathing solution. The activity preferentially occurred in slices originating from between Bregma 27 and 25 in the dorso-ventral axis [42]. The LFPg was recorded with a 24-channel laminar multielectrode array with 50 μm inter-contact distance, placed perpendicularly to the pyramidal cell layer, to record from the entire somato-dendritic axis of the CA3 region. Synchronous population events were detected in the CA3 region (41 / 85 slices, 48.2 %) and consisted of a LFPg transient with superimposed high frequency LFPg oscillations (so-called ripples) and MUA increases. The detected population activity resembled *in vivo* SPW complexes [43] and previously described synchronous population activity in rodent hippocampal slices. The latter of which is considered to be an *in vitro* model of SPWs [3, 4, 6, 7, 15, 20, 23, 24, 44], which is why these *in vitro* synchronous population events are going to be called sharp waves (SPWs) throughout this thesis. Please note that the ripples often accompanying the SPWs will not be discussed in this thesis. Information on ripple power and occurrence can be found in Hofer *et al.* [5].

CSD analysis, which estimates transmembrane currents in the local neuronal population [45, 46] revealed that although the intrahippocampal connections were conserved during the slicing procedure, the SPWs were locally generated in the CA3 region. It was further demonstrated that this activity can be locally generated in the CA3 region as it could be found in mini slices containing the CA3 region only (9 / 16 slices, 56.3 %, not significantly different from whole hippocampal slices (48.2 % as mentioned above, $p > 0.5$, Chi-square test). This fits to previous results found *in vivo* [19, 43] and *in vitro* [3, 4, 6, 7, 15, 23, 24, 44] which encourage the notion that SPWs are generated in the CA3 region. In summary, the CA3 region can generate SPWs *in vitro*, independently of other hippocampal regions.

2.3.2 Two types of SPW activity were identified

Two distinct types of SPW events could be distinguished according to their LFPg and CSD pattern (figure 2.1).

- SPWs with a negative LFPg peak in the str. pyramidale and a positive peak in the str. radiatum (apical dendritic layer) were called type 1. Accordingly, their CSD pattern consisted of a sink-source pair in the str. pyramidale (T1, figure 2.1A).
- On the other hand, positive LFPg peaks in the str. pyramidale as well as in the str. lacunosum-moleculare (distal apical dendrites) combined with a negative LFPg peak in the str. radiatum (apical dendritic layer) were termed type 2. This type exhibited a sink-source triplet: a source in the str. pyramidale, adjoined by one sink each in the str. oriens and str. radiatum. (T2, figure 2.1B).

Apart from their LFPg and CSD patterns, the types further differed in their mean recurrence frequency and their absolute (sign-independent) LFPg amplitude (table 2.2 "overall"). Compared to T2 SPWs, T1 SPWs were significantly less frequent (medians: T1: 0.8 Hz, T2: 1.52 Hz, $p < 1E-05$, Mann-Whitney U-test), but had significantly larger absolute amplitudes (medians: T1: $-54.9 \mu\text{V}$, T2: $29.9 \mu\text{V}$, $p < 1E-05$, Mann-Whitney U-test). The MUA increase tended to be larger for T1 than for T2, but the difference was not significant (medians: T1: $4.46 \mu\text{V}$, T2: $3.20 \mu\text{V}$, $0.05 < p < 0.1$, Mann-Whitney U-test). Data from 33 animals were used for the analysis. T1 SPWs were observed in 26/33 animals, T2 SPWs in 29/33 animals and T1+T2 SPWs in 11/33 animals. There were no striking differences among animals concerning the occurrence of T1, T2, and T1+T2 SPWs.

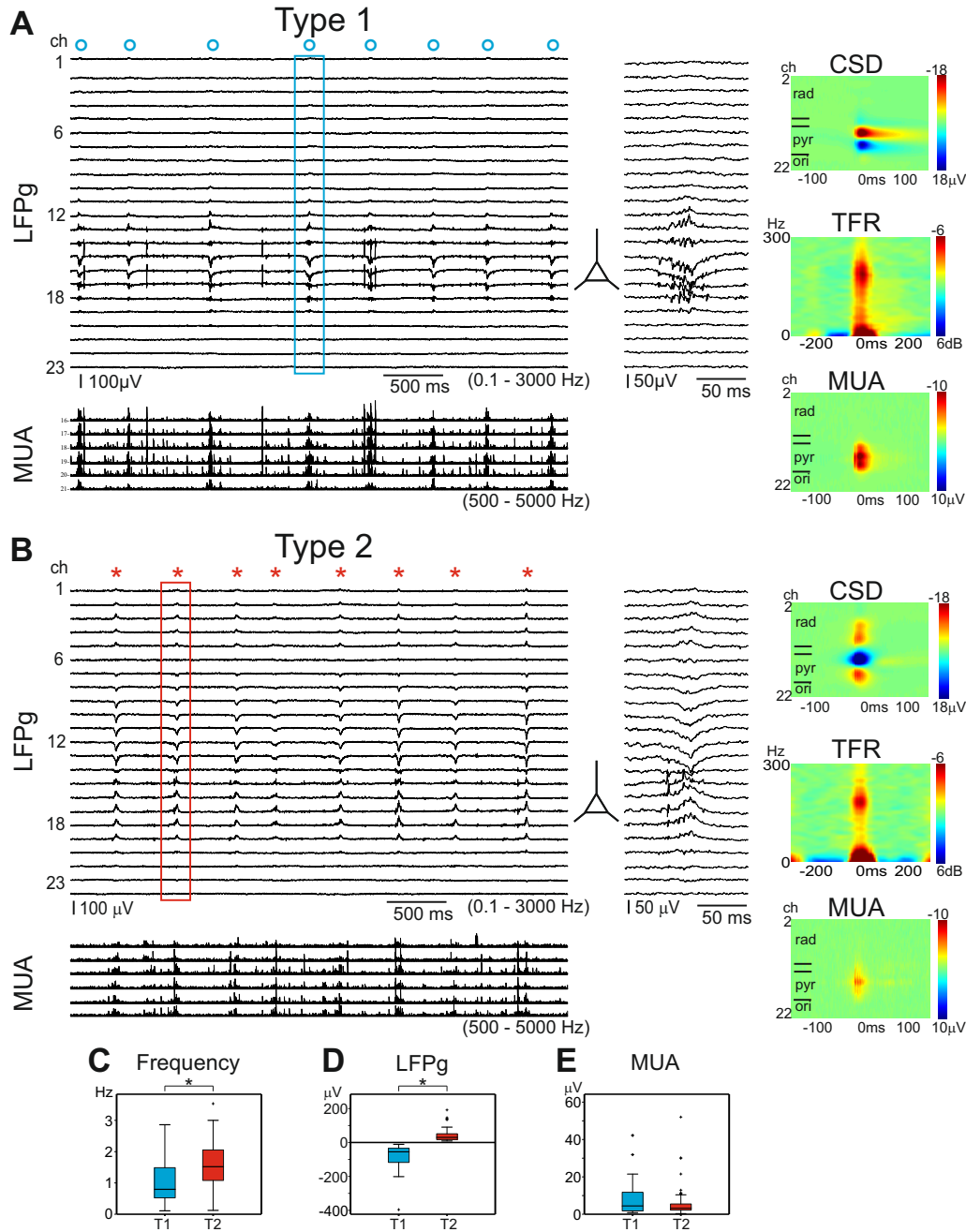


Figure 2.1: Two types of SPW activity in the CA3 region T1 (A) and T2 (B) SPWs could be distinguished according to their LFPg deflection in the str. pyramidale, which was negative for T1 SPWs but positive for T2 SPWs (A, B and D). Above the LFPg traces, SPWs are marked with blue open circles (T1) and red asterisks (T2), the indicated SPWs are magnified on the right side. The location of the str. pyramidale is indicated by a schematic pyramidal cell. In addition to the LFPg, MUA traces (500 – 5000 Hz filtered and rectified LFPg) are displayed. Colour maps show the CSD, the TFR plot and the change in MUA. CSD analysis uncovered a sink-source pair in the str. pyramidale during T1 SPWs, but a source in the str. pyramidale accompanied by two sinks in the str. radiatum and str. oriens during T2 SPWs. TFR plots show the presence of ripple oscillations and MUA plots display an increase in cellular activity during both types of SPWs. On the colour plots warm colours represent current sinks on the CSD maps and/or increases on the MUA and TFR plots while cold colours represent current sources and/or decreases on the MUA and TFR plots. The recurrence frequency (C) as well as the LFPg amplitude (D, absolute value used for testing) of T1 and T2 SPWs were found to be significantly different (both $p < 1E-05$, Mann-Whitney U-test). The MUA change (E) was not significantly different between T1 and T2, but tended to be larger for T1 than for T2 ($0.05 < p < 0.1$, Mann-Whitney U-test). For the values belonging to the box plots see table 2.2 overall values. rad, str. radiatum; pyr, str. pyramidale; ori, str. oriens.

2.3.3 Simultaneous occurrence of T1 and T2

In 10.2 % of slices (15/147), the two types of SPWs could be observed simultaneously in the same recording (figure 2.2A,B and table 2.2 "simultaneous"). In these cases, the frequency of T2 SPWs was significantly higher than that of T1 SPWs (medians: T1: 0.67 Hz, T2: 3.20 Hz, $p < 0.01$, Wilcoxon signed rank test). The LFPg amplitudes of T1 SPWs were consistently negative, while those of T2 were consistently positive, even though they were measured on the same channel within the str. pyramidale. Moreover, the absolute (sign-independent) amplitudes were significantly larger for T1 than for T2 SPWs (medians: T1: $-117.4 \mu\text{V}$, T2: $25.5 \mu\text{V}$, $p < 0.001$, Wilcoxon signed rank test). Although there was no significant difference in MUA increases for the overall T1 vs. the overall T2, this difference existed when MUA increases of simultaneous T1 and T2 SPWs were compared in a pairwise manner (medians: T1: $10.19 \mu\text{V}$, T2: $2.92 \mu\text{V}$, $p < 0.01$, Wilcoxon signed rank test).

	T1		T2	
	exclusive	simultaneous	exclusive	simultaneous
recurrence frequency (Hz)	0.80* [0.68 – 1.21]		1.52* [1.37 – 1.62]	
	1.13 [00.70 – 1.39]	0.67* [00.28 – 0.79]	1.52 [01.37 – 1.64]	1.38* [01.06 – 1.92]
LFPg amplitude (μV)	-54.9* [-84.3 – -44.9]		29.9* [25.5 – 36.0]	
	-46.9 [-67.4 – -41.5]	-117.4* [-168.6 – -69.9]	30.4 [26.0 – 39.7]	25.5* [12.3 – 43.2]
MUA amplitude (μV)	4.46 [3.07 – 7.12]		3.20 [2.52 – 4.10]	
	4.45 [2.73 – 5.53]	10.19* [4.45 – 20.84]	3.33 [2.51 – 4.28]	2.92* [2.33 – 4.68]

Table 2.2: Features of T1 and T2 SPWs The median and its 95 % CI (the latter in square brackets) are given for the mean recurrence frequency, the LFPg amplitude and the MUA amplitude. Values are displayed for overall T1 and T2 SPWs (combining those occurring exclusively and/or simultaneously with the other type), for exclusively occurring T1 and T2, and for T1 and T2 when they occurred simultaneously with the other type. Asterisks indicate significant differences of overall T1 vs. overall T2 SPWs (shown as box plots in figure 2.1C,D and E) and for simultaneous T1 vs. T2. The **recurrence frequency** of T1 SPWs was significantly lower than that of T2 SPWs overall ($p < 1\text{E-}05$, Mann-Whitney U-test) and when directly comparing the simultaneously occurring T1 and T2 ($p < 0.01$, Wilcoxon signed rank test). Moreover, it was significantly lower for simultaneous types than for exclusive types ($p < 0.01$, Mann-Whitney U-test). As the **LFPg amplitudes** of T1 and T2 had opposite signs, their absolute values were used for testing. LFPg amplitudes of T2 SPWs were significantly smaller than those of T1 overall ($p < 1\text{E-}05$, Mann-Whitney U-test) and when comparing the simultaneous types ($p < 0.001$, Wilcoxon signed rank test). The LFPg amplitude appeared to be similar for exclusive and simultaneous types ($p > 0.3$, Mann-Whitney U-test). The **MUA amplitudes** of simultaneous SPWs were significantly larger for T1 than for T2 SPWs ($p < 0.01$, Wilcoxon signed rank test). For overall T1 and T2, this was only a non-significant trend ($0.05 < p < 0.1$, Mann-Whitney U-test). MUA was not significantly different when comparing exclusive vs. simultaneous types ($p > 0.1$, Mann-Whitney U-test).

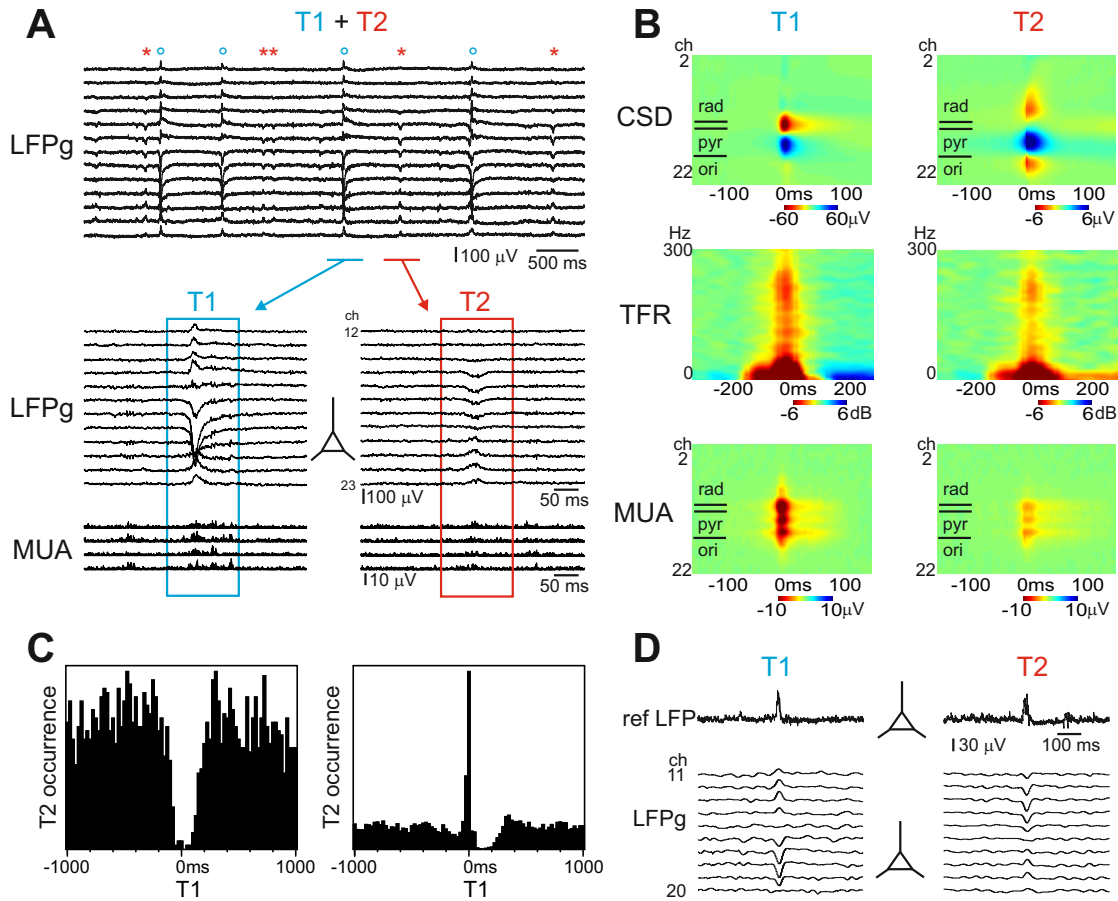


Figure 2.2: Simultaneous occurrence of T1 and T2 SPWs (A) LFPg traces of a recording exhibiting both T1 and T2. SPWs are marked with open blue circles (T1) and red asterisks (T2), the indicated SPWs are magnified below (LFPg filtered 0.1 – 3000 Hz, MUA filtered 500 – 5000 Hz and rectified). The location of the str. pyramidale is indicated by a schematic pyramidal cell. (B) The CSD, the time-frequency plot and the change in MUA of T1 (left) and T2 (right) are characteristic of their respective types (compare to figure 2.1). On the colour plots warm colours represent current sinks on the CSD maps and/or increases on the MUA and TFR plots while cold colours represent current sources and/or decreases on the MUA and TFR plots. Note the different scale for the CSD maps. (C) PETHs showing the occurrence of T2 SPWs around T1 SPWs for two different slices with simultaneous T1 and T2. The two types of SPWs could occur independently from one another (but with a common refractory period, left) or trigger each other (right). (D) T1 and T2 SPWs were indistinguishable in referential recordings made in the pyramidal cell layer. Top sweeps show the recordings made with the referential system (ref LFP), bottom sweeps are from the gradient recording (LFPg, ch 10 – 20, filtered 1 – 30 Hz). Schematic pyramidal cells show the location of the str. pyramidale. rad, str. radiatum; pyr, str. pyramidale; ori, str. oriens.

When occurring simultaneously, the two types of SPWs interacted with each other in various ways. In some slices the only interaction was a shared refractory period, meaning that each of the types could not occur within a short time period (<100 ms) before or after the other type. One example of this is shown in figure 2.2C (left panel). In other slices one type tended to trigger the other type. figure 2.2C (right panel) shows an extreme example of T2 SPWs triggering the occurrence of T1 SPWs, which often resulted in a mixed T1-T2 or T2-T1 SPW type due to the short time delay. However, in most slices some degree of interaction could be found lying in between the two extreme cases shown in figure 2.2C, with varying percentages of mixed and single types. Moreover, if triggering interactions between the two types of SPWs were present, they were not always consistent in their direction and each type could precede the other one at short time delays (<50 ms).

2.3.4 T1 and T2 are indistinguishable on referential recordings

In order to obtain referential recordings in addition to the gradient recordings presented so far, parallel recordings were performed with two acquisition systems in a submerged chamber (n=28 slices, see methods section 2.2.2). Briefly, the LFP was recorded using an extracellular glass electrode in the CA3 pyramidal cell layer and a reference electrode in the rACSF bathing solution. In addition, the LFPg was recorded close-by using the linear multielectrode. SPWs could be recorded in 22/28 slices using the multielectrode system. T1 and T2 SPWs could be identified in 8 and 14 slices, respectively. The referential system recorded positive field potential transients, high frequency oscillations and increased cellular activity in the str. pyramidale during both types of SPWs. While T1 and T2 SPWs were distinguishable on the LFPg recordings performed with the multielectrode, on the referential recordings the two types of SPWs had similar LFP waveforms and amplitudes and could therefore not be distinguished (T1: median: 70.3 μ V, 95 % CI: [35.2 83.2], T2: median: 47.5 μ V, 95 % CI: [30.5 58.3], $p>0.3$, Mann-Whitney U-test, figure 2.2D). It should be noted that - although recorded with the same multielectrode gradient recording system - both types of SPWs displayed larger amplitudes in the dual perfusion chamber (this set of experiments) than in the interface chamber (exclusive T1 or T2 SPWs in all other recordings). This difference was significant for T2 SPWs (medians: submerged: 63.8 μ V, interface: 30.4 μ V, $p<0.01$, Mann-Whitney U-test), but not significant for T1 SPWs (medians: submerged: 75.7 μ V, interface: 46.9 μ V, $p>0.1$, Mann-Whitney U-test). Summarising, a referential recording system was not able to differentiate between the two types of SPWs while they could be observed via the multielectrode system recording in parallel.

2.3.5 T1 and T2 in different CA3 subregions

Both types of SPWs could be recorded in each of the CA3 subregions CA3a, CA3b and CA3c (table 2.3). However, there were significant differences in the abilities of the CA3 subregions generating different types of SPWs. All tests in this section were performed with the Chi-squared test, except where otherwise mentioned. In those cases the chi-squared test's criteria were not met and the Fisher's exact test was used instead.

Subregion	No. of examined subregions	exclusive T1	exclusive T2	simult. T1+T2	no activity
CA3a	83	3 (3.6%)	17 (20.5%)	0 (0.0%)	63 (75.9%)
CA3b	208	35 (16.8%)	51 (24.5%)	8 (3.8%)	114 (54.8%)
CA3c	103	13 (12.6%)	13 (12.6%)	7 (6.8%)	70 (68.0%)
total	394	51 (12.9%)	81 (20.6%)	15 (3.8%)	247 (62.7%)

Table 2.3: T1 and T2 in different CA3 subregions. Numbers and percentages of examined subregions generating different types of SPW activity.

It was found that fewer CA3a than CA3c subregions and fewer CA3c than CA3b subregions produced SPWs (CA3a: 20/83 24.1%, CA3b: 94/208 45.2%, CA3c: 33/103 32.0%, CA3a vs. CA3b: $p < 0.001$, CA3a vs. CA3c: $p < 0.01$, CA3b vs. CA3c: $p < 0.01$). Moreover, the proportion of simultaneous T1+T2 (rather than exclusive T1 or T2) SPWs was significantly higher in CA3c than in CA3a subregions and tended to be higher in CA3c than in CA3b subregions (CA3a: 0/20 0.0%, CA3b: 8/94 8.5%, CA3c: 7/33 21.2%, CA3a vs. CA3b: $p > 0.3$, CA3a vs. CA3c: $p < 0.05$, CA3b vs. CA3c: $0.05 < p < 0.1$, Fisher's exact test). Next the CA3 subregions' ability to generate each SPW type was examined. Case numbers of subregions producing a certain SPW type (exclusively or simultaneously with the other type) were compared to case numbers where no SPW or only the other SPW type was generated. It was found that the CA3a subregion is less capable of generating T1 SPWs than the CA3b or CA3c subregions (CA3a: 3/83 3.6%, CA3b: 43/208 20.7%, CA3c: 20/103 19.4%, CA3a vs. CA3b: $p < 0.001$, CA3a vs. CA3c: $p < 0.01$, CA3b vs. CA3c: $0.05 < p < 0.1$). The ability to generate T2 SPWs was significantly larger in CA3b than in CA3a or CA3c subregions (CA3a: 17/83 20.5%, CA3b: 59/208 28.4%, CA3c: 20/103 19.4%, CA3a vs. CA3b: $p < 0.001$, CA3a vs. CA3c: $p < 0.01$, CA3b vs. CA3c: $0.05 < p < 0.1$). Lastly, the overall tendency of each subregion to one SPW type or the other was checked (using all cases that showed SPWs). It was found that the CA3a subregion tended more to generating T2 rather than T1, while this was not significant for the CA3b or CA3c subregions (CA3a: 3 (T1) vs. 17 (T2) $p < 0.01$, CA3b: 43 (T1) vs. 59 (T2) $p > 0.1$, CA3c: 20 (T1) vs. 20 (T2) $p = 1$, binomial tests). Summarising, the CA3a subregion tends to generate fewer T1 SPWs than T2 SPWs, and differentiates itself from the CA3b or CA3c subregions in other aspects such as generating fewer SPWs overall. Compared to the CA3a or CA3c subregions, the CA3b subregion had a higher proportion of SPW-generating slices in general (for all SPWs) and for T2 SPWs. The CA3c subregion had the highest proportion of simultaneous T1+T2 SPWs, which was significantly higher than that of the CA3a subregion and tended to be higher than that of the CA3b subregion.

The pattern of correlated occurrence of T1 and T2 SPWs between the CA3a, CA3b and CA3c subregions was investigated by consecutive recordings in the different CA3 subregions. A SPW was considered to be correlated when the same SPW type could be found in at least two neighbouring subregions (see methods section 2.2.2 for details). Multiple different patterns could be observed across different CA3 subregions of the same slice. T1 and T2 SPW activity was observed to be correlated to neighbouring CA3 subregions in 14.3% and 32.0% of slices,

respectively and remained local in 85.7% and 68.0% of slices, respectively (table 2.4). Thus, both T1 and T2 SPWs were local events in the majority of cases. Although T2 SPWs appeared to be correlated between subregions more frequently than T1 SPWs, this difference was not significant ($p > 0.1$, Chi square test).

SPW type	correlated SPWs				local SPWs				No. of slices
	a/b	a/c	b/c	total	a	b	c	total	
T1	1	0	2	3 (14.3%)	1	11	6	18 (85.7%)	21
T2	3	2	5	8 (32.0%)	5	9	5	17 (68.0%)	25

Table 2.4: Correlated occurrence of T1 and T2 between neighbouring CA3 subregions. In subsequent recordings from different CA3 subregions, SPWs were considered to be correlated when the same SPW type was present in at least two neighbouring CA3 subregions. If the same type of SPW was not detected in any neighbouring subregion, it was regarded as a local event. Simultaneous T1+T2 SPWs were not treated as a separate type but as containing T1 as well as T2 SPWs. In the special case when the CA3a and CA3c, but not the CA3b subregions displayed T2 SPWs ($n=2$), it was counted as a local SPW for both the CA3a and the CA3c subregion. This is the reason why the sum of local events in the CA3a, CA3b and CA3c subregions is not equal to the number of slices with local events (in the "total" column for local SPWs). T1 and T2 did not show significant differences in terms of the numbers of slices with correlated or local SPWs ($p > 0.1$, Chi square test).

2.3.6 The role of glutamatergic and GABAergic signalling

The role of glutamatergic and GABAergic signalling in the generation of SPW activity was examined using antagonists of excitatory and inhibitory neurotransmitter receptors, respectively.

Both types of SPWs depended on functional AMPA/kainate glutamate receptors as well as GABA_A receptors, as they were suppressed by the receptors' respective antagonists NBQX and bicuculline (figure 2.3A,B). This is consistent with earlier findings [4, 6, 7, 15, 23, 47].

There have been inconsistent findings on the role of NMDA receptors in earlier studies. While some studies reported that a block of NMDA receptors caused increased SPW amplitudes in some studies [23, 48], the results presented here (obtained by bath application of AP5) are consistent with other studies which reported no changes in SPW amplitudes [4, 6, 7, 15] (table 2.5, figure 2.3A). Additionally, in this study AP5 did not induce any significant changes in the recurrence frequency, the LFPg or the MUA amplitude of either SPW type. Moreover, the non-significant trends that were observed in this study were the opposite of those reported in the first group of studies [23, 48].

Except for a reduction in the LFPg amplitude of T2 SPWs, the GABA_B receptor antagonist CGP52432 did not induce any major changes in SPW activity. (table 2.5, figure 2.3B).

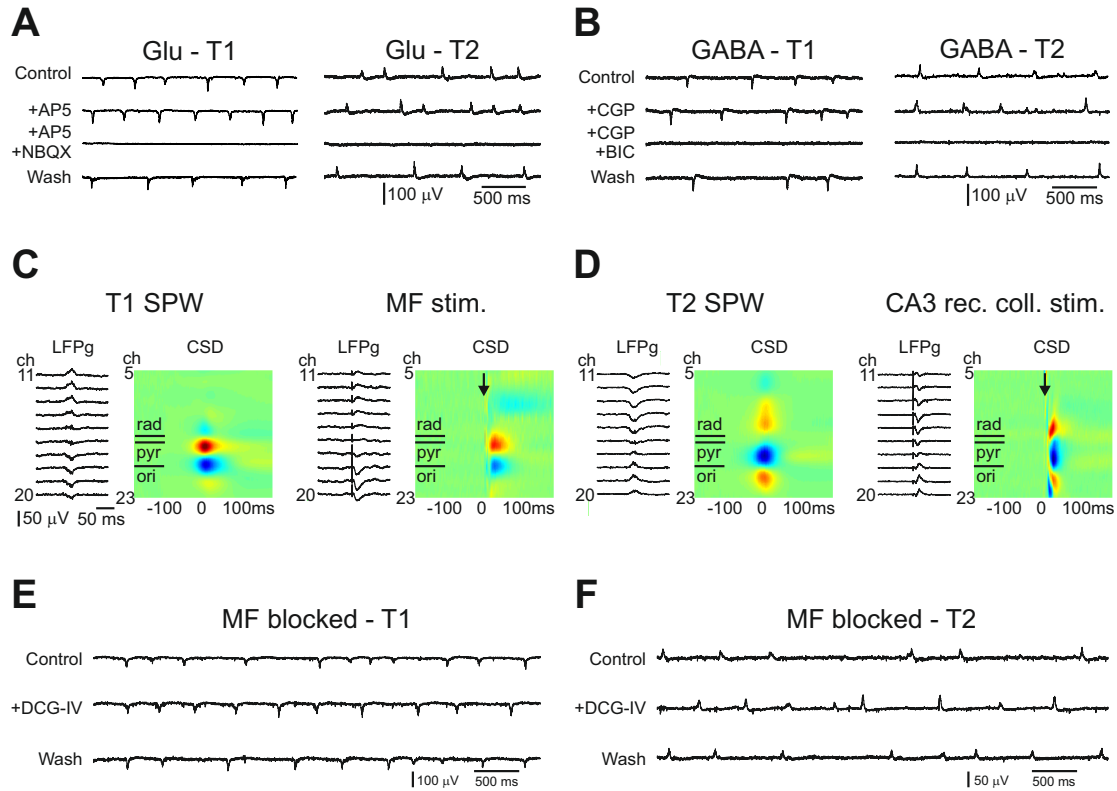


Figure 2.3: Involvement of neurotransmitter receptors and excitatory pathways (A,B) SPWs depend on glutamatergic and GABAergic signalling. **(A)** Blockage of NMDA receptor signalling (via AP5) did not significantly change T1 or T2 SPWs, but blockage of AMPA/kainate receptor signalling (via NBQX) was able to reversibly suppress either type of SPW activity. **(B)** The GABA_B receptor antagonist CGP52432 did not significantly affect SPW activity, except for a reduction in LFPg amplitude in case of T2, but the GABA_A receptor antagonist bicuculline reversibly suppressed both T1 and T2 SPWs. **(C,D)** Stimulation of the MFs **(C)** or the CA3 recurrent collaterals **(D)** evoked slightly different but related responses as spontaneous T1 and T2 SPWs, respectively. The traces on the left side of each panel show the LFPg recorded in the proximal dendritic and somatic layers (channels 11 – 20), colour plots on the right side of each panel show the CSD maps of the entire CA3 region (sinks are represented in red, sources in blue). Arrows depict the stimulation artefacts on the CSD maps. **(E,F)** Blockade of mossy fibre (MF) activity by via the mGluR2 agonist DCG-IV did not suppress the emergence of T1 **(E)** or T2 **(F)** SPWs in the CA3 region.

		recurrence frequency (Hz)	LFPg amplitude (μV)	MUA amplitude (μV)
AP5	T1 (n=5)	112.06 % [97.42 – 121.48] 01.29 → 01.26 p>0.1	102.63 % [67.23 – 132.73] -33.84 → -35.72 p=1	83.43 % [51.26 – 178.98] 01.61 → 01.34 p>0.8
	T2 (n=8)	105.05 % [90.00 – 137.50] 01.16 → 01.28 p>0.7	86.79 % [76.36 – 111.30] 33.69 → 30.27 p>0.5	103.42 % [78.16 – 124.64] 01.72 → 02.27 p>0.5
	T1 (n=10)	97.34 % [93.18 – 106.64] 01.64 → 01.68 p>0.6	109.41 % [72.19 – 128.00] -24.77 → -24.36 p>0.6	109.99 % [72.59 – 159.45] 00.83 → 00.66 p>0.7
	T2 (n=7)	103.96 % [101.74 – 112.37] 01.62 → 01.82 p>0.2	74.33 % [63.82 – 88.18] 29.54 → 23.17 p<0.05	84.51 % [59.39 – 116.84] 01.82 → 01.79 p>0.3
DCG-IV	T1 (n=7)	87.39 % [72.49 – 96.65] 01.57 → 01.52 p<0.05	96.40 % [59.05 – 203.00] -28.67 → -25.45 p>0.6	74.64 % [35.56 – 169.78] 02.92 → 01.98 p>0.5
	T2 (n=7)	147.43 % [94.81 – 157.91] 01.10 → 01.63 0.05<p<0.1	122.30 % [112.06 – 216.84] 32.67 → 38.13 0.05<p<0.1	98.28 % [83.54 – 171.43] 01.42 → 01.25 p>0.6
DAMGO	T1 (n=14 / n=14)	20.95 % [07.33 – 27.06] 01.34 → 00.19 p<0.001	173.63 % [74.45 – 301.60] 57.27 → 94.66 p>0.2	300.24 % [189.79 – 403.00] 01.37 → 05.12 p<0.01
	T2 (n=44 / n=30)	17.60 % [13.99 – 24.13] 01.17 → 00.20 p<0.001	147.28 % [72.55 – 209.09] 58.36 → 79.68 p>0.1	182.00 % [116.29 – 303.44] 01.95 → 05.18 p<0.05

Table 2.5: Pharmacological manipulation of SPWs. Changes in SPW recurrence frequency as well as LFPg and MUA amplitude before and during the application of AP5, CGP52432, DCG-IV or DAMGO. The changes are expressed as percentages in comparison to the values before the drug application (95 % CIs in square brackets). Moreover, the medians for before and during (before → during) the drug application are displayed. P-values reflect the significances as determined by the Wilcoxon signed rank test. In case of DAMGO, 'during' and 'change' values only refer to cases where SPWs persisted. 'before' values also include cases for which SPWs disappeared during the DAMGO application.

2.3.7 The role of excitatory pathways in the generation of SPWs

The CSD pattern of T1 and T2 SPWs showed similarities with the activation patterns of mossy fibres (MFs) and CA3 recurrent collaterals, respectively (figure 2.3C,D). To examine potential contributions of these pathways in the generation of T1 and/or T2 SPWs, multiple kinds of experiments were carried out: A) The activation patterns resulting from electrical stimulation of the pathways in question were compared to spontaneously occurring SPWs, B) the loss of MF connectivity was studied in mini slices and C) glutamate release from MF terminals was suppressed using DCG-IV.

Both MFs and CA3 recurrent collaterals were electrically stimulated in slices with spontaneous T1 (n=5) or T2 (n=6) SPWs. The resulting activation pattern after MF stimulation strongly resembled, but was not identical to, the CSD pattern during T1 SPWs (figure 2.3C). The sink arising from MF activation was shifted by about 50 μm to lie in the str. lucidum compared to the spontaneously occurring sink in the upper str. pyramidale during T1. The accompanying source of the evoked response was also shifted by about 50 μm toward str. oriens compared to the source of the spontaneous SPWs. Interestingly, stimulation of CA3 recurrent collaterals activated transmembrane currents which recalled (but were not identical to) the pattern of spontaneous T2 SPWs: the sinks in the str. oriens and radiatum were about 50 μm closer to the str. pyramidale (figure 2.3D), than during T2 SPWs. In summary, the activation patterns of MFs and CA3 recurrent collateral stimulation resembled T1 and T2 SPWs, respectively, but they were not identical.

As MF stimulation patterns were similar to spontaneous T1 SPWs, it was further examined whether the DG (the source of MFs) is necessary for the generation of T1 SPWs. As mentioned in section 2.3.1, mini slices containing only the CA3 region were able to generate SPWs. Moreover, they were able to generate T1 (3/9 slices), T2 (4/9 slices) and even T1+T2 SPWs (1/9 slices) in various CA3 subregions. Thus, even without the transmission from the DG to the CA3 region, both types of SPWs are possible and MFs are not required for the generation of either SPW type.

The role of the DG in the initiation of SPWs in the CA3 region was further investigated by blocking the glutamate release from MFs using the mGluR2 agonist DCG-IV [40]. While previous findings reported that DCG-IV largely reduced the incidence of SPWs [49], only a slight, but significant decrease in recurrence frequency was found for T1 SPWs in this study (median change to 87.39 %, $p < 0.05$, Wilcoxon signed rank test). Meanwhile, the recurrence frequency and the LFPg amplitude non-significantly tended to increase during DCG-IV application for T2 SPWs (recurrence frequency: median change to 147.43 %, $0.05 < p < 0.1$, LFPg amplitude: median change to 122.30 %, $0.05 < p < 0.1$, Wilcoxon signed rank test, table 2.5, figure 2.3E,F). High variabilities and no significant effects of DCG-IV were found for the LFPg amplitude of T1 SPWs and the MUA amplitudes of either SPW type.

In summary, spontaneous T1 and T2 SPWs showed similar but slightly different CSD patterns than those induced by mossy fibre or CA3 recurrent collateral stimulation, respectively. The suppression of mossy fibre transmitter release reduced the recurrence of T1 SPWs and non-significantly tended to increase that of T2 SPWs. However, none of the SPW types were blocked. Furthermore, the cutting of intrahippocampal connections did not block the emergence of T1 or T2 SPWs in the CA3 region either. These results might imply a possible modulatory role of the DG, which is not necessary for the generation of either SPW type.

2.3.8 Behaviour of pyramidal cells during SPWs

Synaptic inputs to CA3 pyramidal cells and their responses before and during SPWs have been a matter of disagreement. Different studies have emphasised the importance of hyperpolarising [15, 35], depolarising [24] or both [4, 29] types of postsynaptic potentials. Furthermore, depolarising, hyperpolarising, mixed synaptic potentials and no responses were shown to occur in the same CA3 pyramidal cell during SPW activity [23].

Simultaneous intra- and extracellular recordings from 43 putative pyramidal cells were performed in the CA3 str. pyramidale to explore their behaviour during T1 and T2 SPWs (median resting membrane potential: -58.0 mV, 95 % CI: [-60.8 – -55.0]). Recordings were made from 7 cells in slices where T1 SPWs were generated, from 22 cells with T2 and from 14 cells in slices with both T1 and T2 SPWs. Most cells responded with hyperpolarisations during SPWs, some however depolarised or exhibited biphasic responses, during which a longer hyperpolarising response was superimposed by a short depolarising event (figure 2.4, table 2.6).

		excl. T1 (no T2)	response to T2 (during T1+T2)		
			hyperpol.	biphasic	depol.
excl. T2 (no T1)			18 (-,0)	2 (-,2)	2 (-,1)
response to T1 (T1+T2)	hyperpol.	6 (0,-)	8 (0,0)	0 (0,0)	0 (0,0)
	biphasic	1 (1,-)	0 (0,0)	4 (3,3)	0 (0,0)
	depol.	0 (0,-)	1 (1,0)	0 (0,0)	1 (1,1)

Table 2.6: Intracellular responses of putative pyramidal cells during SPWs. Case numbers for responses of 7 cells recorded during T1, 22 cells recorded during T2 and 14 cells recorded during T1+T2 SPWs. Numbers in parentheses represent the number of cells eliciting action potentials during the respective SPW types (during T1, during T2). In case of simultaneous T1+T2 SPWs all cells except for one responded the same way to both SPW types. One cell depolarised and fired during T1 and hyperpolarised during T2. The ratios of cells showing hyperpolarising, depolarising and biphasic responses were not significantly different between T1 and T2 SPWs ($p=1$, Fisher's exact test).

At resting membrane potential, cells responded to consecutive SPWs with similar hyperpolarising, depolarising or biphasic events. However, only one cell showed consistent biphasic responses during all SPW events. In most cells, a depolarising component was associated with most, but not all, SPW events (mean 79.3 % of SPW events). At resting potential, 9 of the 43 pyramidal cells fired during SPWs (table 2.6). All of these cells showed depolarising or biphasic synaptic events in response to the respective SPW type.

When cells were recorded in slices with simultaneous T1+T2, 13/14 cells responded similarly to both SPW types. However, one cell slightly depolarised during T1 and slightly hyperpolarised during T2. This cell fired action potentials during T1, but not during T2 SPWs. In case of biphasic responses during T1+T2 SPWs ($n=4$ cells), the depolarising component was more often associated with T1 (mean 78.3 %), than with T2 (mean 11.1 %) SPWs.

The ratios of cells showing hyperpolarising, depolarising, or biphasic responses were very similar between T1 and T2 SPWs ($p=1$, Fisher's exact test, table 2.6). No significant differences in membrane potentials were found between cells recorded during T1 vs. T2 vs. T1+T2 ($p>0.4$,

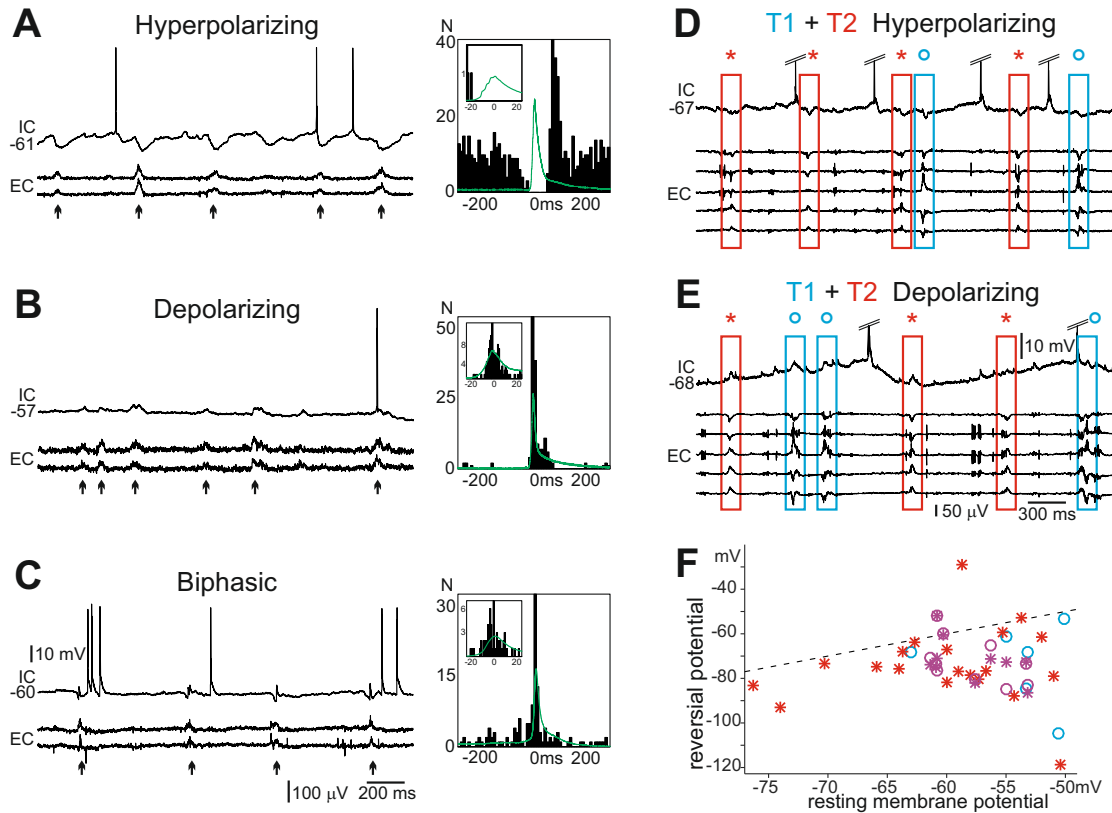


Figure 2.4: Intracellular responses of putative pyramidal cells during SPWs (A-C) Representative examples of hyperpolarising (A), depolarising (B) and biphasic (C) intracellular responses of PCs during SPWs are displayed. Left panels show intracellular traces (IC) and two channels of the extracellular LFPg (EC). Right panels in A-C show the respective cell-SPW PETHs. LFPg averages of the SPWs are overlaid as green lines. While most cells were hyperpolarised (A) and ceased firing during SPWs (arrows), some cells were purely depolarised (B) and discharged during SPWs. Several cells exhibited a biphasic (C) hyperpolarisation+depolarisation response to SPWs. Table 2.6 describes how many cells fall into each category. (D,E) During simultaneous T1+T2 SPWs, the large majority of cells responded similarly to the two SPW types, depolarising (D) or hyperpolarising (E) to both of them. (F) Resting membrane potentials of cells responding with de- or hyperpolarisation (excluding biphasic responses) plotted against the reversion potential of their responses. Cell responses to T1: circles, responses to T2: asterisks. Cells recorded during exclusive T1: blue, during exclusive T2: red, during simultaneous T1+T2: purple. The dashed black line indicates where the reversal potentials are equal to the membrane potentials. Thus, shapes above and below the line represent de- and hyperpolarising responses, respectively. No significant differences in membrane potentials were found between cells recorded during T1 vs. T2 vs. T1+T2 ($p > 0.4$, Kruskal Wallis test, groups represented by colours). No significant differences in reversal potentials were found in responses to T1 vs. T2 ($p > 0.6$, Mann-Whitney U-test, groups represented by shapes).

Kruskal Wallis test, figure 2.4F) nor in reversal potentials in response to T1 vs. T2 ($p > 0.6$, Mann-Whitney U-test, figure 2.4F).

Summarising, most PCs responded to SPWs with hyperpolarisations, though they could also depolarise or show biphasic responses. Almost all analysed PCs showed the same kind of response to to the two types of SPWs.

2.3.9 Behaviour of interneurons during SPWs

As most PCs were inhibited during SPWs, the next step was to investigate the behaviour of inhibitory interneurons during SPWs. For this purpose, single unit interneuron activity was clustered from the extracellular LFPg recordings (see methods section 2.2.4). Reliable single-unit activity was recorded from 71 clustered putative interneurons (table 2.7).

	excl. T1	excl. T2	simult. T1+T2	total
str. lac-mol.	0	1	1	2
str. radiatum	3	8	2	13
str. pyramidale	5	8 (-2)	11 (-1)	24
str. oriens	8	21	2	31
hilus	0	0	1	1
total	16	38	17	71

Table 2.7: Numbers of clustered interneurons. The location of the cell and the type of SPW occurring in the recording are indicated. Three interneurons from the str. pyramidale were not be analysed as their firing frequency was too low to assess their relation to the SPW (values in parentheses: two during T2 SPWs, one during a T1+T2 SPW).

The firing of the clustered neurons was compared to the T1, T2 or simultaneous T1+T2 SPWs present in the same recording via PETHs. In cases where the cell firing was related to the occurrence of SPWs, the observed patterns were grouped into four categories (figure 2.5, table 2.8).

- "SPW": Neurons with this pattern increased their firing during the SPW.
- "SPW+blocked": These neurons showed increased firing during the SPW, followed by a reduction in firing directly afterwards. These neurons could be further subdivided into those with or without rebound firing after the silent period.
- "SPW+after": Neurons in this groups showed increased firing during the SPW, followed by less persistent firing.
- "before+SPW": These neurons showed a slight increase in firing before the SPW onset, followed by a larger increase during the SPW.

Interneuron firing patterns were different during T1 and T2 SPWs. Although there was no difference in the proportion of unrelated neurons (T1: 8.5 %, T2: 8.3 %, $p=1$, Fisher's exact text),

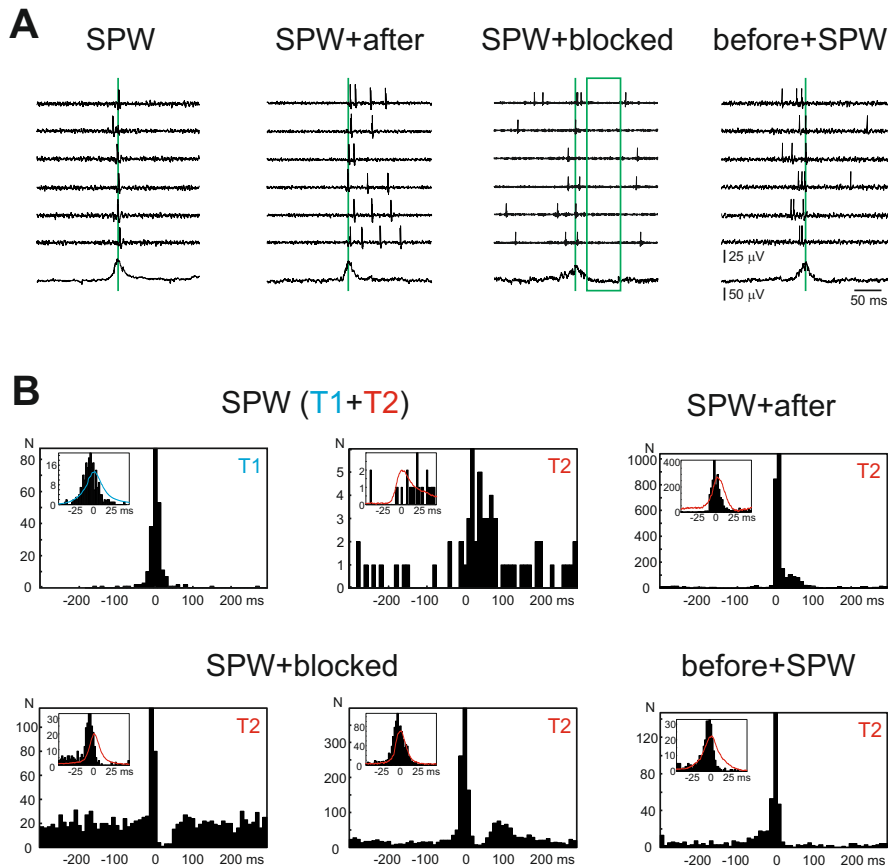


Figure 2.5: Interneuron firing patterns during and around SPWs When related to the SPW, an interneuron's firing followed one out of four patterns. (A) Six consecutive sweeps of interneuron firing (upper traces, bp filtered 500 – 3,000 Hz) and one representative LFPg trace of the SPW (lower trace, bp filtered 0.1 – 500 Hz) are shown for every firing pattern. The time of the SPW peak is indicated by green vertical lines. In SPW+blocked, the cell's silent period is indicated by a green rectangle. (B) PETHs of interneuron firing relative to the SPW events for ± 300 ms. Inset: PETH for ± 30 ms, LFPg averages of the SPWs are indicated in red. The same interneuron can show different firing patterns to the two types of SPWs ("SPW (T1+T2)"). The group of INs showing SPW+blocked behaviour could be further subdivided into subgroups with (right) or without (left) rebound firing after the silent period.

		SPW	SPW+ blocked	SPW+ after	before+ SPW	not related
str. lac-mol.	T1	-7.9 n=1	n=0	n=0	n=0	n=0
	T2	-32.9 n=1	n=0	n=0	-4.0 n=1	n=0
str. radiatum	T1	-2.1 [-10.2 – 3.1] n=4	n=0	n=0	n=0	n=1
	T2	-3.6 [-7.0 – 4.2] n=6	n=0	22.3 [-3.7 – 39.3] n=3	-4.3 n=1	n=0
str. pyramidale	T1	-6.0 [-8.0 – -3.5] n=11	n=0	n=0	n=0	n=4
	T2	3.6 [-2.5 – 14.1] n=8	n=0	-4.1 [-7.9 – 1.1] n=4	n=0	n=4
str. oriens	T1	-6.7 [-8.8 – -4.8] n=7	-7.9 [-13.1 – 1.1] n=3	n=0	n=0	n=0
	T2	-7.3 [-13.1 – -4.3] n=6	-5.8 [-7.3 – -3.3] n=6	-3.6 [-6.6 – -1.2] n=7	-5.8 n=1	n=3
hilus	T1	1.3 n=1	n=0	n=0	n=0	n=0
	T2	n=0	n=0	n=0	n=0	n=1
total	T1	-5.8 [-7.3 – -3.9] n=24	-7.9 [-13.1 – 1.1] n=3	n=0	n=0	n=5
	T2	-2.5 [-6.7 – 3.6] n=21	-5.8 [-7.3 – -3.3] n=6	-3.5 [-4.9 – -0.6] n=14	-4.3 [-5.8 – -4.0] n=3	n=8

Table 2.8: Interneuron firing patterns during and around SPWs. The distribution of INs from table 2.7 over four different firing patterns in association with SPWs and one pattern describing unchanged firing during SPWs ("not related"). In cases where the INs showed a relation to the SPW (all except the "not related" category) the median time of peak firing compared to the SPW peak is displayed in ms for cases of $n > 0$. Additionally, for cases of $n > 1$ the 95 % CI is displayed in square brackets. In the majority of cell-SPW relations (except the "not related" group) the maximal firing preceded the LFPg peak of the SPWs (56/71). Note that "SPW+after" and "before+SPW" firing patterns were only observed in relation with T2, but not T1 SPWs and that "SPW+blocked" behaviour was only observed in str. oriens.

there was a significant difference between T1 and T2 in the distribution of related neurons over the four firing patterns (table 2.8: total over different layers, $p < 0.001$, Fisher's exact test). While the numbers of interneurons showing "SPW+blocked" behaviour were comparable for T1 and T2 SPWs (11.1 % and 13.6 %, respectively) cells only showed "SPW+after" or "before+SPW" firing patterns during T2, but not during T1 SPWs (table 2.8). Although "SPW" was the most common pattern during both types, the proportion of cells firing this way was larger during T1 than during T2 SPWs (88 % and 47.7 %, respectively). During T1+T2 SPWs, 10 interneurons showed different firing patterns during T1 and T2, while 6 showed the same firing pattern (one neuron was undetermined due to too few action potentials, see table 2.7). PETH analysis allowed the analysis of the timing of maximal firing relative to the SPWs. For both T1 and T2 SPWs, the majority of interneurons fired before the LFPg peak associated with the SPW (T1: 81.5 %, T2: 77.3 %, $p > 0.6$, Chi-square test). There was a non-significant tendency for interneurons to fire earlier during T1 than during T2 SPWs (medians [95 % CI] in ms: T1: -6.0 [-7.9 – -4.2], T2: -4.1 [-5.5 – -2.5], $0.05 < p < 0.1$, Kruskal-Wallis). Interneurons located in different layers of the CA3 region behaved differently during SPWs. Cells with a "SPW+blocked" firing pattern only occurred in str. oriens (table 2.8). Moreover, during T2 SPWs, interneurons of different layers fired at different times in respect to the LFPg peak. Cells recorded from str. oriens tended to fire earlier than cells in str. pyramidale ($p < 0.05$, Kruskal Wallis test). No such differences were significant for T1 SPWs.

In summary, the firing of >90 % of interneurons increased in association with SPWs. Several different discharge patterns were observed. Most of the recorded interneurons fired maximally before the peak of SPW fields. Interneuron firing patterns varied according to their location and the type of the SPW. About 60 % of neurons recorded during T1+T2 SPW activity ($n=10/16$) showed different firing patterns in relation to the two types of SPWs.

2.3.10 The role of perisomatic interneurons

Perisomatic inhibitory interneurons have repeatedly been found to play a role in the generation of SPWs *in vitro* [23, 25, 29]. As described in section 2.3.2 and figure 2.1, in the model presented here, a CSD source was found in the str. pyramidale of the CA3 region for both types of SPWs. The high proportion of pyramidal cells being hyperpolarised during SPWs supports the notion that these sources are caused by active inhibitory transmembrane currents, possibly caused by perisomatic interneurons. To examine this hypothesis, the activity of PV⁺ basket cells and somatostatin⁺ dendritic interneurons (the O-LM cells and hippocampo-septal cells [38]) was reduced using the μ -opioid receptor agonist DAMGO [26, 37, 39]. Fourteen slices with T1, 26 slices with T2 and 4 slices with T1+T2 were exposed to DAMGO via the bathing medium (see section 2.2.3). Under the effect of DAMGO, the recurrence frequency of SPWs was significantly reduced, as reported previously for the CA1 region [50] (median changes to 20.95 % and 17.60 % for T1 and T2, respectively, both $p < 0.001$, Wilcoxon signed rank test, table 2.5, figure 2.6A,B). Moreover, the LFPg and CSD pattern of T1 SPWs was reversibly converted into that of T2 SPWs ($n=11/14$, figure 2.6C,E) or to an undefined pattern ($n=3/14$) during DAMGO application. The CSD pattern of T2 SPWs remained unchanged (i.e., source in the pyramidal layer and two sinks in the dendritic layers) in 14/26 slices (figure 2.6D,F), in the other 12/26 slices DAMGO reversibly blocked T2

SPW activity. In two of four slices with both T1 and T2 SPWs only T2 SPWs were detected during the application of DAMGO (figure 2.6G), in the other two slices SPWs with undefined patterns were present. The LFPg amplitude of T1 SPWs changed to 173.63 % ($p > 0.2$, Wilcoxon signed rank test, also see table 2.5), the one of T2 SPWs increased to 147.28 % ($p > 0.1$, Wilcoxon signed rank test). Compared to control, the MUA amplitude of both types significantly increased during DAMGO application, (T1: change to 300.24 %, $p < 0.01$, T2: change to 182 %, $p < 0.05$, Wilcoxon signed rank test).

For the purpose of investigating the effect of DAMGO on individual inhibitory cells, several interneurons were clustered from the str. oriens ($n=11$) and the str. pyramidale ($n=23$). As expected [37, 39], interneurons responded by either increasing ($n=9$) or decreasing ($n=25$) their firing rate during DAMGO application. Moreover, the firing pattern during SPWs either remained unchanged ($n=18$ cells), was blocked ($n=2$ cells), was desynchronised ($n=4$ cells) or synchronised ($n=5$ cells). There was no correlation between the changes in firing rate and the firing pattern, which further increased the heterogeneity of interneuronal responses to DAMGO application.

To reduce the activity of CB1⁺ basket cells [36, 51] in addition to the PV⁺ ones, the acetylcholine receptor agonist CCh was applied. While DAMGO reduced, but did not totally suppress SPW activity (figure 2.6A,B), additional application of CCh blocked the remaining SPWs in almost all slices (T1: 8/8, T2: 4/5, T1+T2: 2/2), inducing a slight gamma activity.

Summarising, the reduction of PV⁺ basket cell and SOM⁺ dendritic inhibitory interneuron activity largely diminished the occurrence of both types of SPWs and reversibly converted T1 into T2 SPW. The remaining T2 SPWs were blocked by reducing the activity of CB1⁺ basket cells.

2.4 Discussion

2.4.1 The rodent CA3 region can generate two types of SPWs *in vitro*

In vitro correlates of SPWs observed in hippocampal slice preparations have been used to study the underlying cellular and network mechanisms of this population activity [3, 4, 6, 7, 22–24, 44], which, *in vivo*, is associated with memory consolidation processes during slow wave sleep and behavioural immobility [1, 2]. In the *in vitro* model used for this study, spontaneous SPWs could be observed in horizontal slices of ventral rat hippocampus. They presented themselves as transients on the LFPg trace associated with increased high frequency oscillations and increased MUA (see figure refrat:fig:2typesofSPWs). The use of a laminar microelectrode placed perpendicularly to the str. pyramidale allowed the estimation of the current source density along the entire extent of the somatodendritic axis of CA3 pyramidal cells. This spatio-temporal characterisation of the detected SPWs allowed the differentiation of two distinct types of SPWs. They differed in various aspects such as recurrence frequency, LFPg pattern and amplitude, the amount of MUA increase and the composition of their CSD pattern (see table 2.2 and figure refrat:fig:2typesofSPWs). Type 1 SPWs were characterised by a negative LFPg transient in the str. pyramidale, the associated sink was confined to the proximal dendrites. Type 2 SPWs were typified by a positive LFPg transient in the str. pyramidale and displayed CSD sinks at the apical and basal dendrites (see figure refrat:fig:2typesofSPWs). Further results from intra- and extracellular recordings of local PCs and INs as well as the administration of pharmacological agents revealed that PCs can be recruited differentially during the different types of SPWs (see figure 2.4 and table 2.6). Moreover, distinct interneuron populations are involved, with the activity of perisomatic INs potentially playing a differential role in the two types of SPWs (see figure 2.6). For this reason it can be excluded that different ways of cutting the hippocampal slices or other procedural variations are the cause of the generation of the two different types of SPWs. The fact that around 10% of slices generated both types of SPWs in the same spot simultaneously further supports this notion (see section 2.3.3).

This leaves the question why the existence of these two SPW types had not been reported previously. One of the possible reasons could lie with problems detecting the differences between the two types when both are present. The 24 channel laminar multielectrode with 50 μm intercontact spacing used in this study allowed the analysis of spatial features that can be easily missed with other types of recording setups. The data presented here demonstrate that the two types of SPWs could be distinguished in LFPg recordings made with the laminar microelectrode, while the separation of the same SPWs was not possible in recordings obtained with a one channel referential recording system (see section 2.3.4 and figure 2.2D). However, Reichinnek *et al.* reported that SPWs could be sorted into distinct types of waveforms even from referential single channel recordings using an unsupervised learning algorithm [52]. Furthermore, since the publication of the study presented here [5], four different types of SPWs have been described in the monkey CA1 region *in vivo*, which differed in the presence and shape of the LFP transient [53]. Each of these SPWs further featured different relationships between the SPW and the accompanying ripple oscillation. Simultaneously performed fMRI further revealed two different brain-wide dynamics

that are differentially associated with the different SPW types. The authors further speculated that these types might be associated with different memory functions [53].

When asking why reports of different types of SPWs are so rare, it has to be considered that they might not be present in all experimental setups as only one type of SPW could be detected in mouse hippocampal slices in spite of using a linear multielectrode [25]. In this case, many experimental factors such as the use of rat or mouse slices, the age of the animals, recordings from the CA1 or CA3 region, dorsal or ventral hippocampus, horizontal, transverse or coronal slices, slice thickness, the use of an interface, classical or dual perfusion [35] submerged chamber, temperature settings and ionic composition of the bathing solution could all contribute to the existence or non-existence of each of the two types.

2.4.2 Cellular interactions during SPWs

Despite various controversies on the generation mechanisms of SPWs, it is generally agreed that a block of AMPA and KA type Glu receptor excitatory signalling blocks SPW activity [4, 6, 15, 23, 24]. Moreover, GABAergic signalling by inhibitory interneurons seems to be crucial for the generation of SPWs as well [6, 20, 22, 23, 25] and perisomatic inhibition has even been described as the major source of the LFP signal during SPWs *in vitro* [25]. Although it seems safe to conclude that an interplay of excitatory as well as inhibitory cellular activity is fundamental for the occurrence of this particular type of population activity, there has been a large amount of disagreement over the kinds of inputs different cell types receive during SPWs. Hyperpolarising [15, 25, 35], depolarising [24], both [4, 29] or mixed [23] responses of PCs during SPWs have been reported. Recent results indicate that synaptic inhibition was dominant in PCs during SPWs, while synaptic excitation was dominant in INs [25]. As a consequence, *in vitro*, only a small fraction of PCs was active during each SPW event, rarely emitting single APs [25]. Although this could be an effect of deafferentation caused by the slice preparation, it is most probably a physiologic phenomenon as the same concept has been described in one of the rare studies performed on the CA3 region *in vivo*: There, the generation of SPWs has been shown to consist of synchronous firing in a small subset of CA3 pyramidal cells accompanied by an increased firing rate of interneurons [19]. In accordance with this, in the present study only a small subset of CA3 PCs fired during both types of SPWs (see table 2.6), which is also consistent with the somatic CSD source (see figure 2.1). Most PCs were hyperpolarised, whereas most INs clustered from the LFPg increased their firing rate, typically discharging before the LFPg peak of the SPWs. However, they showed a multitude of different activation patterns during SPW activity (see figure 2.5) and table 2.8). Interestingly, some patterns were only observed during T2, but not T1 SPWs. Furthermore, IN firing seemed to vary depending on the cell's laminar location. It has been shown that there is a correlation between the function of the interneuron subtype and their anatomical organisation in the hippocampus [26], i.e. cells located in a given layer projecting to a certain other layer have the same function, which can be different from other interneurons located in and projecting to other layers. For example, dendritic targeting O-LM cells are located in str. oriens and project their axons to the str. lacunosum-moleculare, while the perisomatic inhibitory cells are mainly located in str. pyramidale and project to the same layer. Thus, IN firing varying across the hippocampal laminae suggests differences in the involvement of different IN types. It is

known that hippocampal inhibition comes in many flavours and serves different purposes, which is why a distinctive analysis of different IN types is necessary. The importance of the PV⁺ and the perisomatic IN population (which overlap but are not the same) during SPWs has repeatedly been emphasised. *In vivo*, perisomatic basket cells are highly active during SPWs [54] and are implicated in contributing to ripple oscillations accompanying the LFP transient [54–56]. *In vitro*, they are suspected of being important in the initiation of SPWs [23, 25]. Different types of INs have been shown to receive different synaptic inputs during SPWs in mouse hippocampal slices. PV⁺ basket cells were most active during SPWs, whereas axo-axonic cells and CB1⁺ basket cells were active to a lesser extent [25]. Other studies revealed that optogenetic silencing of PV⁺ INs lead to a block of SPW activity [29] and that DAMGO, which reduces the activity PV⁺ basket cells blocked all observed SPWs at a concentration of 20 μ M (n = 4) [30].

The data presented here indicate that DAMGO was able to largely decrease the recurrence frequency of SPWs and block about half of the T2 SPWs (see section 2.3.10 and figure 2.6). Moreover, DAMGO was even able to convert T1 SPWs into T2 SPWs where the latter was not present before the application of DAMGO. Apart from the difference in the applied DAMGO concentration, a possible explanation why all SPWs were blocked in other studies [30] could be that there were only T1 SPWs present in those cases. This raises again the question on the existence of the two types of SPWs in other hippocampal slice models. In any case, the results presented here further support the importance of perisomatic INs during the generation of SPWs as the T2 SPWs remaining during the application of DAMGO could be suppressed by reducing the activity of perisomatic CCK/CB1⁺ basket cells [36] using CCh. This points to a differential role of different subgroups of perisomatic inhibitory cells in the generation of T1 vs. T2 SPWs.

2.4.3 Interaction and Competition between T1 and T2 SPWs

Although only 1 out of 14 PCs recorded during simultaneous T1+T2 SPWs differentially responded to the two types of SPWs (see table 2.6), about 60 % of interneurons showed different firing patterns in relation to the two types of SPWs (see section, 2.3.9). This means that the cell populations involved in the generation of each of the SPW types highly overlap, but also suggests that cells are able to adjust their firing depending on the SPW being generated. In the study by Reichinnek *et al.* mentioned above, cell firing of clustered units also showed preferences to certain SPW waveforms. However, the authors state that the exact mechanisms linking the two are unknown [52].

Since many cells participated in both types of SPWs, there must be a certain amount of interplay between the two types of SPWs in the hippocampus. In fact, in the present study, the recurrence frequency for simultaneous types was lower than for exclusive T1 or T2 (table 2.2). This implies that in cases where both SPW types occur in the same spot, the 2 types are at least to a certain level competing with each other. However, there seem to be interactions between T1 and T2 SPWs as well, as mixed types could also be observed. The extent and manner of interaction seemed to vary from slice to slice as some slices had many mixed types whereas others had none. The latter case might be interpreted as shared refractory period for the two types of SPWs. This recalls other neuronal rhythms in the hippocampus which are mutually exclusive and/or compatible with each other. For example, ripples can only be generated when no theta waves are

present. On the other hand, gamma waves, which are largely generated by the same microcircuit as ripples (via the PING and FINO mechanisms, respectively [29, 35]) can and often do occur at the same time as theta waves [57]. Together with the results gained from pharmacological manipulations discussed above, this indicates that the generation of the two types of SPWs recruits overlapping populations of neurons, but also differentially involves various types of interneurons. Moreover, individual cells seem to be able to discriminate between the two types of SPWs and adjust their firing patterns appropriately.

2.4.4 Differences between CA3 subregions

It has been shown that SPWs are locally generated in the CA3 region and that they are able to spread to other hippocampal subregions *in vivo* [19, 43] and *in vitro* [3, 4, 6, 7, 15, 16, 20–24, 44]. The data presented here confirm that SPWs can be generated locally in the isolated CA3 region. Moreover, the proportion of slices generating SPWs is very similar between the CA3 in isolated mini slices and that in "whole" slices with presumably preserved intrahippocampal connections (section 2.3.1). This suggests that the lack of neighbouring hippocampal regions does not influence the occurrence of SPWs. SPWs have also been shown to travel between subregions within the CA3 region [29, 30]. According to the literature, this process relies on the recurrent connections between PCs of the CA3 region. Connections between PV⁺ cells are not required for synchronising SPWs across CA3 subregions, but play a role in coupling the associated ripple oscillations [29]. In this study, in the majority of cases T1 and T2 SPWs were found to be local events, but the occurrence of both types was found to be sometimes correlated between neighbouring CA3 subregions.

The microcircuit within the subregions has been shown to differ marginally. Compared to the CA3b subregion, the CA3a subregion has been shown to be more intrinsically excitable, it has a higher synaptic connectivity, its PCs receive more excitatory connections and they have more complex dendritic trees [58]. These variations in connectivity might be connected to the differences in SPW generation ability observed in the present study. However, it is surprising that the CA3a subregion generated SPWs significantly less often than the CA3b or CA3c subregions (section 2.3.5 and table 2.3). Differences in the used models of the two studies (transverse slices of the middle third of guinea pig hippocampus [58] vs. horizontal slices of ventral rat hippocampus in this study) could also be the reason for these apparent inconsistencies. However, if the differences between the CA3a and CA3b subregions described in the guinea pig are applicable to the tissue used in the present study, this seems to suggest that higher synaptic connectivity and higher excitability do not necessarily result in a higher tendency to generate SPWs. Thus, it can be speculated that SPW generation relies on a certain microcircuit architecture rather than merely high excitability and/or connectivity. Additionally, the CA3a subregion tended more towards generating T2 rather than T1 SPWs, while this trend was not as pronounced in the CA3b or CA3c subregions. Thus, the generation of T1 and T2 SPWs might be favoured by slightly different underlying microcircuits.

3. Synchronous population activity in the human neocortex

Part of the presented results describing SPAs and IIDs are included in a submitted manuscript with the title "Hyperexcitability of the network contributes to synchronisation processes in the human epileptic neocortex". Data describing clustered cell activity will be part of a further publication which has not been submitted yet.

3.1 Introduction

Epilepsies are characterised by the presence of interictal spikes detected on scalp electroencephalographic (EEG) recordings. They represent one of the most important diagnostic signs of focal cortical epilepsies. Interictal discharges in both human and experimental focal epilepsies were characterised by high amplitude, fast EEG spikes, followed by a slow wave [59]. Interictal spikes were either generated locally in the neocortex of epileptic patients, or were found to propagate from distant sites. Local interictal spikes emerged in infragranular layers, while propagated spikes appeared in the granular layer, both with a large initial current sink and with a considerable increase in cellular firing [32]. About half of the intracortically recorded single neurons were modulated in their firing rate during or around interictal discharges in patients with focal epilepsies, with a very heterogeneous firing pattern, suggesting that interictal discharges reflect a complex and dynamic network phenomenon, emerging from a heterogeneous neuronal population [60]. Spontaneous synchronous discharges are known to be generated by slices prepared from the neocortex [12, 14, 61] or the hippocampal formation [8–11] of epileptic patients, in a physiological perfusion solution. When filtered as the EEG (1-100 Hz), *in vitro* events are composed of a high-amplitude fast transient followed by a longer lasting wave [8], while a wide band filtering (1-3000 Hz) shows the increase of cellular activity and fast oscillations during interictal-like events *in vitro* [11, 62], similar to *in vivo* interictal discharges [32, 34]. Synchronous population events in neocortical specimens of epileptic patients were detected in all layers, but most frequently emerged in the supragranular layers, associated with a current sink [63]. Although the population bursts were called sharp wave [12], or were termed interictal-like activity [8, 10, 14, 64], all groups agreed that they might be epilepsy related phenomena. The question of control tissue is always problematic in case of human studies. Anatomical studies usually include human autopsy tissue [65–67], or healthy monkey tissue [11, 68] as a control, while electrophysiological studies typically operate with rodent tissue [69], sometimes together with one of its corresponding epilepsy models [70].

Furthermore, sclerotic hippocampus is usually compared to non-sclerotic hippocampus derived from epileptic patients [71–74], and human neocortex with focal cortical dysplasia is compared to adjacent non-dysplastic neocortex [75, 76]. The present study investigates cell activity and neuronal population activity using the best available control for the human epileptic neocortex: neocortical tissue of patients without any clinical signs of epilepsy, which are operated for other reasons such as brain tumours. In the presented work it is shown that spontaneously occurring synchronous population activity (SPA) arises not only in slices from epileptic but also from tumour patients without epilepsy. Our data demonstrate that SPAs emerging in slices derived from epileptic and non-epileptic patients are basically similar in their network and cellular characteristics, but they considerably differ from interictal spikes of epileptic patients, and therefore cannot be regarded as their *in vitro* correlate.

3.2 Methods

3.2.1 Patients

All patients gave written consent and the protocol was approved by the Hungarian Ministry of Health. The study was approved by the Regional and Institutional Committee of Science and Research Ethics of the Scientific Council of Health (ETT TUKEB 20680-4/2012/EKU) and performed in accordance with the Declaration of Helsinki. It is known that some forms of brain tumours such as gliomas can be epileptogenic [77]. In order to keep the non-epileptic group clean from any signs of epileptic activity, tumour patients which had had at least one seizure were treated as epileptic. The patients were grouped according to epilepsy severity: Patients in the NoEpi group, as mentioned, had never had a single seizure as far as could be determined. Moreover, preoperative clinical EEG was performed to additionally assess the patients' epilepsy status. Patients in the ContrEpi group exhibited epilepsy which could be successfully controlled with antiepileptic medication (pharmacoresponsive epilepsy). The third group of patients, ResEpi, displayed pharmacoresistant epilepsy, which could not be successfully treated with pharmacological means. In case of tumour patients, the surgeons provided information on whether the tissue sample was close or distant (minimum > 3 cm, usually > 5 cm) compared to the tumour. Not all patients' tissue samples produced neuronal population activity *in vitro*. Neocortical synchronous activity (NSA) and in many cases single unit activity were detected and analysed in only a subset of the available recordings, as NSA detection and cell clustering are very time-consuming. In total, 49 recordings from 14 ResEpi patients, 12 recordings from 5 ContrEpi patients and 33 recordings from 7 NoEpi patients were processed for the purposes of this study (table 3.1 displays an overview over the case numbers of patients, slices and recordings; table 3.2 provides information about the patients).

	No. of patients	No. of slices	No. of recordings
NoEpi	7 (7)	23 (21)	33 (29)
ContrEpi	5 (3)	12 (7)	12 (7)
ResEpi	14 (13)	41 (37)	49 (45)
total	26 (23)	76 (65)	94 (81)

Table 3.1: Case numbers for patients, slices and recordings Numbers of patients, slices and recordings in which NSAs were detected. Numbers in parentheses describe only those cases in which cellular activity was clustered also.

3.2.2 Tissue preparation

Tissue samples obtained during brain surgery were transported to the laboratory (located in the same building) in cold oxygenated sucrose solution as described in section 2.2.1. After removing the pia mater and large blood vessels, neocortical slices of 500 μm thickness were prepared using a vibratome. They were transferred and maintained at 35–37 °C in an interface chamber perfused with a physiological solution (hACSF: 124 mM NaCl, 26 mM NaHCO₃, 3.5 mM KCl, 1 mM MgCl₂, 1 mM CaCl₂ and 10 mM glucose, equilibrated with 5 % CO₂-95 % O₂, note the slight difference to rACSF described in section 2.2.1) at 34–35 °C and left to recover for at least one hour before recording.

3.2.3 Electrophysiological recordings

LFPg recordings were performed while the slices were kept in the interface chamber similarly as described in section 2.2.2, with the exception that the inter-contact spacing of the laminar multielectrode was 150 μm (instead of the 50 μm spacing used for rat hippocampal slices). The increased inter contact spacing was necessary to be able to cover the entire extent of the neocortical grey matter from the pia to the beginning of the white matter when the multielectrode was placed perpendicularly to the pial surface and the neocortical layers. The slices were scanned from one end to the other, moving the electrode in increments of around 300–400 μm .

3.2.4 Data analysis

Population activities

The initial steps of the data analysis of electrophysiological recordings from human neocortical slices were analogous to those for rat hippocampal slices described in section 2.2.4. Synchronous population activity (SPA) and interictal discharge (IID) in human neocortical slices was detected using the methods corresponding to the detection of SPWs in the rat hippocampus. As for the rat hippocampal SPWs, the quality of the detection was visually assessed and the threshold adjusted if necessary. Averaged waveforms, the CSD and the MUA were calculated using the same techniques as described in section 2.2.4. Waveform analysis was performed on the averaged LFPg and MUA with a home written C++ routine. The largest positive or negative LFPg peak relative

Patient ID	Gender & Age	Cortical lobe	Epilepsy severity	Diagnosis	Time since first seizure	Distance to tumour	Morphology
T04◇	F 69	te	NoEpi	glioblastoma multiforme		distant	normal
T06◇	M 31	fr	NoEpi	cavernoma, haematoma intracerebralis acuta		distant	normal
T07◇	F 58	te	NoEpi	glioblastoma multiforme, meningitis		close	infiltrated
T08◇	F 78	te	NoEpi	glioblastoma multiforme, astrocytoma grade IV		distant	normal
T11◇	F 57	oc	NoEpi	glioblastoma multiforme grade IV		distant	normal
T17◇	F 74	pa	NoEpi	glioblastoma multiforme grade IV		distant	normal
T18◇	M 68	pa	NoEpi	melanoma malignum metastaticum		distant	normal
T03◇	F 18	fr	ContrEpi	anaplastic ependymoma grade III	1 mo	distant	normal
T05◇*	F 35	oc	ContrEpi	oligodendroglioma grade III	1 mo (1 seizure)	close	infiltrated
T09◇	F 48	oc	ContrEpi	lung small cell carcinoma metastaticum	2 wks (1 status epilepticus)	close	infiltrated
T10◇	M 44	te	ContrEpi	glioblastoma multiforme, astrocytoma grade IV	3 wks	distant	normal
T13◇	M 53	fr	ContrEpi	radionecrosis (6 years earlier: anaplastic oligoastrocytoma grade III)	6 yrs (1 seizure)	distant	N/A
E01◇*	F 22	pa	ResEpi	encephalitis	1 mo		normal / cell loss
E02◇	F 21	fr	ResEpi	focal cortical dysplasia with glioneural heterotopia	2 yrs		dysgenetic

Patient ID	Gender & Age	Cortical lobe	Epilepsy severity	Diagnosis	Time since first seizure	Distance to tumour	Morphology
E04◇	M 24	te	ResEpi	ganglioglioma grade I	4 yrs	distant	normal
E05◇	F 18	te	ResEpi	focal cortical dysplasia II B	5 yrs		dysgenetic
E06◇	M 51	te	ResEpi	hippocampal sclerosis	50 yrs		normal
E08◇	F 33	oc	ResEpi	focalis corticalis dysplasia II B	31 yrs		normal + dysgenetic
E10◇	M 21	te	ResEpi	hippocampal sclerosis	21 yrs		normal
E12◇	M 40	te	ResEpi	hippocampal sclerosis	35 yrs		normal
E13◇*	F 53	te	ResEpi	hippocampal sclerosis	40 yrs		normal
E15◇	M 35	te	ResEpi	focal cortical dysplasia + hippocampal sclerosis	34 yrs		normal
E16◇*	M 26	te	ResEpi	subependymal gliosis (dysgenesis) + hippocampal sclerosis	24 yrs		normal
E17◇	F 38	fr	ResEpi	focal cortical dysplasia + hippocampal sclerosis	31 yrs		normal
E21*	M 56	te	ResEpi	haemangioma cavernosum	26 yrs		N/A
O42◇	M 72	fr	ResEpi	glioblastoma multiforme	9 mos (1 seizure)	distant	normal

Table 3.2: Patients Demographics and diagnosis for NoEpi, ContrEpi and ResEpi patients from which neocortical population activity (SPA◇ and/or IID*) and/or single unit activity was detected and analysed. Abbreviations: F, female; M, male; fr, frontal; pa, parietal; te, temporal; oc, occipital; wks, weeks; mos, months; yrs, years.

to the baseline was determined from the averaged LFPg using a moving average. Its amplitude as well as its width and asymmetry at half the maximal LFPg amplitude were determined (see appendix section 6.1.1 for details on the algorithm). SPAs were differentiated from IIDs manually, taking into account the amplitude of the LFPg/CSD peak, the MUA amplitude and the recurrence frequency.

Table 3.3 summarises the numbers of SPAs and IIDs detected and analysed in this study. As described in the table, there was only one IID detected in the ContrEpi group. It was not considered appropriate to group the ContrEpi IID together with those of the ResEpi group, especially as it would have formed an outlier within that group in terms of neocortical location, LFPg amplitude as well as patient diagnosis group (see figure 3.3E, purple asterisk). On the other hand, it would not lead to significant or interpretable results if it were used as its own group with $n=1$. Thus, the IID in the ContrEpi group (patient T05) was not included in any data analysis (except when describing the number of incidence: table 3.3, figure 3.3E, table 3.5 and figure 3.6).

	SPA	IID	total
NoEpi	48 (100.0%)	0 (0.0%)	48
ContrEpi	13 (92.9%)	1 (7.1%)	14
ResEpi	57 (87.7%)	8 (12.3%)	65
total	118 (92.9%)	9 (7.1%)	127

Table 3.3: Detected NSAs Numbers (and row percentages) of NSAs detected from extracellular recordings by type of NSA (SPA or IID) and tissue of origin. The proportion of different NSAs is not equal across the three patient groups ($p<0.05$, Fisher's exact test). Post-hoc testing revealed that the number of IIDs in the NoEpi group tends to be lower than expected by chance ($0.05<p<0.1$).

The location of the SPA or IID within the neocortical layers was determined by hand. As the microelectrode covered all layers of the neocortex in almost all cases, the channel number indicated the position within the neocortical layers. Usually channels 1–8 were in the supragranular, channels 9–13 in the granular and channels 14–23 in the infragranular layers. Channel positions were established according to the thickness of the neocortex of the given patient, and corrected if necessary. The location of the SPAs/IIDs was determined on the raw recordings by verifying the extent of the field potential transient, high frequency oscillation and increase in MUA all over the different electrode channels. This resulted in the categorisation of SPAs into SPAs covering the supra, sup+gran, gran, gran+inf, infra or the entire extent of the neocortical grey matter. For the regression analysis, this information was reorganised into three larger groups separating NSAs mainly located in the supra and granular layers from those mainly located in the infra layer and those covering the entire radial extent of the neocortex. In total, 118 SPAs and 9 IIDs were identified across all patients and slices. However, of the nine IIDs, eight were in the ResEpi and only one in the ContrEpi group (see table 3.3). As it was not deemed meaningful to interpret results from a group where $n = 1$, nor appropriate to pool the IIDs (and SPAs) from the ResEpi and the ContrEpi group, only the IIDs from the ResEpi group were analysed and compared to the SPA from the ResEpi group. The IID detected in the ContrEpi group was thus not analysed.

Clustered neuronal activity

Single unit activity was clustered using a home-written Matlab routine or the program Klusters [41], see section 2.2.4 for details. The location of the single units – supragranular (supra), granular (gran) or infragranular (infra) – was determined from the channel number on which the averaged action potential (AP) showed its largest amplitude and the position of the multielectrode on the slice. However, in case of the human neocortex, the location of a given cell does not assist in determining its cell type (principal cell or interneuron) as it does in rat hippocampus (compare to section 2.2.4). Instead, a program for unbiased cell type categorisation was written in Matlab. The user of this program is shown the unfiltered and 300 – 3000 Hz filtered averaged AP waveform as well as the autocorrelogram of the cell's spike train. The AP width at 50 % and 10 % height as well as the delay of the afterhyperpolarisation are measured and annotated to assist the user, as the width of principal cell (PC) APs is significantly larger on average than that of INs [78–80]. Due to the considerably different conditions *in vitro*, the firing frequency of a cell does not supply information useful for cell type characterisation, as is the case in *in vivo* conditions [1, 79]. The autocorrelogram helps judging the discharge dynamics of the cell, which is characteristic for different cell types: a high peak at 3 – 5 ms followed by a fast exponential decay is characteristic for bursting PCs, a slowly rising phase without initial peak marks regular firing PCs, while an exponentially rising phase around 10 ms followed by a very slow decay is typical for INs [79, 80]. 860 clustered cells were categorised with the aid of this Matlab program, with the following criteria: first the AP width at 50 % amplitude was examined on the unfiltered average. Cells with an AP width <0.2 ms were considered to be INs, while neurons with AP width >0.4 ms were taken to be PCs. In case of an AP width between 0.2 and 0.4 ms the autocorrelogram and AHP were also considered. Cells with an $0.2 \text{ ms} < \text{AP width} < 0.25 \text{ ms}$ and with an autocorrelogram typical for INs and/or fast AHP were judged to be INs, while cells with $0.35 \text{ ms} < \text{AP width} < 0.4 \text{ ms}$ and with an autocorrelogram typical either to bursting or to regular firing PC and/or slow AHP were taken as PCs (ref to figure). Cells that could not be categorised as either PC or IN were classified as unclear cells (UCs) and included in the analysis as a third group beside PCs and INs. Table 3.7 (in the results section) summarises the clustered cells used in this study.

Multiple features were measured from the averaged AP: the amplitude (μV), the width and right/left asymmetry at 50 % amplitude, the amplitude of the afterhyperpolarisation (in % to the amplitude of the main spike) and the peak-to-peak (p2p) delay (from the peak of the main spike to the peak of the AHP). For details on the algorithm see the appendix section 6.1.2. The spike trains of clustered units were investigated using custom written algorithms in C++ and Matlab. Interspike intervals were calculated as the time delays between pairs of consecutive events, i.e. the first time derivative of the cell spike times. For each neuron, multiple features describing firing properties were calculated:

- The mean recurrence frequency (firing frequency) in Hz
- The median interspike interval (ISI) further characterises a cell's firing behaviour. However, as ISIs generally do not follow a normal distribution (see figure 3.7), neither the mean recurrence frequency nor the median ISI are enough to fully describe a neuron's firing pattern.

- The ISI QCD (quartile coefficient of dispersion) is a dimensionless measure for variability. It quantifies the distance of the first and third quartiles of the ISI distribution (called Q_1 and Q_3). The QCD is defined as $(Q_3 - Q_1)/(Q_3 + Q_1)$. As it uses non-parametric quantifications (the quartiles), it is a robust measure, but, as it only uses two values for its calculation, unfortunately not a very sensitive one.
- The ISI varcoeff (variation coefficient) is another dimensionless measure for variability. However, other than the QCD, the varcoeff relies on parametric measures such as the standard deviation and the mean. Thus, it is more sensitive to outliers and skewed distributions, which makes it mostly suited for symmetric distributions. However, it is a widely used measure to quantify the variability of neuronal firing in the literature [81].
- Burstiness, a measure for the amount of cell bursting, was expressed as the percentage of APs within bursts. A burst was defined as a group of spikes during which each spike occurred within 10 ms of the last spike [82].
- The firing stability was calculated as the proportion of the recording during which the cell fired continuously (cut-off for continuous firing: $5 \times$ the median ISI).

With the exception of burstiness, these features were also calculated for the spike trains of NSAs.

Interaction of cellular and population activity

For SPAs, but due to low spike counts not for IIDs, PETHs describing cell firing were generated for the time period of ± 300 ms around the peak of the SPA (bin size: 5 ms). Each PETH was standardised using the geometric mean of the total number of cell spikes and the SPA events for colour coded visualisations. An example of a colour coded PETH and its respective bar diagram is shown in figure 3.1 under the PETH labelled "original".

Moreover, for each combination of one SPA and one cell it was assessed how significantly the cell changes its firing during the SPA. One of the most straightforward approaches to quantify the firing change would be to calculate the firing frequency for the time period ± 50 ms around the SPA, standardised by the baseline firing. However, this calculation is very sensitive to the recurrence frequency of the involved cell and/or SPA: If one or both of the latter are very low, even cells that did not change their firing during the SPA often didn't display action potentials during the SPA by chance alone. To avoid wrongly identifying these cells as exhibiting decreased firing during the SPA, a randomisation step was added to the calculation. Figure 3.1 shows how shuffled spike trains were generated from randomly permuted interspike intervals, preserving many of the cells' (and population activities') recurrence properties such as e.g. the median ISI and the average recurrence frequency. Subsequently, the number of APs during the SPA (± 50 ms) was counted for each shuffled spike train. In this way 10,000 randomised values were generated for each value derived from the original spike trains. Each original value was then compared to that of their own shuffled spike trains. The cell-SPA relationship was then quantified by assessing where the original value fell into the randomised ones, calculating the quantile within the randomised values that was equal to the original value (see "quantile of original within shuffled values" in figure 3.1).

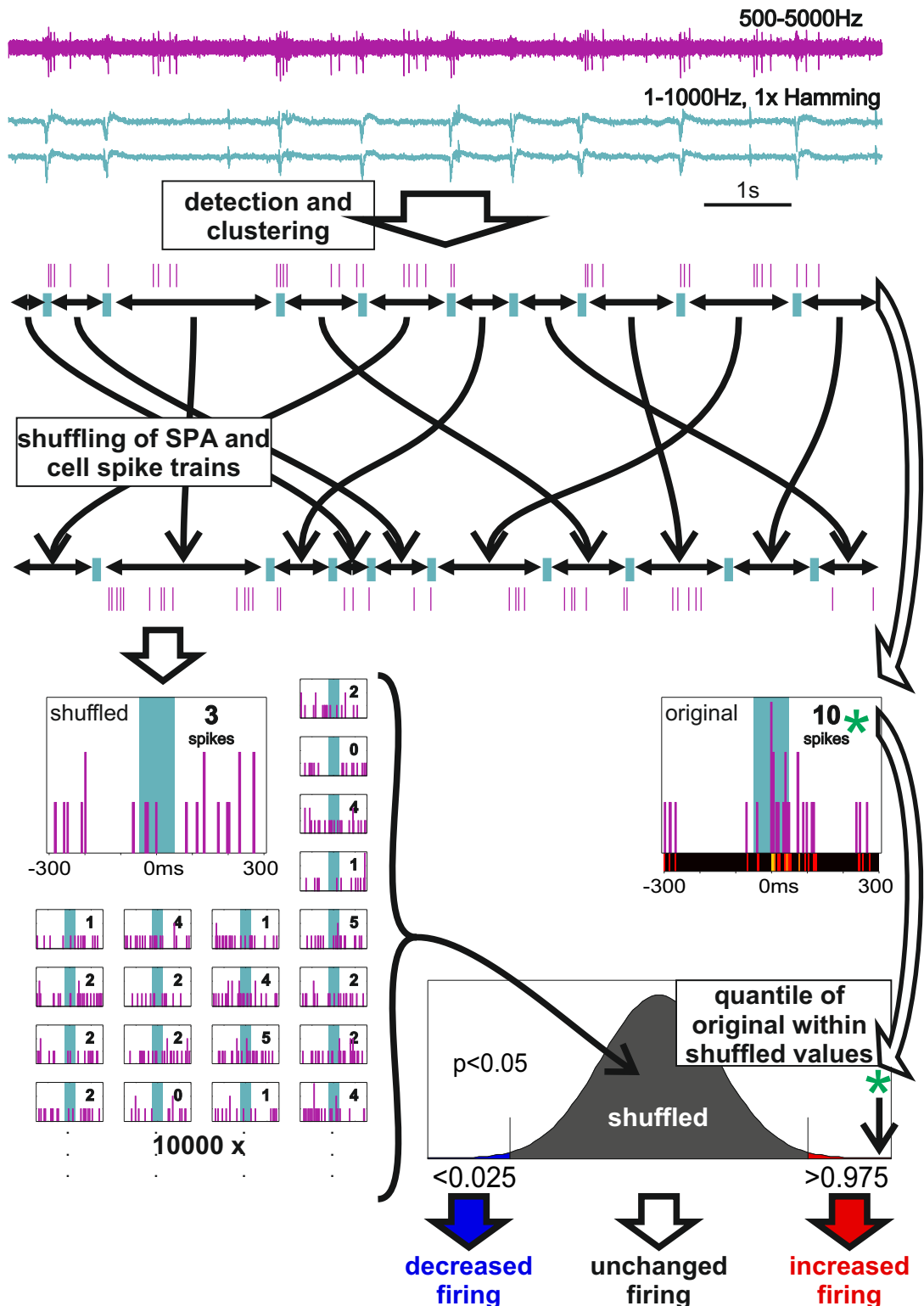


Figure 3.1: Calculation of firing change quantiles The original cell (purple) and SPA (grey-blue) spike trains were detected from the LFPg ("detection and clustering"). Both were shuffled by random permutation of their interspike intervals ("shuffling of SPA and cell spike trains"). For the original as well as the shuffled spike trains, the numbers of cell spikes during the SPAs ± 50 ms were counted. This is visualised by PETHs: purple bars which overlap the grey-blue background reflect spikes which happened during the SPA. In case of the original spike train, a colour coded PETH is included for comparison. The collected randomised spike trains provide a distribution of shuffled values, which the original value (green asterisk) is compared to. The resulting quantile determines the categorisation of the cell as decreasing, not changing or increasing its firing during the respective SPA.

Thus, a value of zero or one reflects that the actual number of cell spikes during the SPA is lower or higher than any of the randomised values, respectively. A value of 0.55 means that the original value is larger than 55 % of the shuffled values, which does not reflect a substantial change in firing during the SPA. As the shuffled spike trains have the same number of events as the original spike train, the quantile calculated from the number of spikes during the SPA is the same to the one that could have been calculated from the firing changes. As the firing change quantile reflects how likely it is to attain the original firing change value (or a more extreme value) due to chance alone, there are similarities to p-values. The difference is that quantiles close to zero *and* close to one reflect extreme results, whereas only small but not large p-values reflect significant results. Thus, firing change quantiles up to 0.025 and above 0.975 were considered significant firing decreases or increases at a 5 % significance level, respectively. As this statistic assesses how significantly a cell changed its firing during the ± 50 ms around the SPA, it is less sensitive to problems associated with low recurrence frequencies than the firing change calculated without the randomisation step. Due to the comparison of the actual value to values generated from shuffled spike trains, very low recurrence frequencies result in cells being identified as not significantly changing their firing rate, rather than wrongly identifying them as decreasing their firing rate. As this analysis is performed for each single combination of cells and SPAs (provided they stem from the same recording), a cell can display different behaviour during different SPAs. In addition to the quantile calculated for the time period of ± 50 ms to determine whether a cell in- or decreases its firing, quantiles were also calculated for each of the 5 ms time bins in the ± 300 ms histogram for visualisation (resulting graph in figure 3.9).

In addition to the firing change quantile, two more features were calculated for all cell-SPA pairs describing how and whether a cell was linked to an SPA:

- The reliability of a cell is defined as the proportion of SPA time windows during which the cell fired at least one action potential. The reliability is related to the conditional probability $P(\text{cell event during } \pm 50\text{ms around SPA})/P(\pm 50\text{ms around SPA})$.
- The dependency of a cell on the SPA is defined as the proportion of action potentials which fell within the ± 50 ms time window around the SPA. The dependency is related to the conditional probability $P(\text{cell event during } \pm 50\text{ms around SPA})/P(\text{cell event})$.

Furthermore, additional features were calculated further characterising the behaviour of cells that showed increased firing during the SPA:

- The firing change (or firing change intensity) is calculated from a cell's firing frequency within (A) and outside of (B) the ± 50 ms SPA time window in the form $A/(A + B)$. Thus, a value of zero reflects the complete stop of firing during the SPA, a value of one signifies that a cell only fired during the ± 50 ms around the SPA peak, while a value of 0.5 indicates the same mean firing rate inside and outside of the SPA ± 50 ms time window. In other words, a firing change intensity of 0.5 reflects that SPAs and cell events occurred independently from one another, as defined by their probabilistic independence $P(\text{cell event during } \pm 50\text{ms around SPA}) = P(\text{cell event}) \times P(\pm 50\text{ms around SPA})$.
- The fano factor describes how consistent or variable the cell response is among SPA events. It is defined as the variance divided by the mean of the number of spikes during the different

SPA events. This means that a lower fano factor indicates a more consistent response to the SPAs, but not necessarily a higher one. Cells that steadily respond with no spikes or steadily respond with ten spikes are very consistent, which will be reflected in a low fano factor. On the other hand, a cell that fires no action potential during one SPA event, ten in another and three in another displays a high variability in responses to the SPA, which will be reflected in a higher fano factor.

- The time of maximal firing (max firing) was determined from the PETH describing cellular firing during the SPA. It was defined as the time bin (in ms) of the PETH displaying the highest firing frequency (the mode of the PETH). To increase reproducibility, an initial smoothing step was performed on the PETH (weighted moving average using the kernel [0.25, 0.5, 0.25]). If there was no unique mode in the PETH after the initial smoothing steps, additional smoothing was performed.
- Relative maximal firing (rel max firing) was determined to better investigate the timing of a cell's firing in relation to the LFPg wave of an SPA. The procedure was equivalent to the one described for max firing above, however, using time bins that were stretched or squeezed depending on the duration of the respective SPA ("relative time", figure 3.2). In short, 100 relative bins were defined depending on the duration (width) of the SPA. Those time bins (50 on each side of the peak) were not uniform in length, but reflected during which phase of the SPA a cell fired maximally (such as the ascending, peak or descending phase).

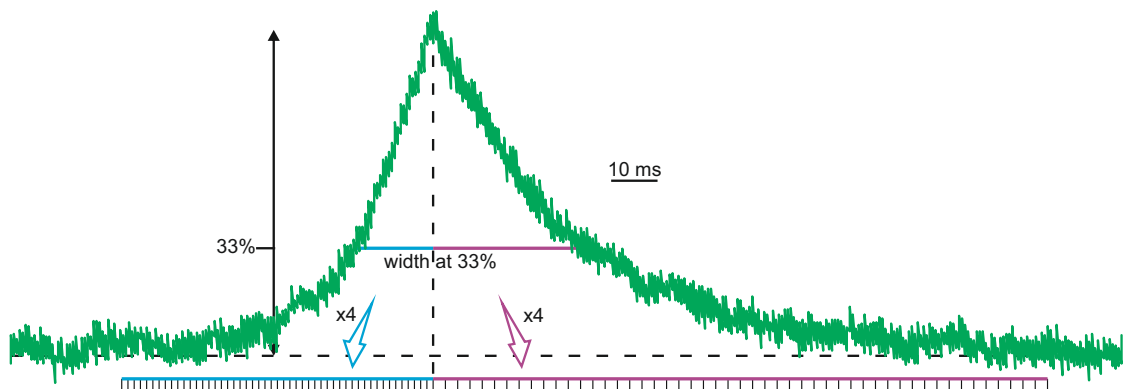


Figure 3.2: Time bins relative to the SPA shape For describing the timing of a cell in relation to the SPA, the width of the LFPg waveform of the SPA was measured at 33 % of its height, as described in the appendix section 6.1.1. The time periods four times the width on the left as well as on the right side of the SPA peak were each divided into 50 bins, resulting in 100 bins in total. Note that SPAs were not left-right symmetric, and thus the size of the bins before the peak were not equal to those after the peak. Five phases were defined via the bins: before (25 bins), ascending (22 bins), peak (6 bins centred around the peak), descending (22 bins) and after (25 bins).

Cell responses during multiple SPAs

In slices with two or three simultaneous SPAs and clustered cells, responses of the same cell during different SPAs were compared. For this purpose, responding (increased or decreased) and not-responding (unchanged) cell firing was distinguished. Subsequently, for each cell it was assessed whether it responded to all SPAs present ("all"), to none of the SPAs present ("none") or showed differential responses to the simultaneous SPAs by responding to some but not all SPAs ("differential"). The resulting percentages of all, none or differential responses were analysed in two different ways: In the first case, a Chi-squared test was applied to check for differences between the patient groups (NoEpi and ResEpi, multiple SPAs were observed in one recording from ContrEpi tissue but no cells could be clustered from that recording; resulting significances are visualised in appendix table 6.10). In the second analysis, each patient group was evaluated separately. The number of none, differential and all responses (to multiple SPAs) expected by chance was calculated from the numbers of increased, unchanged and decreased responses (to each SPA) observed in the recordings with multiple SPAs of that patient group. Then, the observed numbers of none, differential and all were compared to the expected numbers via a one-way goodness-of-fit test (resulting significances are visualised in appendix table 6.11).

Other statistical tests used

The non-parametric Mann-Whitney U-test (also called Wilcoxon rank sum test), the Kruskal–Wallis test and/or the Wilcoxon signed rank test as well as the Chi-square test and/or Fisher's exact test were used as described in section 2.2.4.

As each measured and/or calculated property of NSAs, cells or cell-SPA interactions is potentially influenced by (and correlated with) multiple known (independent) variables such as age, patient group, gender, neocortical lobe of origin, etc., multiple regression analysis was performed. For an explanation what multiple regression does and what the resulting parameters stand for, see appendix section 6.2. In short, R^2 and the adjusted R^2 , beta-coefficients and heteroskedasticity-robust p-values (White heteroskedasticity-robust t-statistic [83–86]) were calculated, as almost all regressions comprised heteroskedastic residuals (Breusch-Pagan heteroskedasticity test, modified by Koenker [87, 88]). As no heteroskedasticity-robust statistics are available for binomial regressions (logit / probit model), linear regression was applied also to limited dependent variables. Before each regression, dependent as well as independent variables were transformed using the natural logarithm (ln) or cube roots as required to achieve asymptotically normally distributed residuals. Regressions for which assumptions such as asymptotically normally distributed residuals could not be fulfilled (despite multiple attempts using variable transformations) are not interpretable and are thus not presented. Categorical independent variables (patient group, cell location, etc.), were encoded as dummy variables. To obtain a single p-value for the beta-coefficient of each categorical variable, non-heteroskedasticity-robust and heteroskedasticity-robust LM statistics were calculated as described in [86, Chapters 5-2a and 8-2a]. Note that ideally, another categorical independent variable would have been included to differentiate each patient from the others (resulting in *number of patients* – 1 additional dummy variables). However, due to the high number of patients this overparameterised the model, lead to problems with overfitting and was thus not included. As the generation mechanism of SPAs and IIDs could potentially be very

different, so might the associations of some of their properties and various independent variables. Thus, if they would be analysed using regression, interaction terms for all independent variables and a variable differentiating SPAs from IIDs would be necessary, which is analogous to running two separate regressions for the two types of NSAs. However, due to the low case number of IIDs, one would face issues with overfitting the available data. Thus, regression analysis was only applied to SPAs and not to IIDs.

3.3 Results

3.3.1 SPA and IID in the human neocortical slice

Synchronous population activity (SPA) was spontaneously generated in neocortical slices from epileptic and non-epileptic patients in a physiological solution. They resembled SPWs observed in rat hippocampal slices, consisting of a LFPg transient often superimposed by MUA increases as well as high frequency LFPg oscillations (ripples at 130-250 Hz and fast ripples at 300-800 Hz). Figure 3.3A,B,C shows examples of SPAs observed in the NoEpi, ContrEpi and ResEpi group, respectively. The LFPg trace, CSD and MUA of a typical SPA example from each patient group can be seen in figure 3.3A-C. In some slices, a considerably larger type of activity emerged, which occurred at a lower recurrence frequency. It resembled epileptiform activity induced by 4-aminopyridine [89] and was thus called interictal activity (IID). This type of activity was only observed in epileptic patients and was distinguishable from SPAs by CSD & MUA amplitude and recurrence frequency (figure 3.3E). For the numbers of detected NSAs (neocortical synchronous activity, the umbrella term for SPAs and IIDs), see table 3.3 in the methods section. The different patient groups did not generate SPAs and IIDs at the same proportions ($p < 0.05$, Fisher's exact test). Post-hoc testing revealed that the NoEpi group tends to generate fewer IIDs than expected by chance ($0.05 < p < 0.1$). The LFPg trace, CSD and MUA of a typical IID example from the ResEpi group is shown in figure 3.3D.

Table 3.4 displays quantifications of recurrence properties and features of the averaged traces of SPAs and IIDs for the different patient groups. The mean recurrence frequency, the ISI median, the LFPg as well as the MUA amplitudes are visualised in figure 3.3F. Interestingly, SPAs occurring in the three patient groups appeared to be very similar in many aspects. The only features exhibiting significant differences between the patient groups were the LFPg and the CSD amplitude (note that the CSD is calculated from the LFPg). In both cases, SPAs in the ResEpi group displayed larger amplitudes than those in the NoEpi group (LFPg: $p < 0.01$, CSD: $p < 0.05$, both: Kruskal Wallis, also see figure 3.3F and the quantifications in table 3.4).

However, while SPAs appeared largely similar between patient groups, considerable differences were found between IIDs and SPAs in the ResEpi group. The two types of neocortical population activity differed in almost every aspect investigated. Compared to SPAs, IIDs had a lower recurrence frequency ($p < 1E-04$), a longer ISI median ($p < 1E-04$), a higher ISI variability (ISI QCD: $p < 0.05$, ISI varcoeff: $p < 0.01$), and a lower stability throughout the recording ($p < 0.01$, all Mann-Whitney), reflecting that IID events often disappeared for relatively long stretches of time before reoccurring. Moreover, IIDs comprised larger LFPg ($p < 1E-04$), CSD ($p < 1E-05$) as

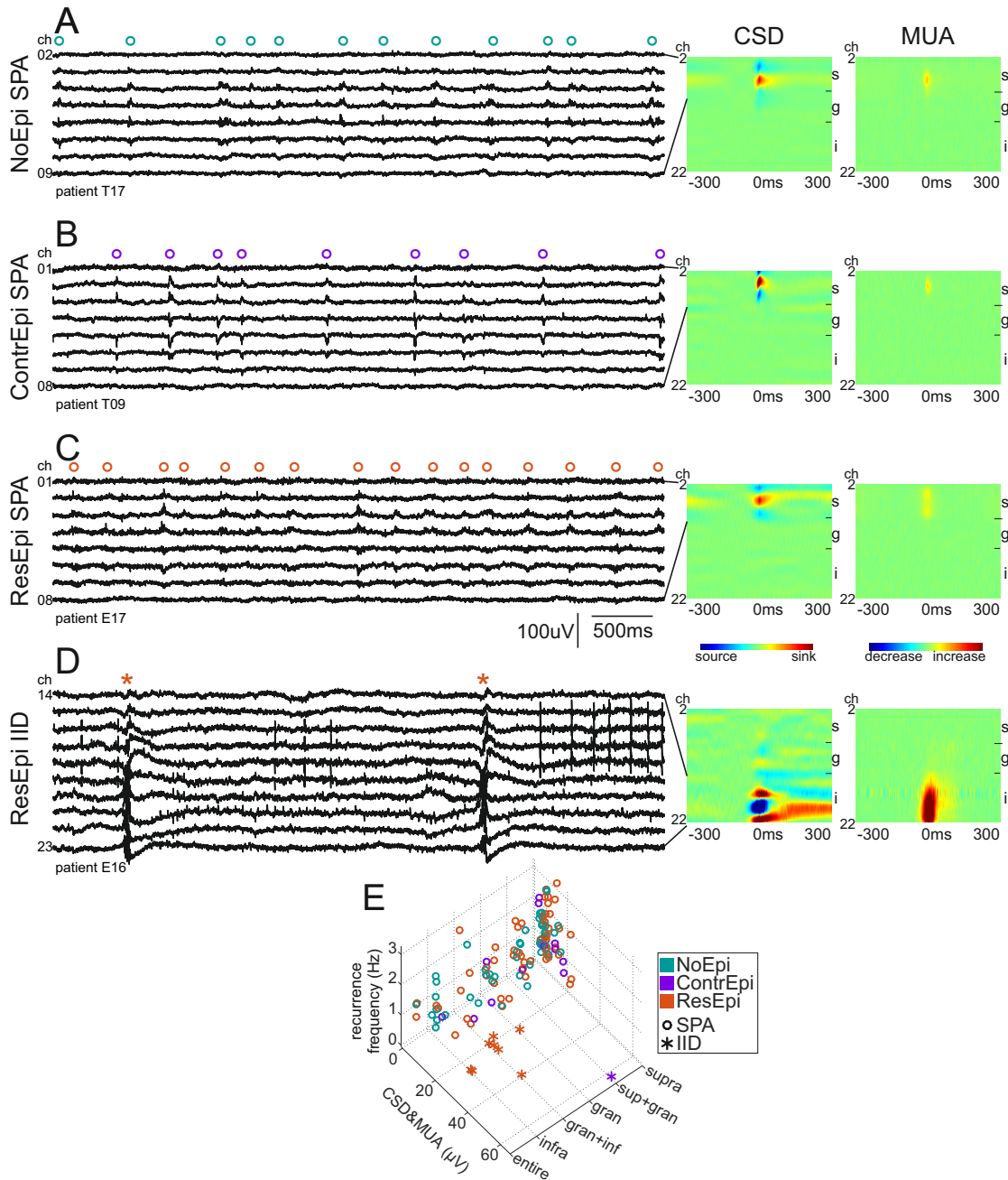


Figure 3.3: SPA and IID in neocortical tissue (A-D) Example LFPg traces (5 s), as well as CSD and MUA plots of averaged SPAs (A-C) or an IID (D) in NoEpi (A), ContrEpi (B) and ResEpi (C,D) tissue. LFPg traces, CSD plots and MUA plots are, respectively, each on the same scale from A-D. On the LFPg traces, open circles and asterisks indicate the detected SPA and IID, respectively. Note the similarities in appearance of the SPAs between different patient groups, as well as the difference between SPAs and IIDs. (E) 3D scatter plot illustrating the distinction of SPAs (open circles) and IIDs (asterisks). Different patient groups are indicated by colour (NoEpi: turquoise, ContrEpi: purple, ResEpi: orange). Note how IIDs form a cluster of larger LFPg and/or MUA amplitudes and are mostly located in the deep neocortical layers (gran+inf and infra), with the exception of the IID in the ContrEpi group, which was excluded from the data analysis (also see table 3.5 and figure 3.6). In contrast, SPAs can occur in all layers, but appear preferentially in the supragranular layers.

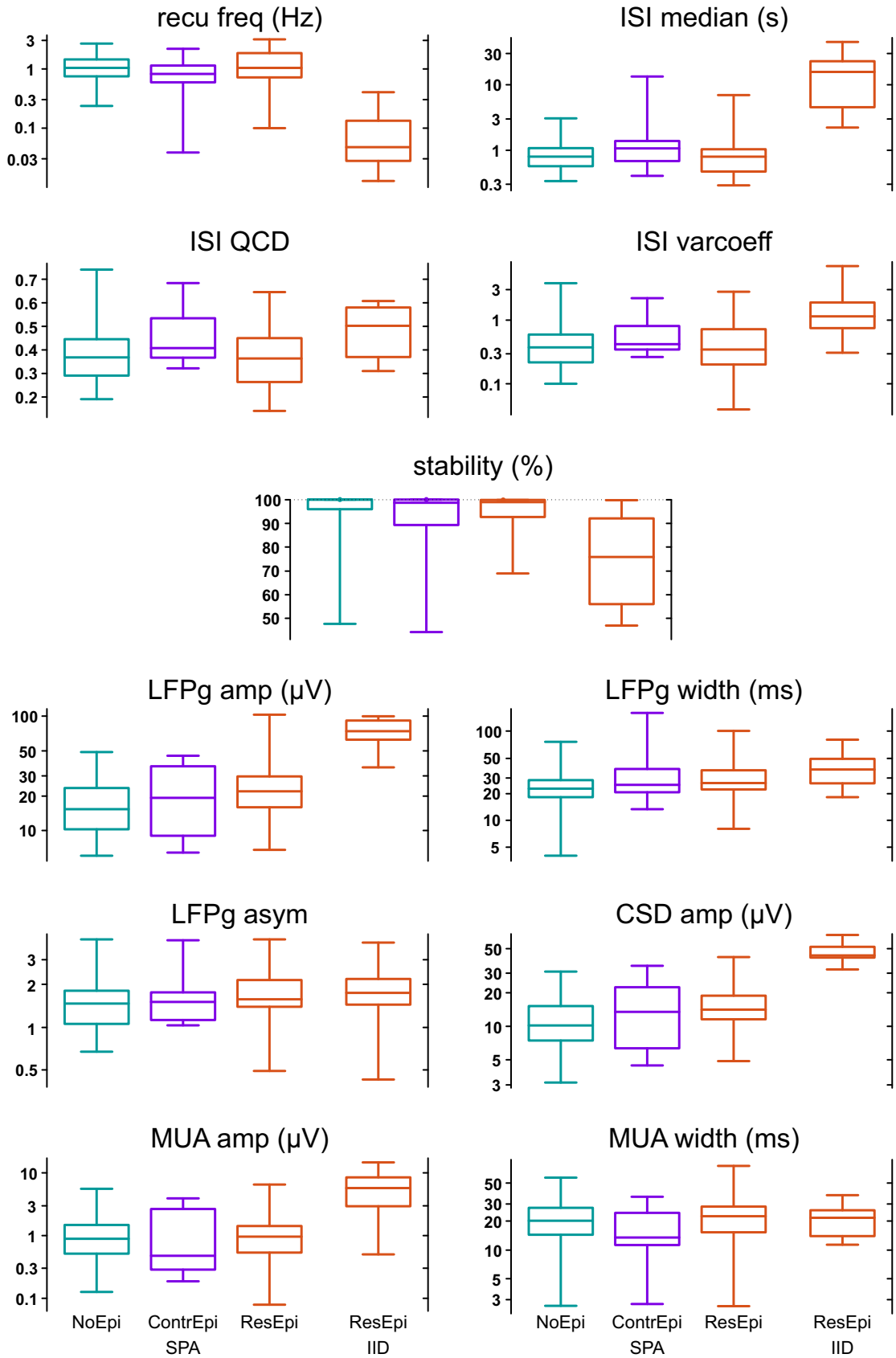


Figure 3.4: NSA properties Box plots visualising SPA and IID recurrence and wave shape properties. Note the logarithmic scale for all variables except for the ISI QCD and the stability. For medians and their CIs see table 3.4, for significant differences see appendix table 6.1.

	all SPA	NoEpi SPA	ContrEpi SPA	ResEpi SPA	ResEpi IID
n	118	48	13	57	8
recu freq (Hz)	1.03 [0.93 – 1.17]	1.06 [0.90 – 1.38]	0.82 [0.66 – 1.15]	1.04 [0.96 – 1.45]	0.05 [0.02 – 0.14]
ISI median (s)	0.82 [0.71 – 0.89]	0.80 [0.63 – 0.94]	1.05 [0.71 – 1.31]	0.80 [0.63 – 0.89]	15.62 [4.06 – 28.24]
ISI QCD	0.37 [0.35 – 0.40]	0.37 [0.33 – 0.40]	0.41 [0.37 – 0.53]	0.36 [0.31 – 0.42]	0.50 [0.36 – 0.61]
ISI varcoeff	0.39 [0.33 – 0.45]	0.38 [0.29 – 0.49]	0.41 [0.36 – 0.81]	0.35 [0.25 – 0.53]	1.13 [0.58 – 2.06]
stability (%)	99.4 [98.5 – 100.0]	99.8 [98.2 – 100.0]	98.5 [89.6 – 100.0]	99.0 [97.4 – 100.0]	76.0 [55.5 – 100.0]
LFPg amp (μV)	20.24 [17.43 – 22.27]	15.41 [12.82 – 20.37]	19.44 [9.02 – 35.88]	22.27 [19.05 – 25.66]	74.36 [60.16 – 92.62]
LFPg width (ms)	25.10 [23.30 – 27.41]	23.05 [21.00 – 25.85]	25.50 [21.45 – 36.85]	26.10 [23.75 – 31.15]	37.00 [19.30 – 52.55]
LFPg asym	1.52 [1.44 – 1.62]	1.46 [1.20 – 1.59]	1.51 [1.13 – 1.77]	1.57 [1.45 – 1.71]	1.77 [1.30 – 2.62]
CSD amp (μV)	13.15 [11.92 – 13.99]	10.31 [8.05 – 13.06]	13.52 [6.68 – 22.25]	14.00 [13.06 – 16.09]	42.97 [40.86 – 51.15]
MUA amp (μV)	0.90 [0.75 – 1.09]	0.90 [0.68 – 1.17]	0.47 [0.31 – 2.61]	0.95 [0.73 – 1.11]	5.81 [1.66 – 8.94]
MUA width (ms)	20.23 [18.13 – 22.85]	19.88 [18.05 – 22.55]	13.60 [11.50 – 23.65]	22.50 [17.90 – 25.65]	21.58 [14.13 – 27.70]

Table 3.4: NSA properties Properties of SPA and IID recurrence and shape for different patient groups. The median and its 95 % CI (in square brackets) are displayed. For box plot visualisations see figure 3.4, for significant differences see appendix table 6.1.

well as MUA ($p < 0.001$) amplitudes. It should be noted that the differences in amplitudes are not surprising, as they were a major criterion for differentiating IIDs from SPAs (see figures 3.3C-E and 3.4 and table 3.4).

Summarising, two types of NSAs could be observed. One type, called SPA occurred in epileptic as well as non-epileptic patients and was very similar across all patient groups. The other type, called IID, was larger in amplitude, lower in recurrence frequency and was only observed in tissue from epileptic patients (ContrEpi and ResEpi).

3.3.2 Spatial subtypes of NSAs

SPAs, but also IIDs were observed to occur in different cell layers within the neocortex. Judging the LFPg pattern and the positioning of the multielectrode on the slice, they were categorised into supra, sup+gran, gran, gran+inf, infra and entire NSAs (see figure 3.5A). Out of these categories, sup+gran, gran+inf and entire describe cases when the LFPg transient spanned across more than one neocortical cell layer, which was observed in 27.1 % of SPA cases (NoEpi: 25.0 %, ContrEpi: 15.4 %, ResEpi 31.6 %, not significantly different: $p>0.4$, Chi-squared test). The distributions of SPAs across all spatial groups were not significantly different between the patient groups (table 3.5 and figure 3.6, $p>0.8$, Fisher's exact test). However, within the ResEpi patient group (the only one whose IIDs were analysed), the distribution of SPAs and IIDs differed across the neocortical layers ($p<0.001$, Fisher's exact test). Post-hoc tests indicated that IIDs are preferably generated in the gran+inf layer ($p<0.001$). Additionally, IIDs tended to occur more often in the infra layer but less often in the supra layer (both n.s. trends, $0.05<p<0.1$). The tendency of IID being generated in the deeper layers is in accordance with the literature, which describes that locally generated spikes in the human neocortex emerge in the deep layers (layer V) [32].

		supra	sup+gran	gran	gran+inf	infra	entire	total
SPA	NoEpi	22 (45.8 %)	8 (16.7 %)	6 (12.5 %)	3 (6.3 %)	8 (16.7 %)	1 (2.1 %)	48
	ContrEpi	8 (61.5 %)	1 (7.7 %)	2 (15.4 %)	1 (7.7 %)	1 (7.7 %)	0 (0.0 %)	13
	ResEpi	28 (49.1 %)	11 (19.3 %)	8 (14.0 %)	5 (8.8 %)	3 (5.3 %)	2 (3.5 %)	57
	Total	58 (49.2 %)	20 (16.9 %)	16 (13.6 %)	9 (7.6 %)	12 (10.2 %)	3 (2.5 %)	118
IID	ContrEpi	0 (0.0 %)	1 (100 %)	0 (0.0 %)	0 (0.0 %)	0 (0.0 %)	0 (0.0 %)	1
	ResEpi	0 (0.0 %)	0 (0.0 %)	1 (12.5 %)	5 (62.5 %)	2 (25.0 %)	0 (0.0 %)	8
	Total	0 (0.0 %)	1 (11.1 %)	1 (11.1 %)	5 (55.6 %)	2 (22.2 %)	0 (0.0 %)	9

Table 3.5: NSA location Numbers (and row percentages) of NSAs located in different neocortical layers by type of NSA (SPA or IID) and tissue of origin. The numbers of SPAs in different locations do not differ between the three patient groups ($p>0.8$, Fisher's exact test). Similarly, the distribution of IIDs over different locations is also not significantly different between the patient groups ($p>0.2$, Fisher's exact test), although this is very probably due to the low case numbers (The less conservative Chi-squared test resulted in a significant result $p<0.05$, but is not appropriate due to low observed frequencies). Interestingly, within the ResEpi group, the distribution over neocortical locations differed between SPAs and IIDs ($p<0.001$, Fisher's exact test). Post-hoc testing revealed that IIDs occur more often than expected in the gran+inf layer ($p<0.001$). There were also non-significant trends of IIDs occurring less often in the supra layers and more often in the infra layers (both $0.05<p<0.1$). For examples illustrating the different spatial SPA types see figure 3.5A, for a bar graph visualising the incidences of different NSA locations see figure 3.6.

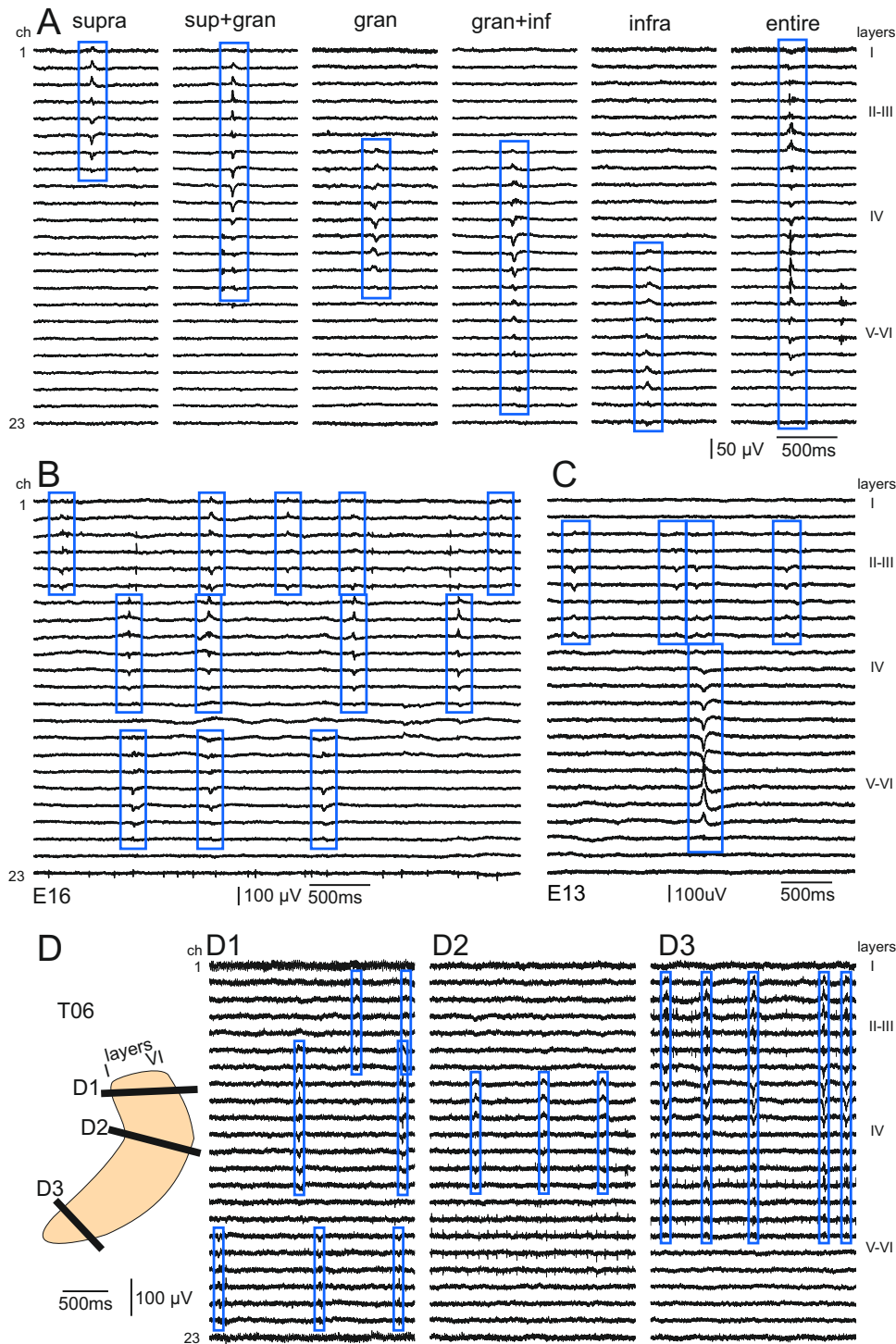


Figure 3.5: Multiple spatial types of SPAs (A) Six different spatial types of SPAs were identified. From left to right: supra, sup+gran, gran, gran+inf, infra and entire. Traces are single events taken from different recordings. For case numbers of SPAs and IIDs occurring in different locations, see table 3.5 and figure 3.6. (B) Different types of SPAs can occur simultaneously in one recording (example taken from patient E16). Example trace exhibiting supra (green), gran (purple) and infra (orange) SPA simultaneously. (C) IIDs and SPAs have also been observed to occur simultaneously in the same recording (example taken from patient E13). The example trace displays simultaneous supra SPA (blue) and gran+inf IID (red). (D) Different spots in the same slice can display different spatial SPA types (example taken from patient T06). Recordings D1, D2 and D3 were performed sequentially on the same slice. D1 displays three simultaneous SPA types (supra: green, gran: purple, infra: orange), D2 shows one SPA type (gran: pink), D3 shows another different type of SPA (sup+gran: blue). The schematic drawing on the left indicates the position of the multielectrode on the slice during each of the recordings.

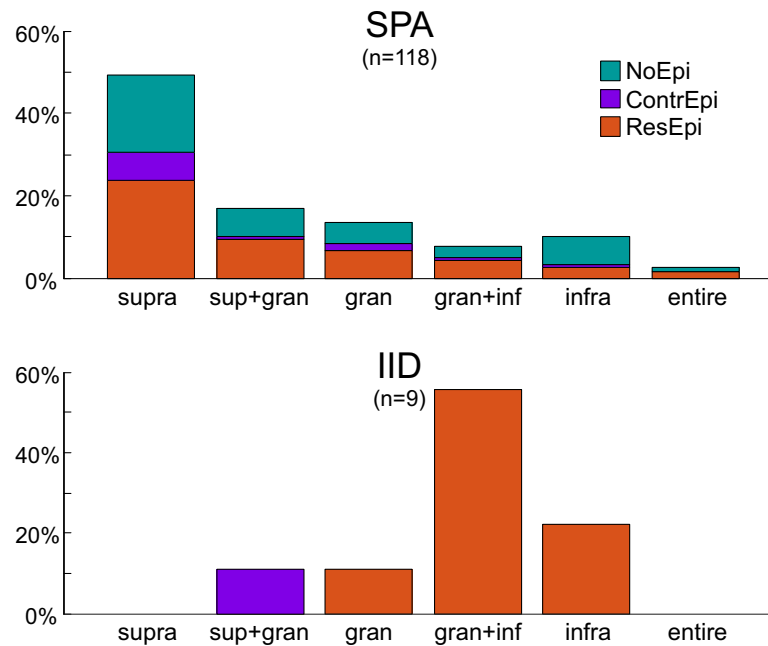


Figure 3.6: NSA locations Bar graph visualising the incidences of different locations of SPAs and IIDs. Bar heights are relative to the numbers of all SPAs and all IIDs, respectively (i.e. all SPAs are 100 % and all IIDs are 100 %). For absolute numbers see table 3.5.

3.3.3 Simultaneous occurrence of multiple NSAs

In 26.6 % of recordings (25/94), two or more (up to four) NSAs could be observed simultaneously in the same recording. This phenomenon occurred at similar ratios in the three patient groups (NoEpi: 33.3 %, ContrEpi: 8.3 %, ResEpi: 26.5 %, not significantly different $p > 0.2$, Chi-squared). Moreover, the number of NSAs in each recording was also similar between the patient groups (medians are all 1, mean \pm SD: NoEpi: 1.45 ± 0.71 , ContrEpi: 1.17 ± 0.58 , ResEpi: 1.33 ± 0.63 , not significantly different, $p > 0.2$, Kruskal Wallis). An example of multiple SPAs occurring simultaneously can be seen in figure 3.5B. The example illustrates that the different types can occur independently of each other. However, some crosstalk between the populations generating the distinct types can be assumed, as the different types sometimes occur within few milliseconds of each other, possibly triggering one another. Cases of simultaneous NSAs with overlapping locations (e.g. supra & sup+gran or gran & gran+inf) have also been observed (not shown). In these cases it is possible that the overlapping types are generated by non-interacting non-overlapping populations. However, it is also possible that these are cases of two (possibly overlapping) populations A and B generating synchronous activity where A always triggers B but not vice versa. Strikingly, the concept of simultaneous population activities was not restricted to SPAs. Cases of simultaneous SPAs and IIDs in the same recording could also be observed (see figure 3.5C). This is interesting as it implies that the state in which the neuronal network can generate IID and the one in which it can generate SPA are not mutually exclusive, at least on the time scale of seconds.

As mentioned in methods section 3.2.3, within an experiment, each neocortical slice was scanned by sequential recordings, moving the electrode successively in parallel to the neocortical layers. During this scanning, different types of NSAs were sometimes visible in different spots on

the slice. Figure 3.5D shows an example where three different spots revealed different kinds of SPA activity. Spots in-between the three indicated ones either had no population activity or SPAs similar to the ones shown in D1, D2 and D3. In many cases, the same type of NSA (e.g. supra SPA) was visible across a large proportion of the slice. For more information about multiple spots of NSAs in one slice including differences between patient groups see the appendix section 6.3.1.

In summary, different spatial subtypes of SPAs as well as SPAs and IIDs could occur simultaneously in the same recording and in neighbouring regions from the same neocortical slice (in subsequent recordings).

3.3.4 Regression on SPA properties

The previously described table 3.4 describes differences between the patient groups according to their epilepsy diagnosis status. However, there are many other potentially contributing factors such as the cortical lobe of origin or patient features such as age or gender. To investigate the influence of each of these aspects, multiple regression analysis was performed. Table 3.6 displays the results of the regression analysis on SPA properties. Selected findings are discussed in the following paragraphs.

For a detailed interpretation of the results concerning the regression on SPA recurrence (table 3.6 rows 1-6), including a discussion about the effects of different patient age please see appendix section 6.3.2. In short, the recurrence frequency and the ISI median were found to be inversely proportional. However, while this might seem trivial, it is not at all obvious and although this does not necessarily imply a normal or even symmetric distribution of ISIs, it points to the existence of a structured relationship between the recurrence frequency and the ISI median. Accordingly, the different measures of ISI variability as well as the stability could be predicted moderately to well. As discussed later, the same relationship between recurrence frequency and ISI median was not found for the spike trains of the analysed cells.

The predictability of the LFPg and CSD amplitudes was very low (R^2 : 0.150 and 0.135, respectively, rows 7 and 9). The only significant (n.s. trend in case of the CSD amplitude) predictor was the epidiagnosis (NoEpi<ResEpi). Another interesting aspect was that the LFPg as well as the CSD amplitudes could not be predicted from the mean recurrence frequency or the ISI median (p-values: 0.83, 0.98, 0.73 and 0.97). This is relevant as it is an indication of a reproducible SPA detection. Random or arbitrary thresholding would lead to higher recurrence frequencies being associated with smaller LFPg amplitudes (more small events included) and vice versa (fewer small events included). According to this analysis, this did not seem to be the

Table 3.6: (Regressions on SPA properties cont.) E.g. For the regression on the recurrence frequency "i 0.23 s 0.36 e" indicates, that (when all the other independent variables are kept the same), the recurrence frequency of infra SPAs was on average 0.23 times smaller than that of supra or granular SPAs, which were in turn on average 0.36 times smaller than entire SPAs. The dull red background indicates that the effect of SPA location on recurrence frequency is not significant ($0.1 \leq p < 0.2$). For more explanations of R^2 , adj. R^2 or the x-fold interpretation of the beta-coefficients in case of ln transformed variables, see appendix section 6.2. Abbreviations: s, SPA in supragranular and granular layers; i, SPA in infragranular layers; e, entire SPA (across all layers); fr, frontal lobe; pa, parietal lobe; oc, occipital lobe; te, temporal lobe; f, female; m, male.

	R ² (adj. R ²)	Recu. frequency (ln)	Median ISI (ln)	SPA location (layers)	Cortical lobe	Epilepsy diagnosis group	Patient age	Patient gender
recu freq (ln)	0.183 (0.115)			i 0.23 s 0.36 e	oc 0.08 pa 0.07 te 0.09 fr	ContrEpi 0.13 NoEpi 0.35 ResEpi	0.15	f 0.04 m
ISI median (ln)	0.190 (0.122)			e 0.24 s 0.29 i	fr 0.10 te 0.05 pa 0.10 oc	ResEpi 0.30 NoEpi 0.12 ContrEpi	-0.13	m 0.04 f
ISI median (ln)	0.975 (0.972)	-0.86		s 0.07 e 0.02 i	pa 0.01 fr 0.01 oc 0.00 te	ResEpi 0.00 NoEpi 0.01 ContrEpi	0.00	m 0.01 f
ISI QCD	0.588 (0.545)	-0.48	-0.45	e 0.03 i 0.04 s	fr 0.07 te 0.11 pa 0.06 oc	ResEpi 0.01 NoEpi 0.03 ContrEpi	0.00	f 0.01 m
ISI varcoeff (ln)	0.795 (0.773)	-4.75	-4.68	e 0.30 i 0.12 s	fr 0.09 pa 0.01 oc -0.03 te	ResEpi 0.12 NoEpi 0.03 ContrEpi	0.00	f 0.01 m
stability (ln)	0.807 (0.787)	0.81	0.81	e 0.04 i 0.00 s	fr 0.11 te 0.06 pa 0.01 oc	ContrEpi 0.00 NoEpi 0.01 ResEpi	0.00	f 0.03 m
LFPg amp	0.150 (0.062)	-0.01	0.12	i 0.16 s 0.19 e	pa 0.04 oc 0.09 te 0.13 fr	NoEpi 0.09 ContrEpi 0.27 ResEpi	0.00	m 0.07 f
LFPg width	0.244 (0.165)	1.24	1.46	i 0.23 s 0.25 e	oc 0.12 te 0.11 fr 0.16 pa	NoEpi 0.25 ResEpi 0.06 ContrEpi	0.02	f 0.23 m
CSD amp	0.135 (0.046)	0.01	0.16	i 0.20 s 0.14 e	oc 0.02 pa 0.08 te 0.13 fr	NoEpi 0.15 ContrEpi 0.18 ResEpi	0.01	m 0.11 f
MUA amp	0.176 (0.090)	1.30	1.48	s 0.11 i 0.35 e	te 0.05 fr 0.15 pa 0.00 oc	ContrEpi 0.26 ResEpi 0.24 NoEpi	-0.14	m 0.34 f
MUA width	0.073 (-0.023)	0.66	0.78	i 0.04 s 0.35 e	pa 0.01 fr 0.02 oc 0.01 te	ContrEpi 0.35 ResEpi 0.05 NoEpi	-0.05	f 0.06 m
Colour legend		p<1E-10	p<0.001	p<0.05	p<0.1	p>0.1	p≥0.2	

Table 3.6: Regressions on SPA properties. Independent variables are represented by columns, regressions run on different dependent variables by different rows. R² and adjusted R² indicate how well the regression describes the variation in the dependent variable. The colour of each cell represents significance (see colour legend, LM statistic in case of categorical variables with more than 2 categories (SPA location, cortical lobe, epilepsy diagnosis group), t-statistic otherwise). For significant differences for categorical variables with more than two groups see table 6.2. Empty grey cells indicate that this independent variable was not included in the respective regression, otherwise, numbers represent beta-coefficients. Beta-coefficients describing the change for patients of different ages are given for increments of 10 years. '(ln)' indicates that the variable was transformed using the natural logarithm. In these cases, beta-coefficients can be interpreted as x-fold changes rather than additions of x. In case of categorical independent variables, the groups are sorted from smaller to larger, beta-coefficients indicate the differences between adjoining groups. See the continuation on the left page.

case. Thus, the absence of this relationship indicates that the detection threshold was chosen appropriately for different files.

Out of all the dependent variables tested in this analysis, the epilepsy diagnosis group (third column from the right) only predicted the LFPg amplitude in a significant way. This is in accordance with the results using Mann-Whitney and Kruskal-Wallis tests (described in section 3.3.1). The CSD amplitude provides a minor exception, as a significant difference (NoEpi<ResEpi, $p<0.05$) was identified using the Kruskal-Wallis test, while the regression analysis only identified a non-significant trend ($0.05<p<0.1$). However, for two such different analysis approaches, such small differences in p-values do not constitute a contradiction.

Summarising, multiple regression analysis of SPA properties was in agreement with the results described above (table 3.4). Moreover, it indicated good SPA detection quality, as the LFPg amplitudes were not related to the recurrence frequencies.

3.3.5 Characterisation of cellular activity

In addition to the population activity detected, single cell activity was clustered from the extracellular recordings in order to gain insight into neuronal behaviour within the slice. After detection and averaging, the AP shape as well as the autocorrelogram were used to manually categorise the cells into principal cells (PCs), interneurons (IN) and unclear cells (UC). During this process no information other than the autocorrelogram and the averaged action potential was displayed to the user in order to avoid bias (see methods section 3.2.4 for more details). Table 3.7 summarises the cells analysed in this study.

	PC	IN	UC	total
NoEpi	132 (32.5 %)	104 (25.6 %)	170 (41.9 %)	406
ContrEpi	18 (24.3 %)	35 (47.3 %)	21 (28.4 %)	74
ResEpi	131 (34.5 %)	106 (27.9 %)	143 (37.6 %)	380
total	281 (32.7 %)	245 (28.5 %)	334 (38.8 %)	860

Table 3.7: Clustered neurons Numbers (and row percentages) of single units clustered from extracellular recordings by cell type and tissue of origin. The proportion of different cell types is not equal across the three patient groups ($p<0.01$, Chi-squared). Post-hoc testing revealed that the number of INs is larger than expected in the ContrEpi group. A separate Chi-square test revealed no significant differences between the NoEpi and the ResEpi group in terms of detected cell types ($p>0.4$).

Strikingly, the proportion of different cell types was not uniform across the patient groups ($p<0.01$, Chi-squared). As determined by post-hoc testing, the ContrEpi group exhibits more clustered INs than expected by chance (47.3 %, in comparison to 25.6 % in NoEpi and 27.9 % in ResEpi, table 3.7). This was not caused by a compromised purity of the ContrEpi IN group, as the properties which differ most between the cell types, i.e. AP width, the peak-to-peak delay as well as the ahp amplitude were not different from that of the IN groups of NoEpi or ResEpi ($p>0.3$, $p>0.1$ and $p>0.4$, Kruskal Wallis, see table 3.8, appendix table 6.3 and figure 3.7). Similarly, there were no differences between the patient groups for PCs or UCs. However, as a larger proportion of INs was found in tissue from ContrEpi patients, this might distort/affect the patient group totals

for some cell properties. To accommodate for this fact, totals over each patient group are not presented or considered. Instead, cell properties are exclusively compared across cell types within each patient group and across patient groups within each cell type. For more information on the differences in AP shape between the patient groups and cell types (shown in table 3.8 rows 7-11), please see appendix section 6.3.3.

In summary, the ContrEpi group had more clustered (and thus active) INs than the other two patient groups. The AP shape properties showed the expected differences between the differentiated cell types.

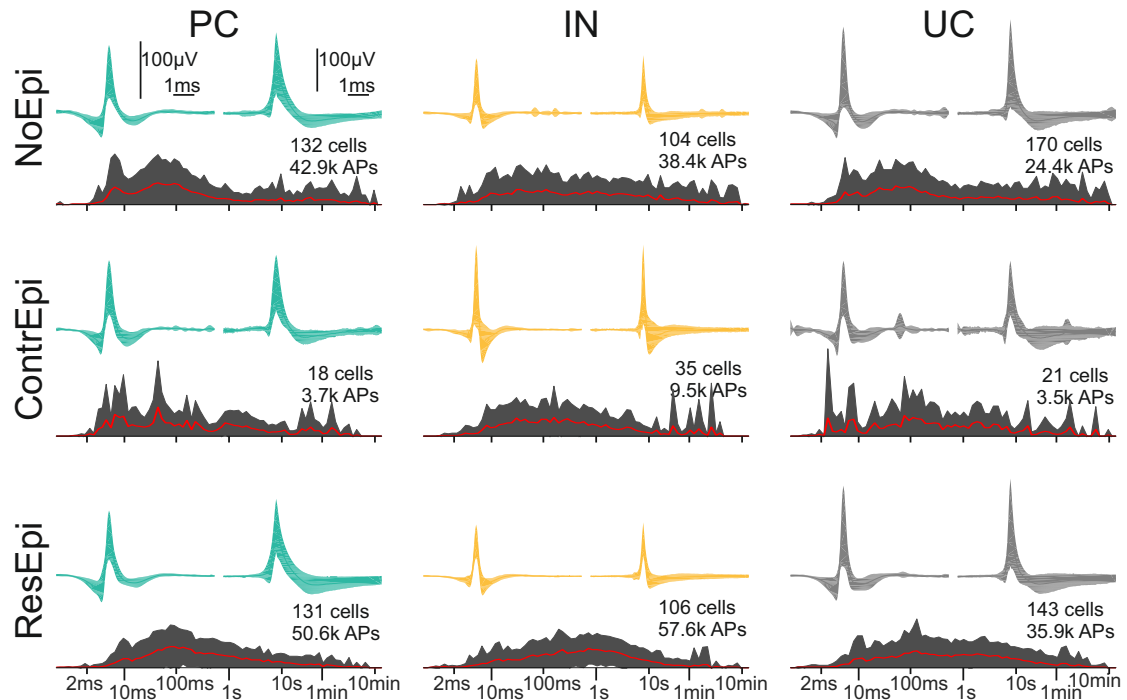


Figure 3.7: Cell AP shapes and ISI histograms At the top of each panel: Mean \pm SD (line and shaded area, respectively) of the averaged APs (-2.5 – 5 ms) of all cells in the respective group: 300 – 3000 Hz bp filtered (left) and unfiltered (right). The scale bars are valid for all filtered and all unfiltered traces, respectively. On the bottom of each panel: Histograms of ISIs, averaged across all cells (mean \pm SD: red line and grey area, respectively), weighted so that each cell carries the same weight (rather than each AP). Note the logarithmic scale on the x-axes of the histograms. For better comparison, the y-axes were adjusted to equalise the total areas of the bars within each histogram. The lower smoothness of the histograms in the ContrEpi group is due to the lower number of cells (and APs). Case numbers describe the numbers of cells and the total number of APs in each group (“k APs” stands for 1000 action potentials). For quantifications see table 3.8 and figure 3.8.

With regard to cell firing properties, multiple differences were found between cell types and patient groups. For example, the mean recurrence frequency of cells was larger in the ResEpi group than in the NoEpi group for each cell type (PC: $p < 1E-04$, IN: $p < 0.01$, UC: $p < 0.01$, table 3.8 and figure 3.8). Although both PCs and INs displayed higher firing frequencies in ResEpi, the difference was larger for PCs than for INs (medians: PCs: NoEpi: 0.17 Hz, ResEpi: 0.47 Hz, $p < 1E-04$; INs: NoEpi: 0.24 Hz, ResEpi: 0.59 Hz, $p < 0.01$, both Kruskal Wallis). This might point to increased excitability in the pharmacoresistant epileptic neocortical network.

However, while the recurrence frequency describes how much a neuron fires, the ISI median is more closely related to the typical firing pattern of a neuron. Strikingly, the analysis of the

	NoEpi PC	NoEpi IN	NoEpi UC	ContrEpi PC	ContrEpi IN	ContrEpi UC	ResEpi PC	ResEpi IN	ResEpi UC
n	132	104	170	18	35	21	131	106	143
recu freq (Hz)	0.17 [0.12–0.22]	0.24 [0.15–0.34]	0.15 [0.12–0.20]	0.22 [0.08–0.39]	0.41 [0.23–0.70]	0.26 [0.07–0.33]	0.47 [0.33–0.59]	0.59 [0.46–0.73]	0.28 [0.22–0.35]
ISI median (s)	0.08 [0.07–0.09]	0.43 [0.20–0.63]	0.13 [0.11–0.19]	0.13 [0.05–0.53]	0.24 [0.09–0.53]	0.15 [0.07–0.55]	0.18 [0.15–0.24]	0.50 [0.28–0.70]	0.37 [0.23–0.61]
ISI QCD	0.73 [0.66–0.83]	0.77 [0.71–0.84]	0.83 [0.77–0.90]	0.93 [0.69–0.98]	0.74 [0.57–0.81]	0.78 [0.63–0.95]	0.74 [0.71–0.79]	0.69 [0.64–0.74]	0.83 [0.74–0.87]
ISI varcoeff	8.02 [6.83–9.65]	2.66 [1.66–4.20]	5.12 [4.21–6.06]	5.86 [2.43–11.19]	8.49 [3.34–19.38]	6.15 [4.35–11.27]	6.20 [4.70–7.47]	2.37 [1.88–3.07]	3.63 [3.31–4.52]
stability (%)	1.42 [0.92–2.26]	26.41 [10.54–62.34]	2.57 [1.41–4.67]	2.41 [1.12–7.70]	15.73 [1.67–36.39]	5.23 [1.01–16.50]	6.46 [4.36–14.45]	56.39 [38.28–64.78]	16.42 [8.88–31.07]
burstiness (%)	14.29 [9.31–17.72]	3.48 [1.38–6.96]	10.00 [6.25–12.43]	22.33 [7.29–43.85]	1.27 [0.00–8.57]	6.67 [2.02–24.04]	2.67 [1.15–5.98]	1.17 [0.45–2.52]	2.69 [0.86–4.79]
AP amp (μV)	59.90 [53.49–64.67]	42.18 [38.18–48.66]	52.07 [47.90–61.04]	52.32 [42.69–84.42]	50.99 [42.95–62.69]	52.52 [34.52–95.89]	58.49 [51.29–65.31]	52.29 [48.43–56.89]	65.99 [60.33–75.11]
AP width (ms)	0.36 [0.35–0.37]	0.24 [0.23–0.24]	0.29 [0.29–0.30]	0.36 [0.34–0.38]	0.23 [0.21–0.24]	0.30 [0.28–0.31]	0.36 [0.35–0.37]	0.24 [0.23–0.25]	0.30 [0.29–0.30]
AP asym	1.45 [1.36–1.53]	1.24 [1.17–1.37]	1.42 [1.29–1.47]	1.41 [1.10–1.50]	1.08 [0.86–1.15]	1.16 [0.97–1.47]	1.43 [1.35–1.51]	1.05 [0.97–1.13]	1.24 [1.19–1.30]
AHP amp (%)	22.0 [19.8–24.0]	29.4 [26.2–32.3]	22.8 [21.8–23.6]	23.4 [20.5–31.0]	32.3 [28.1–42.5]	25.2 [21.3–28.8]	19.2 [18.3–20.5]	31.5 [28.2–35.0]	23.1 [21.5–24.1]
p2p delay (ms)	1.10 [1.07–1.15]	0.45 [0.40–0.55]	0.90 [0.85–0.95]	1.00 [0.85–1.15]	0.40 [0.35–0.50]	0.65 [0.45–0.85]	1.20 [1.10–1.30]	0.40 [0.35–0.45]	0.80 [0.70–0.90]

Table 3.8: Cell properties Cell recurrence and AP shape features for different cell types and patient groups. The median and its 95 % CI (in square brackets) are displayed. For box plot visualisations see figure 3.8, for significant differences see appendix table 6.3.

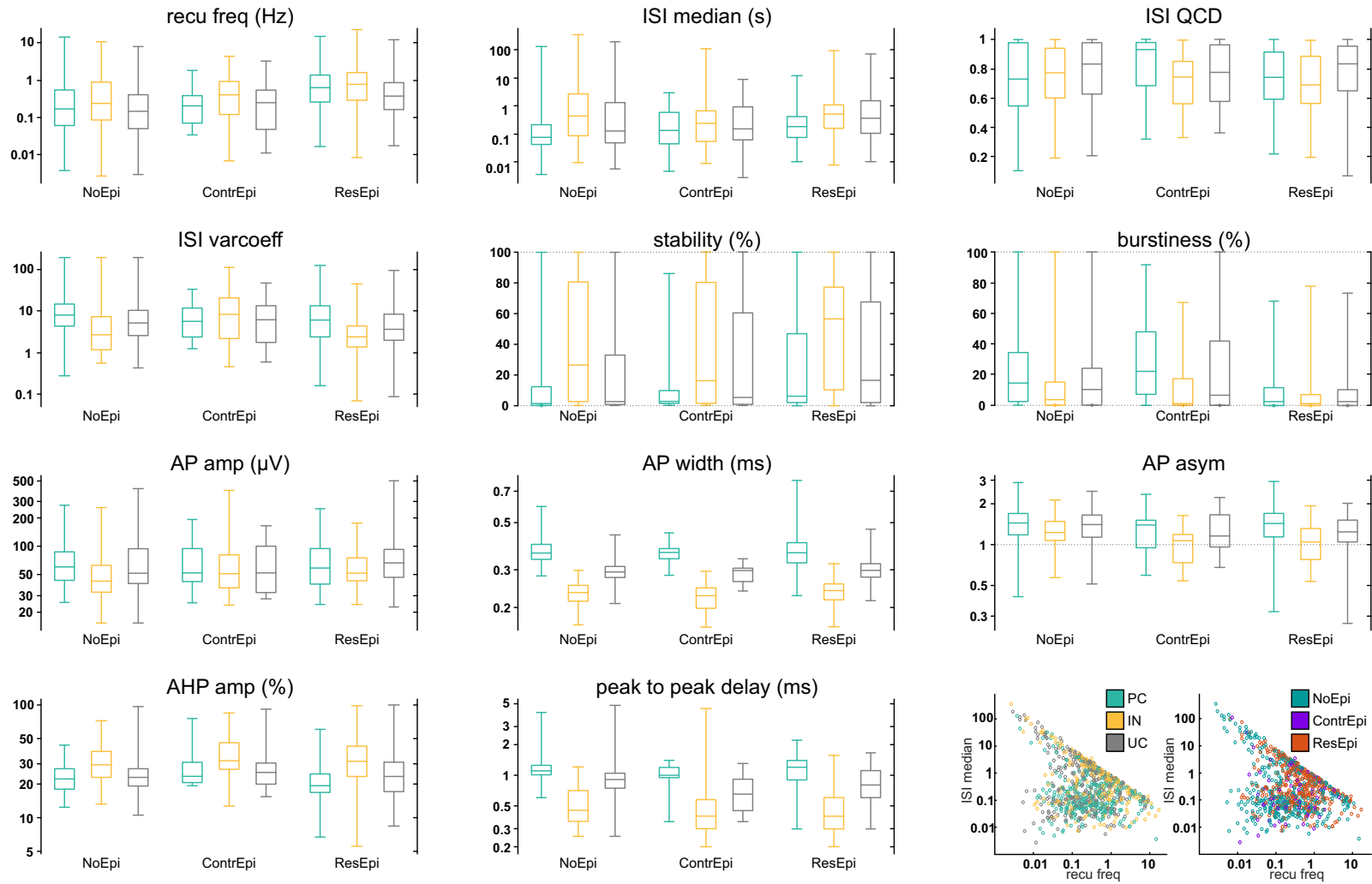


Figure 3.8: Cell firing and AP shape properties Box plots visualising firing and AP shape properties of cells for different cell types and patient groups. Note the logarithmic scale for all variables except for the ISI QCD, stability and burstiness. For medians and their CIs see table 3.8, for significant differences see appendix table 6.3.

ISI median resulted in a different picture from that of the recurrence frequency. The discrepancy between the recurrence frequency and the ISI median in case of cells is visualised in the scatter plot in figure 3.8. Its origin is the disparity of the mean and the median for (almost all) distributions that are non-symmetric. ISI distributions were sometimes log-normal, but very often they were bi- or multimodal (e.g. due to burstiness, compare to the combined cell ISI histograms in figure 3.7, although those are the combined histograms over many cells). This multimodality resulted in non-trivial relationships between the mean and the median of ISI distributions (and thus also to the mean recurrence frequency, which is the inverse of the ISI mean). Interestingly, PCs seemed to diverge more often from the expected negative relationship than INs (left scatter plot in figure 3.8). This was presumably caused by more complex ISI distributions of PCs.

In both NoEpi and ResEpi, the ISI median was smaller for PCs than for INs and UCs (NoEpi: PC<IN: $p<1E-06$, PC<UC: $p<0.01$, UC<IN: $p<0.05$, ResEpi: PC<IN: $p<0.001$, PC<UC: $p<0.001$, UC<IN: $p>0.8$). The smaller ISI median of PCs might be in relation with bursting behaviour. Indeed, in NoEpi tissue, the burstiness of PCs was larger than that of INs ($p<0.001$). While the same difference in burstiness could be found between PCs and INs of ContrEpi tissue ($p<0.01$), this was not the case for cells from ResEpi tissue ($p>0.3$). Moreover, differences in ISI medians could also be found between patient groups: PCs as well as UCs had shorter ISI medians in NoEpi than in ResEpi tissue ($p<0.001$ and $p<0.05$, respectively). This fits to the finding that ResEpi PCs and UCs burst less than their NoEpi counterparts ($p<1E-05$ and $p<0.001$, respectively, also see figure 3.8) and that ContrEpi PCs burst more than ResEpi PCs ($p<0.001$). This loss of short ISIs in ResEpi PCs is also visible in the ISI histograms in figure 3.7. The peak below the 10 ms tick mark is nicely visible in NoEpi PCs and UCs and less clearly (due to noisier histograms) also in ContrEpi. However, this peak is absent or far less pronounced in INs of all patient groups and for PCs of the ResEpi group. Overall, this points to a loss of short ISIs and the associated burstiness in PCs of the ResEpi group.

Due to the often multimodal distributions of cell ISIs, their variability was difficult to quantify. This had the unfortunate consequence that different quantifications lead to different results. As mentioned in the methods (section 3.2.4, under 'Clustered neuronal activity'), the QCD, which is robust and independent of the underlying distribution, is not very sensitive. On the other hand, the ISI varcoeff, which is used in the literature [81], relies on parametric measures to describe cell firing, such as the mean and SD, which are mostly suited for symmetric distributions. Judging from the ISI varcoeff, PCs fire more irregularly than UCs, which in turn fire more irregularly than INs in NoEpi and ResEpi tissue (NoEpi: IN<PC: $p<1E-07$, UC<PC: $p<0.01$, IN<UC: $p<0.01$, ResEpi: IN<PC: $p<1E-06$, UC<PC: $p<0.05$, IN<UC: $p<0.01$). It is also noteworthy that there is no such difference in the ContrEpi group ($p>0.7$ and reversed relationships: INs have the largest ISI varcoeff in the ContrEpi group, compare to table 3.8). Additionally, ContrEpi INs also fire more irregularly than NoEpi or ResEpi INs (NoEpi<ContrEpi: $p<0.05$, ResEpi<ContrEpi: $p<0.01$). This could be related to the (successful) application of antiepileptic drugs. Last but not least, stability (as defined in this analysis, see section 3.2.4) is also related to firing regularity. For both NoEpi and ResEpi, INs fire more stably than PCs and UCs (NoEpi: PC<IN: $p<1E-08$, UC<IN: $p<1E-04$, ResEpi: PC<IN: $p<1E-05$, UC<IN: $p<0.01$, also see figure 3.8). This is in accordance with the findings regarding the ISI varcoeff (higher firing stability/regularity corresponds to a

lower ISI variability / firing irregularity). Moreover, UC as well as PC are more consistently active (more stable) in ResEpi than in NoEpi (PC: $p < 1E-06$, UC: $p < 0.001$). For medians and their CIs of the properties discussed in this paragraph, please see table 3.8.

In contrast to the regression on SPA properties where the contributions of different independent variables to the recurrence frequency and ISI median was very similar (see table 3.6, rows 1 and 2 and appendix section 6.3.2), this did not seem to be the case for cells (table 3.9, rows 1 and 2). I.e. the independent variables contributed differently to the recurrence frequency and the ISI median. For example, the recurrence frequency, but not the ISI median could be predicted using the epidiagnosis status (recurrence frequency: NoEpi<ResEpi: $p < 1E-05$, ContrEpi<ResEpi: $p < 0.001$), ISI median: $p > 0.2$). However, the R^2 values are very low, which means that the overall predictive power is very low for these two regressions. Moreover, even when the mean was taken into account (row 3), the median could still only be predicted to an R^2 of 0.22 (for comparison, the same regression for SPAs resulted in an R^2 of 0.972). As the recurrence frequency was of little help in predicting the ISI median, in the case of cells, these two variables seem to have stood in a more complex relation to each other than in the case of SPAs (compare again to the left scatter plot in figure 3.8).

Another reflection of these apparently more intricate ISI distributions was that the ISI variability (rows 4-7) was harder to quantify than was the case with SPAs. Depending on the measurement for dispersion, the contributions of the various independent variables differed a lot, sometimes even contradicting each other (as e.g. in case of gender (rows 4 and 6): ISI QCD: female<male: $p < 0.001$, ISI varcoeff: male<female: $p < 0.05$). As the results on cell firing variability too strongly depend on how it is defined and calculated, these findings remain inconclusive.

The regression results on burstiness indicate that the patient group ($p < 1E-05$) and the cell type ($p < 0.001$) were the main predictors (row 8, unless the median ISI is taken into account, row 9). In accordance with the findings using Kruskal-Wallis tests, INs were found to burst less than PCs and UCs (IN<PC: $p < 1E-04$, IN<UC: $p < 0.01$, UC<PC: $p > 0.1$). Further confirming the findings from earlier, the analysis shows that ResEpi cells had reduced bursting ability compared to the other groups (ResEpi<NoEpi: $p < 1E-06$, ResEpi<ContrEpi: $p < 0.001$, ContrEpi<NoEpi: $p > 0.9$).

In accordance with the results using Kruskal-Wallis tests, the stability (the last two rows) of INs seems to be larger than that of PCs or UCs (PC<IN: $p < 1E-04$, UC<IN: $p < 0.01$, PC<UC: $p > 0.1$). Similarly to burstiness, the effect of the cell type is largely taken away when the ISI median is included in the regression. This indicates that the differences between the cell types in terms of bursting and stability could largely be explained by their differences in firing pattern (the ISI median).

Overall, the cell type, the cell location within the neocortical layers as well as the cortical lobe of origin and sometimes the patient gender, but not patient age affected cell firing.

Summarising the results obtained by Kruskal-Wallis tests and multiple regression analysis, ResEpi cells had a higher firing rate than NoEpi cells. PCs burst more than INs in NoEpi and ContrEpi tissue, while burstiness and short ISIs seemed to be reduced in ResEpi tissue. Moreover, although ISI variability and/or firing irregularity was hard to quantify, it seems that INs fired most regularly while PCs fired most irregularly among the cell types. Moreover, ContrEpi INs were found to fire more irregularly than NoEpi or ResEpi INs.

	R ² (adj. R ²)	Recur- rence frequency (ln)	Median ISI (ln)	Cell type	Cell location (layers)	Cortical lobe	Epilepsy diagnosis group	Patient age	Patient gender
recu freq (ln)	0.107 (0.095)			UC 0.38 PC 0.23 IN	g 0.29 s 0.16 i	pa 0.25 te 0.22 oc 0.03 fr	NoEpi 0.05 ContrEpi 0.85 ResEpi	0.02	m 0.34 f
ISI median (ln)	0.102 (0.091)			PC 0.79 UC 0.30 IN	i 0.16 g 0.45 s	oc 0.40 te 0.45 pa 0.24 fr	NoEpi 0.07 ContrEpi 0.28 ResEpi	-0.02	f 0.07 m
ISI median (ln)	0.220 (0.209)	-0.45		PC 0.62 UC 0.58 IN	g 0.04 i 0.54 s	oc 0.30 te 0.33 pa 0.47 fr	NoEpi 0.10 ContrEpi 0.67 ResEpi	-0.01	m 0.08 f
ISI QCD	0.205 (0.194)	-0.05		PC 0.01 IN 0.02 UC	i 0.03 s 0.01 g	pa 0.07 fr 0.00 te 0.03 oc	ContrEpi 0.01 NoEpi 0.02 ResEpi	0.01	f 0.07 m
ISI QCD	0.205 (0.193)	-0.06	0.00	PC 0.01 IN 0.02 UC	i 0.03 s 0.01 g	pa 0.07 fr 0.00 te 0.03 oc	ContrEpi 0.01 NoEpi 0.02 ResEpi	0.01	f 0.07 m
ISI varcoeff (ln)	0.140 (0.127)	0.08		IN 0.38 UC 0.39 PC	s 0.30 i 0.15 g	fr 0.06 pa 0.32 te 0.23 oc	ResEpi 0.37 ContrEpi 0.03 NoEpi	-0.03	m 0.27 f
ISI varcoeff (ln)	0.406 (0.397)	-0.08	-0.36	IN 0.17 UC 0.17 PC	s 0.11 i 0.14 g	pa 0.11 fr 0.09 te 0.12 oc	ResEpi 0.12 NoEpi 0.00 ContrEpi	-0.03	m 0.30 f
bursti- ness ($\sqrt{\cdot}$)	0.117 (0.104)	-0.01		IN 0.06 UC 0.03 PC	i 0.02 s 0.01 g	pa 0.05 te 0.01 oc 0.02 fr	ResEpi 0.16 ContrEpi 0.00 NoEpi	-0.01	f 0.04 m
bursti- ness ($\sqrt{\cdot}$)	0.269 (0.258)	-0.03	-0.06	IN 0.02 PC 0.01 UC	i 0.03 g 0.02 s	pa 0.02 oc 0.01 te 0.07 fr	ResEpi 0.12 NoEpi 0.00 ContrEpi	-0.01	f 0.04 m
stability (ln)	0.318 (0.309)	0.62		PC 0.66 UC 0.67 IN	g 0.04 i 0.61 s	oc 0.32 te 0.42 pa 0.46 fr	NoEpi 0.12 ContrEpi 0.65 ResEpi	-0.01	m 0.17 f
stability (ln)	0.978 (0.309)	1.11	1.09	UC 0.01 PC 0.03 IN	i 0.01 g 0.02 s	te 0.00 fr 0.00 oc 0.05 pa	ResEpi 0.05 NoEpi 0.02 ContrEpi	0.00	m 0.08 f
Colour legend		p<1E-10	p<0.001	p<0.05	p<0.1	p>0.1	p≥0.2		

Table 3.9: Regressions on cell properties. Independent variables are represented by columns, regressions run on different dependent variables by different rows. R² and adjusted R² indicates how well the regression describes the variation in the dependent variable. The colour of each cell represents significance (see colour legend, LM statistic in case of categorical variables with more than 2 categories (cell type, cell location, cortical lobe, epilepsy diagnosis group), t-statistic otherwise). For significant differences for categorical variables with more than two groups see table 6.4. Empty grey cells indicate that this independent variable was not included in the respective regression, otherwise, numbers represent beta-coefficients. Beta-coefficients describing the change for patients of different ages are given for increments of 10 years. ' $\sqrt{\cdot}$ ' and '(ln)' describe variable transformations. In the case of 'ln', beta-coefficients can be interpreted as x-fold changes rather than additions of x. In case of categorical independent variables, the groups are sorted from smaller to larger, beta-coefficients indicate the differences between adjoining groups. Abbreviations: s, supra; g, gran; i, infra; fr, frontal lobe; pa, parietal lobe; oc, occipital lobe; te, temporal lobe; f, female; m, male.

3.3.6 Cell-SPA interactions

In the following section, results about the cells' activity during SPA is presented. In case of multiple SPAs occurring in the same recording, each cell was analysed in respect to each SPA. This explains the higher case numbers for cell-SPA interactions than for SPAs or for cells. Due to the low case number of IIDs (n=8) overall and the low number of events in each case (medians: number of events: 20, recurrence frequency: 0.046 Hz), it was not deemed reasonable to carry out analysis investigating cell activity during IID. Thus, only interactions of cells and SPAs, but not of cells and IIDs were considered.

Local and distant cells

Local and distant cells were differentiated according to whether or not the SPA was visible in the cell layer (supra, gran or infra) where the respective cell was located. Table 3.10 shows that in NoEpi tissue the distribution of different cell types across local and distant cells is not equal. PCs were more likely to be found where SPA was present rather than where SPA was not present. As it is not expected that PCs moved within the tissue to the location of the SPA, the causality is probably reversed, leading to the notion that in NoEpi tissue, SPA was more likely to be generated where larger proportions of (active) PCs could be found. These trends were not present in ContrEpi or ResEpi tissue. However, in terms of the spatial distribution of cell types, it is difficult to compare ContrEpi to the other two as ContrEpi comprised a higher ratio of INs overall as discussed earlier.

		PC	IN	UC	Total
NoEpi	local	113 (43.3 %)	50 (19.2 %)	98 (37.5 %)	261 (100 %)
	distant	104 (30.4 %)	94 (27.5 %)	144 (42.1 %)	342 (100 %)
ContrEpi	local	12 (35.3 %)	12 (35.3 %)	10 (29.4 %)	34 (100 %)
	distant	6 (15.0 %)	23 (57.5 %)	11 (27.5 %)	40 (100 %)
ResEpi	local	66 (32.0 %)	64 (31.1 %)	76 (36.9 %)	206 (100 %)
	distant	68 (36.6 %)	50 (26.9 %)	68 (36.6 %)	186 (100 %)

Table 3.10: Numbers of local and distant cells. For each patient group, the division into local cells (SPA occurs in the layer of the cell) and distant cells is described. Absolute numbers as well as row percentages are displayed. The split into local and distant is not equal for different cell types in case of NoEpi ($p < 0.01$) and tends to be unequal in case of ContrEpi ($0.05 < p < 0.1$, both Chi-square). Post-hoc analysis revealed that in NoEpi there was a higher number of local PCs ($p < 0.05$) and tended to be a lower number of distant PCs ($0.05 < p < 0.1$).

Heterogeneous firing patterns during SPA

Figure 3.9 shows the PETH of each of the 1069 cell-SPA interactions analysed. It can be seen that PCs, INs as well as UCs actively participated in the SPA, but that a large proportion of cells in each group did not change its firing during the SPA. White lines in **A** and black lines in **B** indicate the borders between increased (top), unchanged (middle) and decreased (bottom) cell responses. It is clearly visible that a higher proportion of cells increased its firing in ResEpi than in NoEpi tissue (discussed in more detail below). Moreover, cells that increased their firing during the SPA fired in diverse temporal patterns during SPAs. There was no obvious difference in the firing patterns of PCs, INs and UCs. The PETHs in figure 3.9 show that there were examples of cells showing increased firing before, during and after the SPA peak in all the cell type groups.

In an attempt to quantify the involvement of a cell in an SPA, the cells' reliabilities and dependencies were determined. Here, a cell's reliability during an SPA is defined as the proportion of SPA events (± 50 ms) during which the cell fired at least one action potential, i.e. how reliably the cell fired during an SPA. It was found that cells in ResEpi tissue fired much more reliably during SPAs than NoEpi cells (significant for each cell type: PC: $p < 1E-09$, IN: $p < 1E-05$, UC: $p < 1E-06$, Kruskal-Wallis, for medians and CI see table 3.12, also see figure 3.11). However, the results of the regression on reliability (table 3.13 row 1) indicate that the patient group is not a significant predictor of reliability ($p > 0.1$) and that the observed differences were probably due to the differences in cell firing frequency between the patient groups. However, both the group-based (Kruskal-Wallis) and the regression analysis agree that INs show a higher reliability than PCs in both NoEpi and ResEpi tissue (NoEpi: $p < 0.05$, ResEpi: $p < 0.01$, Kruskal-Wallis, $p < 0.001$, regression). Moreover, a tighter connection of local than of distant cells to the SPA was reflected by a higher reliability of local cells ($p < 1E-10$, regression). The dependency of a cell, defined as the proportion of APs the cell fired during the SPA (± 50 ms) showed a similar picture (see table 3.12, figure 3.11 and table 3.13). Although a significant difference could be observed between the patient groups, with ResEpi cells showing a higher dependency than NoEpi cells (significant for each cell type: PC: $p < 0.01$, IN: $p < 0.01$, UC: $p < 0.01$), the results of the regression imply that this was due to the higher recurrence frequency of cells in the ResEpi group. Regression analysis (but not the comparison between groups using Kruskal-Wallis) also discovered that INs depend on SPAs to a larger extent than PCs ($p < 0.01$). Furthermore, the results of the regression imply that in

Figure 3.9: (PETHs of cell firing around SPA events cont.) (A): Within each panel, each row reflects the activity of one cell during one SPA expressed as a colour coded PETH. The x-axis represents time (± 150 ms, the green lines indicate the time of the SPA), the cell's firing frequency during the respective SPA is encoded by colours (white and yellow indicate high, black and red low firing frequencies, see the colour legend, compare to figure 3.1 under "original"). For visualisation purposes, each PETH was standardised using the number of cell and SPA events (see methods section 3.2.4). The 1069 PETHs are arranged into nine panels according to epilepsy status and cell type. Within each panel, white horizontal lines separate increased, unchanged and decreased cells as determined by the firing change quantile. The PETHs/rows are sorted from top to bottom according to the significance with which the cell increased or decreased its firing during the SPA (firing change quantiles), except for PETHs of increased cells, which are sorted by their time of maximal firing (see table 3.12). (B): Same arrangement as in (A). However, instead of the firing frequency, the firing change quantile is represented by colours (red for increased firing, blue for decreased firing, see the colour map). For these PETHs, the quantiles were assessed for each time bin separately. Analogous to (A), black horizontal lines separate increased, unchanged and decreased cells.

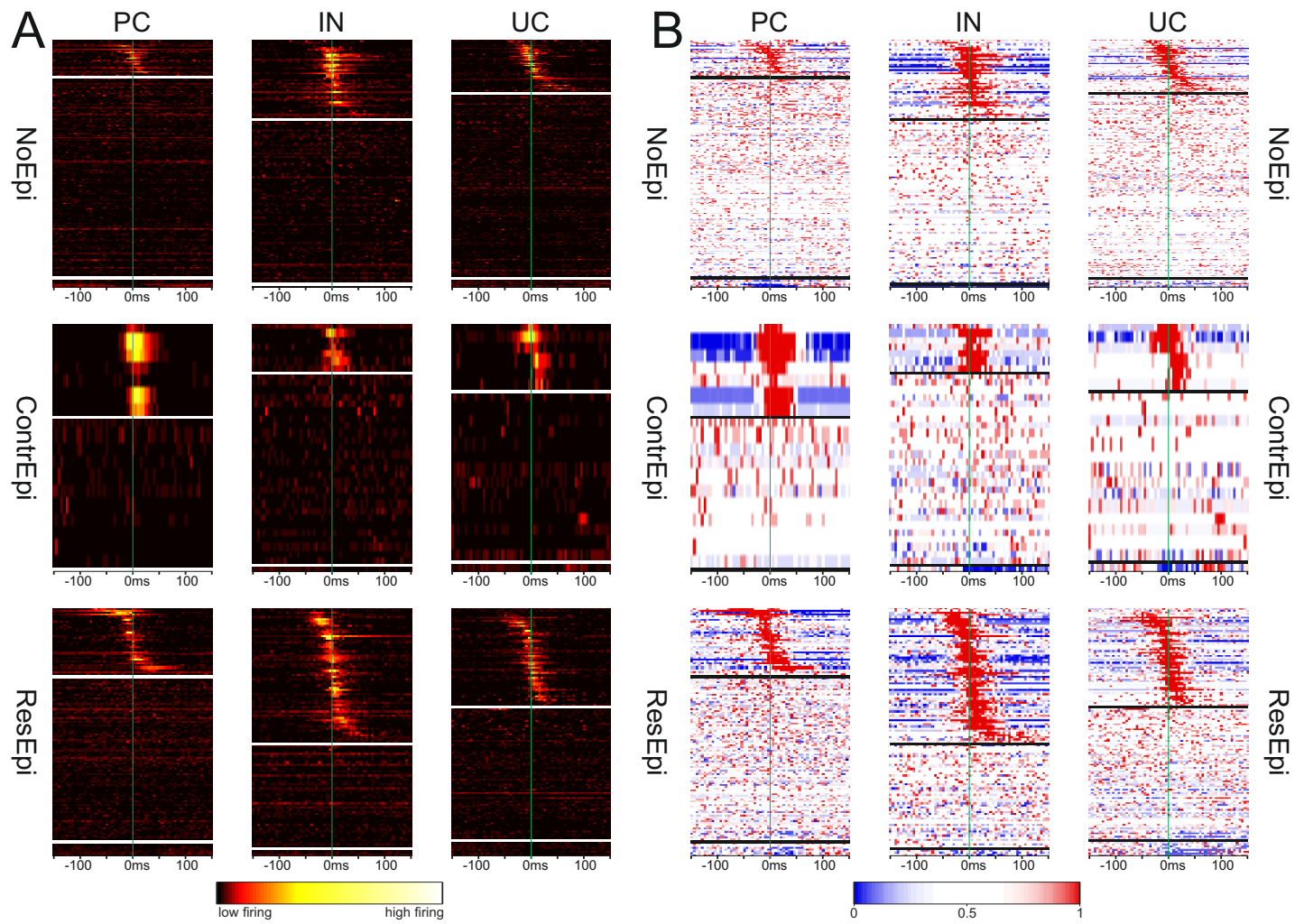


Figure 3.9: PETHs of cell firing around SPA events Description on the left page.

addition to a higher reliability, local cells also display a higher dependency on SPAs than distant cells.

In summary, ResEpi cells show a tighter connection to SPAs than NoEpi cells, which can be partially explained by their differences in firing frequency. Moreover, INs show a stronger involvement in SPAs than PCs and local cells are more engaged in SPAs than distant cells.

Increased and decreased cell responses

To assess whether a cell significantly changes its firing frequency during the SPA, firing change quantiles were computed. In short, the firing of a cell during the SPA was compared to the firing in randomised versions of the same SPA and cell spike trains. The values computed from the randomised spike trains reflected the firing change expected by chance alone (the null hypothesis). If the quantile of the actual firing frequency fell within extreme regions within the randomised values (between 0 and 0.025 or between 0.975 and 1), it was considered to be unlikely to happen by chance alone. In other words, that cell was considered to significantly change its firing during the SPA (for a more detailed explanation see section 3.2.4 and figure 3.1). Table 3.12 and figure 3.11 show the firing change quantiles for the different cell types and patient groups. However, the quantile itself is hard to interpret, as only values close to 0 or to 1 are meaningful and differences between values of e.g. 0.4 and 0.6 are close to meaningless. Thus, although the group medians and box plots displayed in table 3.12 and figure 3.11, respectively, suggest general tendencies of cell behaviour during SPA, it is more adequate to use the quantiles to distinguish between "increased", "unchanged" and "decreased" cell-SPA interactions and interpret those groups. Figure 3.10A-C shows five example cell responses during SPAs. Overall, only 3.3 % (35 / 1069) of cells showed a decreased firing response. This is probably due to the fact that a high baseline firing rate is necessary to detect a significant decrease in firing during the SPA. 28.9 % of cells (309 / 1069) significantly increased their firing, but the majority of cells (67.8 %, 725 / 1069) did not significantly change their firing rate during SPAs. Note that many of those cells might actually have responded to SPAs, but due to a low number of cell spikes or SPA events, the change was not significant. A Chi-square test revealed that the numbers of increased, unchanged and decreased responses were not equal across the three patient groups ($p < 1E-08$, Chi-square, see figure 3.10D, rows labelled "total" in table 3.11 and appendix table 6.7). Post-hoc testing revealed that ResEpi has a higher number of increased cells ($p < 1E-04$) and a lower number of unchanged cells ($p < 0.01$), while NoEpi has a lower number of increased cells ($p < 0.01$) and a higher number of unchanged cells ($p < 0.05$) than expected by chance. No significant post-hoc results were found for decreased cells or ContrEpi cells, probably due to low case numbers. This is in accordance with the increased participation of cells in ResEpi compared to NoEpi, as determined by their reliability and dependency, as described above.

Different cell types showed different response tendencies within the NoEpi ($p < 0.01$) and within the ResEpi group ($p < 0.001$, figure 3.10F, table 3.11 and appendix table 6.8). In both of these two groups, post-hoc analysis revealed that INs showed more increased responses and PCs showed fewer increased responses than expected by chance (NoEpi: $p < 0.01$ and $p < 0.05$, respectively, ResEpi: $p < 0.05$ both). The results of the regression predicting whether or not a cell increased its firing (table 3.13 row 3) confirmed the tendency that INs increased their firing more often

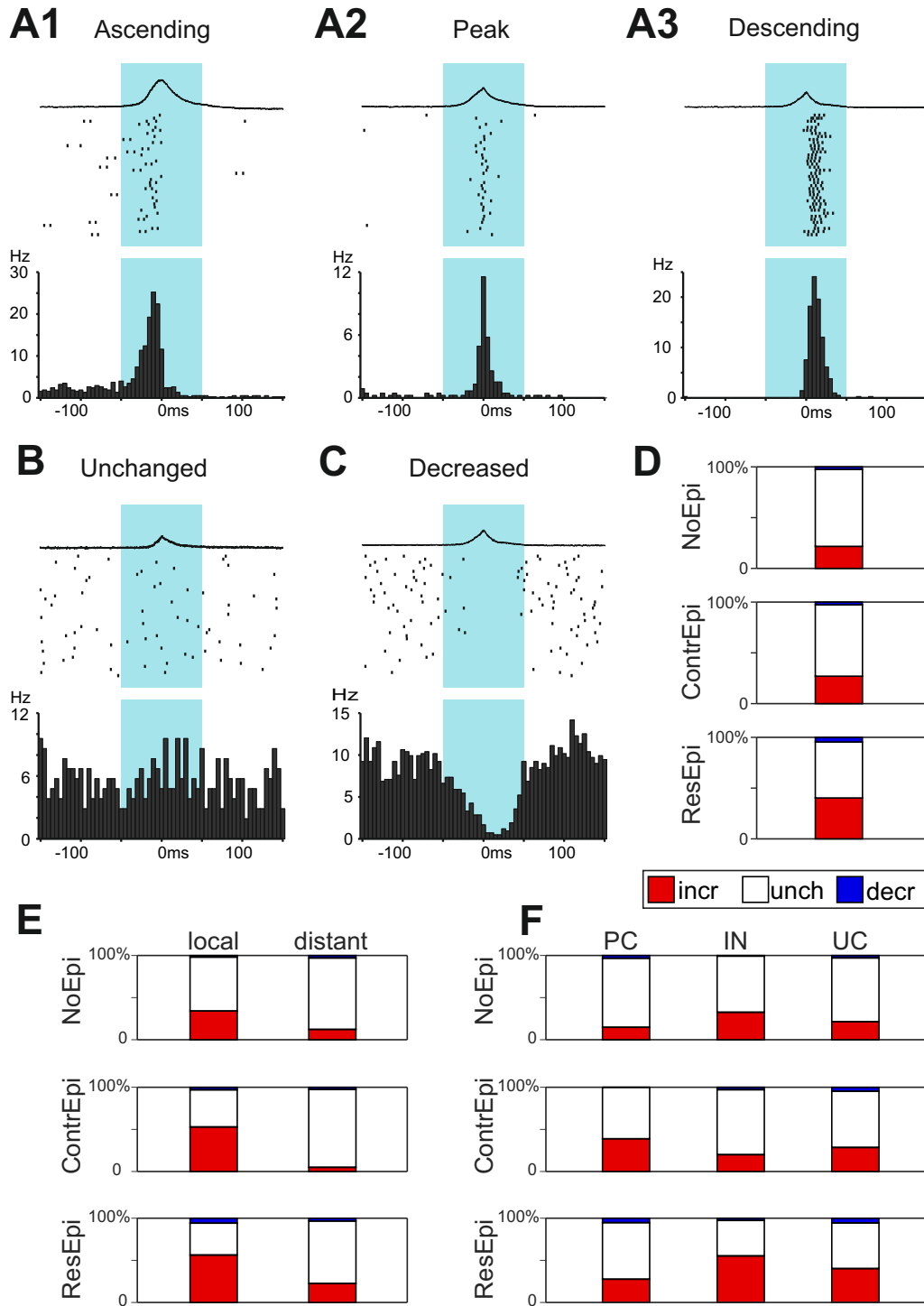


Figure 3.10: Cell firing patterns during SPA (A-C) Example raster plots (upper panels) and PETHs (lower panels) for different firing patterns relative to the SPA events. Three examples of increased firing (A1-3) as well as one for unchanged (B) and one for decreased (C) firing are displayed. The LFPg average of the respective SPA is shown at the top of each panel. Blue shading indicates the ± 50 ms time period used for calculating the firing change during the SPA. (D-F) Numbers of increased (red), unchanged (white) and decreased (blue) cells for each patient group. E also differentiates between local and distant cells, F between cell types (also see tables 3.11 and 3.14).

		incr.	unch.	decr.	total
NoEpi	PC	32 (14.7%)	178 (82.0%)	7 (3.2%)	217 (100%)
	IN	47 (32.6%)	96 (66.7%)	1 (0.7%)	144 (100%)
	UC	52 (21.5%)	183 (75.6%)	7 (2.9%)	242 (100%)
	total	131 (21.7%)	457 (75.8%)	15 (2.5%)	603 (100%)
ContrEpi	PC	7 (38.9%)	11 (61.1%)	0 (0.0%)	18 (100%)
	IN	7 (20.0%)	27 (77.1%)	1 (2.9%)	35 (100%)
	UC	6 (28.6%)	14 (66.7%)	1 (4.8%)	21 (100%)
	total	20 (27.0%)	52 (70.3%)	2 (2.7%)	74 (100%)
ResEpi	PC	37 (27.6%)	90 (67.2%)	7 (5.2%)	134 (100%)
	IN	63 (55.3%)	48 (42.1%)	3 (2.6%)	114 (100%)
	UC	58 (40.3%)	78 (54.2%)	8 (5.6%)	144 (100%)
	total	158 (40.3%)	216 (55.1%)	18 (4.6%)	392 (100%)

Table 3.11: Numbers of increased, unchanged and decreased PCs, INs and UCs For each patient and cell type group, the division into increased (incr.), unchanged (unch.) and decreased (decr.) cells is described. Absolute numbers as well as row percentages are displayed. For bar plots see figure 3.10F. For significant differences see appendix tables 6.7 and 6.8.

	NoEpi PC	NoEpi IN	NoEpi UC	ContrEpi PC	ContrEpi IN	ContrEpi UC	ResEpi PC	ResEpi IN	ResEpi UC
n (n*)	217 (32*)	144 (47*)	242 (52*)	18 (7*)	35 (7*)	21 (6*)	134 (32*)	114 (63*)	144 (58*)
firing reliability	1.05 [0.70 – 1.41]	2.24 [1.66 – 4.13]	1.33 [0.87 – 1.74]	2.61 [1.00 – 5.93]	3.75 [1.48 – 6.90]	2.00 [0.91 – 7.50]	3.97 [3.23 – 5.25]	11.83 [7.55 – 15.34]	3.18 [2.46 – 4.29]
firing dependency	12.50 [10.59 – 15.29]	13.67 [11.70 – 16.02]	13.61 [11.76 – 15.89]	15.44 [10.60 – 58.70]	12.64 [10.71 – 16.30]	12.39 [9.52 – 28.57]	14.88 [12.83 – 19.23]	21.07 [17.39 – 27.77]	19.38 [15.73 – 24.08]
quantiles	0.55 [0.47 – 0.63]	0.73 [0.63 – 0.86]	0.67 [0.58 – 0.78]	0.83 [0.57 – 1.00]	0.73 [0.56 – 0.90]	0.60 [0.28 – 0.82]	0.77 [0.70 – 0.88]	1.00 [0.92 – 1.00]	0.90 [0.71 – 0.97]
fir. incr.*	0.81 [0.69 – 0.84]	0.87 [0.82 – 0.93]	0.87 [0.83 – 0.92]	0.99 [0.94 – 0.99]	0.84 [0.79 – 0.97]	0.92 [0.90 – 0.97]	0.77 [0.73 – 0.87]	0.84 [0.78 – 0.92]	0.87 [0.81 – 0.93]
fano factor*	1.64 [1.34 – 2.00]	1.00 [0.96 – 1.19]	1.15 [1.04 – 1.50]	1.10 [0.93 – 1.27]	0.81 [0.73 – 1.11]	1.03 [0.96 – 1.99]	1.01 [0.95 – 1.38]	0.95 [0.91 – 0.98]	0.98 [0.97 – 1.03]
max firing* (ms)	0.00 [-7.50 – 5.00]	0.00 [0.00 – 5.00]	0.00 [-5.00 – 5.00]	5.00 [0.00 – 10.00]	0.00 [-5.00 – 5.00]	7.50 [0.00 – 15.00]	0.00 [-5.00 – 5.00]	0.00 [0.00 – 5.00]	0.00 [-5.00 – 5.00]
rel max firing*	1.50 [-1.50 – 3.00]	1.50 [0.50 – 2.50]	1.50 [-0.50 – 5.50]	1.50 [0.50 – 2.50]	1.50 [0.50 – 2.50]	3.50 [-0.50 – 8.00]	1.50 [0.50 – 2.50]	1.50 [1.50 – 2.50]	1.00 [0.50 – 2.50]

Table 3.12: Properties of cell-SPA interactions Properties of neuronal behaviour during SPA for different cell types and patient groups. The median and its 95 % CI (in square brackets) are displayed. An asterisk (*) next to the variable name indicates that only increased cells were analysed. For box plot visualisations see figure 3.11, for significant differences see appendix table 6.5.

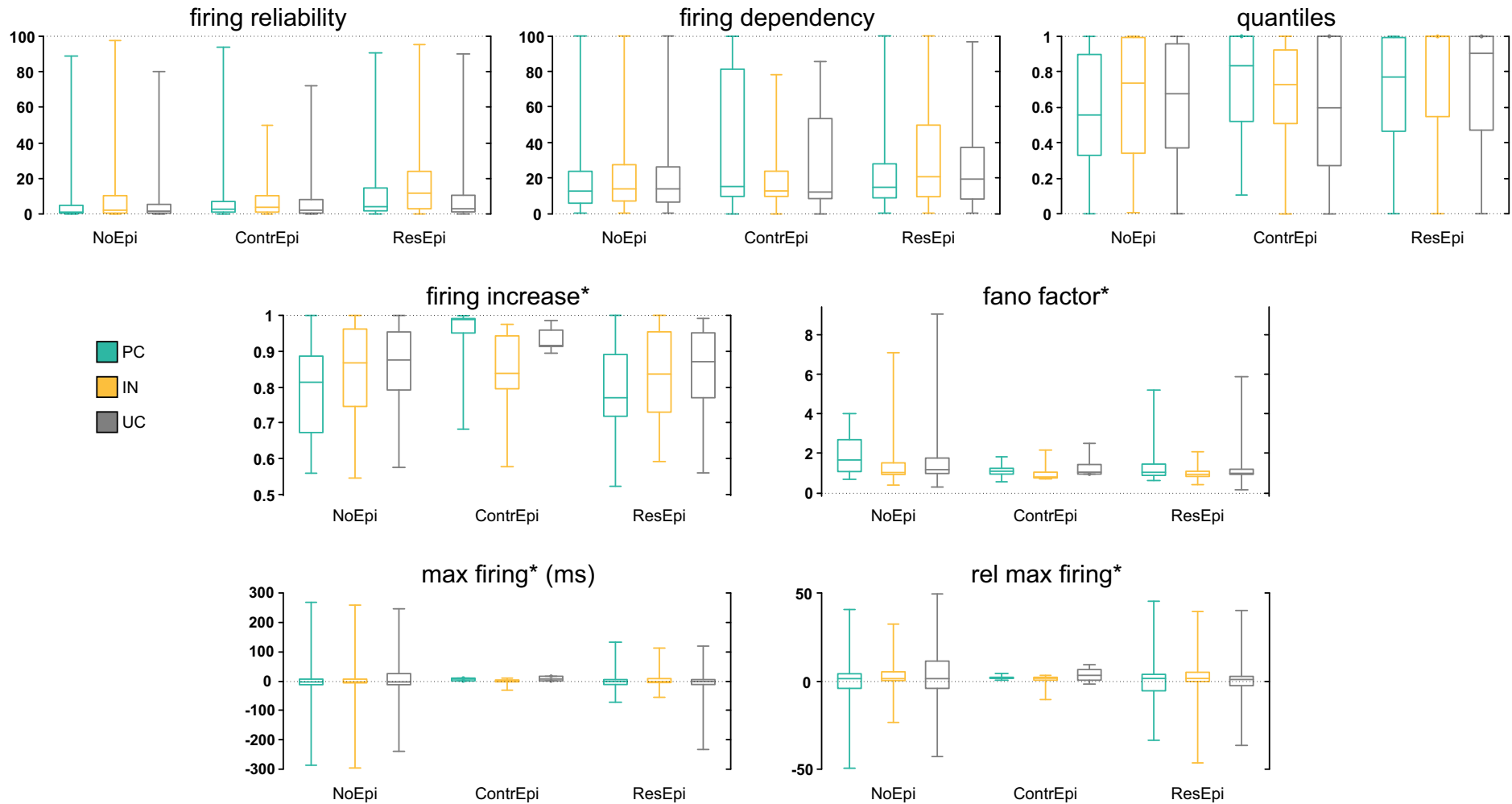


Figure 3.11: Properties of cell-SPA interactions Box plots visualising the properties of neuronal behaviour during SPA for different cell types and patient groups. An asterisk (*) next to the variable name indicates that only increased cells were analysed. For medians and their CIs see table 3.12, for significant differences see appendix table 6.5.

	R ² (adj. R ²)	SPA median ISI (ln)	SPA freq (ln)	Cell median ISI (ln)	Cell freq (ln)	Cell burst- ness	Cell type	SPA location (layers)	Cell location (layers)	Local / distant cell	Cortical lobe	Epilepsy diagnosis group	Patient age	Patient gender
reliability ($\sqrt[3]{}$)	0.769 (0.765)	0.48	0.27	0.11	0.57	0.22	PC 0.12 UC 0.04 IN	s 0.09 i 0.38 e	s 0.02 g 0.02 i	di 0.29 lo	oc 0.04 te 0.01 fr 0.10 pa	NoEpi 0.03 ResEpi 0.12 ContrEpi	-0.04	m 0.00 f
dependency ($\sqrt[3]{}$)	0.276 (0.263)	0.61	1.11	0.05	0.15	-0.26	PC 0.23 UC 0.02 IN	s 0.04 i 0.27 e	s 0.09 g 0.05 i	di 0.55 lo	oc 0.03 fr 0.02 te 0.06 pa	NoEpi 0.10 ResEpi 0.11 ContrEpi	-0.06	m 0.11 f
whether increased	0.253 (0.240)	0.42	0.31	0.04	0.07	0.18	PC 0.11 UC 0.06 IN	s 0.02 i 0.28 e	i 0.05 g 0.02 s	di 0.23 lo	oc 0.05 te 0.02 fr 0.09 pa	NoEpi 0.04 ContrEpi 0.00 ResEpi	-0.03	m 0.06 f
firing increase intensity*	0.417 (0.379)	0.03	-0.02	0.03	-0.02	0.27	PC 0.03 UC 0.01 IN	i 0.03 s 0.09 e	i 0.00 g 0.01 s	di 0.05 lo	oc 0.12 pa 0.03 fr 0.07 te	ResEpi 0.03 NoEpi 0.07 ContrEpi	-0.01	m 0.04 f
fano factor*	0.648 (0.625)	0.18	0.29	-0.16	-0.21	0.44	UC 0.03 IN 0.03 PC	e 0.12 s 0.00 i	i 0.07 s 0.00 g	lo 0.09 di	pa 0.00 fr 0.05 te 0.14 oc	ContrEpi 0.04 ResEpi 0.08 NoEpi	0.00	f 0.06 m
max firing* ($\sqrt[3]{}$)	0.082 (0.021)	1.27	1.11	0.03	-0.02	-0.38	PC 0.21 UC 0.43 IN	i 0.30 e 0.11 s	s 0.18 g 1.03 i	di 0.04 lo	pa 0.13 fr 0.02 oc 0.01 te	ResEpi 0.66 NoEpi 0.15 ContrEpi	-0.08	f 0.19 m
rel max firing*	0.095 (0.035)	-2.49	-1.91	-0.31	1.05	0.69	PC 2.85 IN 0.47 UC	e 4.21 s 3.54 i	g 2.13 s 6.53 i	lo 1.69 di	pa 0.02 fr 0.06 oc 0.00 te	ContrEpi 0.47 ResEpi 2.38 NoEpi	-0.87	m 2.53 f
		Colour legend		p<1E-10	p<0.001	p<0.05	p<0.1	p>0.1	p≥0.2					

Table 3.13: Regressions on cell-SPA relation properties. Independent variables are represented by columns, dependent variables by different rows. The colour of each cell represents significance (see colour legend). The numbers in each cell represent beta-coefficients. Those for age are given for increments of 10 years. ' $\sqrt[3]{}$ ' and '(ln)' describe variable transformations. For categorical independent variables, the groups are sorted from smaller to larger, beta-coefficients indicate the differences between adjoining groups. For significant differences for categorical variables with more than two groups see table 6.6.

than PCs (overall: $p < 1E-05$, PC<IN: $p < 1E-05$, PC<UC: $p < 0.001$, UC<IN: $0.05 < p < 0.1$). The difference in cell responses between cell types is also nicely visible in the colour coded PETHs in figure 3.9. Note that although the trend of INs showing a larger proportion of increased cells (in NoEpi and ResEpi) was reversed in ContrEpi, this was not significant due to the low case number in that patient group ($p > 0.5$, Fisher's exact test).

Summarising, a higher proportion of ResEpi cells seemed to increase their firing during SPA events than in the other two patient groups. Moreover, increased firing seemed to be more common in INs than in PCs.

Strong differences in responses were found within each patient group between cells that were local or distant to the SPA (NoEpi: $p < 1E-09$, Chi-square, ContrEpi: $p < 1E-05$, Fisher's exact test, ResEpi: $p < 1E-11$, Chi-square). In all three patient groups, there was a higher number of increased local and unchanged distant cells while there was a lower number of unchanged local and increased distant cells than expected by chance (see figure 3.10E, table 3.14 and appendix table 6.9). This suggests that local cells were much more involved in SPAs than distant cells, confirming the results concerning reliability and dependency. Likewise, regression analysis revealed that the location of a cell relative to the SPA was one of the strongest predictors for whether or not a cell increased its firing (table 3.13 row 3, $p < 1E-10$). Interestingly, the location of the cell within the neocortical layers itself (i.e. not in comparison to the location of the SPA) did not significantly affect whether or not a cell increased its firing ($p > 0.1$). However, although not significant, the largest difference that could be observed between cells from different cell layers was that infra cells participated slightly less in SPAs than supra cells did ($0.05 < p < 0.1$, table 3.13 row 3). This is noteworthy as it is the opposite of what would be expected if SPAs were to be considered epileptiform events [32]. The location of the SPA itself (i.e. not in comparison to the location of the cell) did not significantly affect the involvement of the cell ($p > 0.2$).

Overall, this implies that SPAs were a very local event within the neocortical layers, as distant cells participate much less than cells located in the area where the SPA was visible on the averaged LFPg trace, independent of the specific cell layers involved.

Intensity and variability of increased cell responses

In order to further characterise increased cell responses, the intensity and the variability (fano factor) of the responses were assessed (see table 3.12 and figure 3.11). Decreased cells were not analysed separately due to their low case number overall ($n=35$). The change in firing frequency was calculated as the ratio of the firing frequency within ± 50 ms around each SPA to the firing frequency outside those time periods. There were no significant differences in the intensity with which increased cells increased their firing between patient groups and cell type groups (all $p > 0.2$, Kruskal-Wallis, see table 3.12). However, regression analysis revealed a weak but significant effect which the epilepsy diagnosis status had on the firing change intensity ($p < 0.05$, table 3.13 row 4). Surprisingly, ContrEpi cells showed a higher firing increase than ResEpi and NoEpi cells (NoEpi<ContrEpi: $p < 0.05$, ResEpi<ContrEpi: $p < 0.01$). Moreover, taking differences such as firing frequency into account, regression analysis further identified a weak difference in firing change intensity between the cell types. According to this analysis, INs increased their firing more strongly during SPA than PCs ($p < 0.01$). How intensely a cell responds further seemed to

		incr.	unch.	decr.	total
NoEpi	local	89 (34.1 %)	167 (64.0 %)	5 (1.9 %)	261 (100 %)
	distant	42 (12.3 %)	290 (84.8 %)	10 (2.9 %)	342 (100 %)
	total	131 (21.7 %)	457 (75.8 %)	15 (2.5 %)	603 (100 %)
ContrEpi	local	18 (52.9 %)	15 (44.1 %)	1 (2.9 %)	34 (100 %)
	distant	2 (5.0 %)	37 (92.5 %)	1 (2.5 %)	40 (100 %)
	total	20 (27.0 %)	52 (70.3 %)	2 (2.7 %)	74 (100 %)
ResEpi	local	116 (56.3 %)	78 (37.9 %)	12 (5.8 %)	206 (100 %)
	distant	42 (22.6 %)	138 (74.2 %)	6 (3.2 %)	186 (100 %)
	total	158 (40.3 %)	216 (55.1 %)	18 (4.6 %)	392 (100 %)

Table 3.14: Numbers of increased, unchanged and decreased cells: local and distant cells For each patient and cell location relative to the SPA, the division into increased (incr.), unchanged (unch.) and decreased (decr.) cells is described. Absolute numbers as well as row percentages are displayed. For bar plots see figure 3.10E. For significant differences see appendix tables 6.7 and 6.9.

depend on the recurrence frequency of the cell and whether it was a local or distant cell compared to the SPA (distant<local, $p<0.001$). Moreover, cells that showed bursting behaviour increased their firing more intensely than non-bursting cells ($p<1E-11$).

In terms of the variability of cell responses of increased cells (fano factor, see methods section 3.2.4), NoEpi PCs were found to be the group with the largest variance in their responses. Their responses were significantly more variable than those of NoEpi INs or ResEpi PCs ($p<0.01$ and $p<0.05$, respectively, Kruskal-Wallis). According to regression analysis, these differences can be attributed to other features such as differences in cell recurrence frequency or burstiness (see table 3.13 row 5). Interestingly, local increased cells were found to have more stable responses than distant increased cells ($p<0.05$), which fits to the finding that local cells also show higher reliability overall (discussed above).

As mentioned earlier, figure 3.10 shows that cells display diverse firing patterns during the SPA. Moreover, in figure 3.9 it is visible how some cells started firing 50 ms and in rare cases even 100 ms before the SPA, while others fired only during a very short time period or kept firing after the SPA. In an attempt to quantify the temporal firing pattern of a cell, the time of maximal firing frequency was assessed for the cell-SPA PETHs of increased cells in milliseconds (ms) as well as relative to the SPA shape (see figure 3.11, table 3.12 and section 3.2.4). Neither the Kruskal-Wallis test nor the regression analysis could identify significant differences between patient or cell type

groups (table 3.12, all $p > 0.7$). This indicates that there was no clear temporal firing sequence of different cell types and that there was no association between the time of maximal firing and the cell type. Regression analysis (table 3.13) confirmed that the cell type did not influence the timing of a cell's firing. However, the results indicated that, independent of the location of the SPA, infragranular cells fired later than supragranular and granular cells (max firing: $p < 0.05$, rel max firing: $p < 0.01$; gran earlier than infra: max firing: $p < 0.05$, rel max firing: $p < 0.01$; supra earlier than infra: max firing: $p < 0.05$, rel max firing: $0.05 < p < 0.1$).

Cell firing during multiple simultaneous SPAs

Cellular responses during multiple simultaneous SPAs were investigated as described in the methods section 3.2.4. In short, responses of cells to multiple simultaneously occurring SPAs were evaluated based on how many ("none", some: "differential" or "all") SPAs the cell responded to with in- or decreased firing. When ResEpi and NoEpi were compared directly, it could be seen that ResEpi cells tended to produce more uniform responses than expected (table 3.15 Chi-square: $p < 0.01$, post-hoc: more uniform responses in ResEpi: $p < 0.05$, post-hoc significances are visualised in appendix table 6.10). However, when the expected none, differential and uniform responses were calculated from the number of increased, unchanged and decreased cells (analysed and tested independently for NoEpi and ResEpi), the results indicated that both NoEpi and ResEpi non-significantly tended to prefer "uniform" and/or "none" responses compared to "differential" responses (NoEpi: $p > 0.1$, ResEpi: $0.05 < p < 0.1$, post-hoc significances are visualised in appendix table 6.11). Thus, there seem to have been slightly more cells that responded to no or all SPAs than expected and fewer cells that only respond to some but not all SPAs. This implies that some cells were more prone to participating in SPAs than other cells and the participation of a cell in one SPA raised the chance of it also participating in other SPAs. As explained in the methods section, increased and decreased responses were both counted as "responding" and not differentiated for this analysis. For the vast majority of cases (23 / 24, 95.8%), a uniform response meant that the cell increased its firing during all SPAs or decreased its firing during all SPAs. However, one cell (from patient E15, ResEpi group, located in the supragranular layer) has been observed which increased its firing during one SPA (supra SPA, quantile = 1) and decreased its firing during the other SPA (infra SPA, quantile = 0.0045). This cell was counted as responding to all SPAs. It should be noted that although the in- and decreases in cell firing were significant, they were not very intense changes.

		none	differ- ential	uni- form	total
NoEpi	PC	52 (72.2 %)	16 (22.2 %)	4 (5.6 %)	72 (100 %)
	IN	12 (44.4 %)	13 (48.1 %)	2 (7.4 %)	27 (100 %)
	UC	27 (44.3 %)	28 (45.9 %)	6 (9.8 %)	61 (100 %)
	total	91 (56.9 %)	57 (35.6 %)	12 (7.5 %)	160 (100 %)
ResEpi	PC	8 (47.1 %)	7 (41.2 %)	2 (11.8 %)	17 (100 %)
	IN	6 (33.3 %)	5 (27.8 %)	7 (38.9 %)	18 (100 %)
	UC	9 (37.5 %)	12 (50.0 %)	3 (12.5 %)	24 (100 %)
	total	23 (39.0 %)	24 (40.7 %)	12 (20.3 %)	59 (100 %)

Table 3.15: Cell responses during multiple SPAs For each patient and cell type group, the division into none, differential and uniform cells is described. Absolute numbers as well as row percentages are displayed. For significant differences see appendix tables 6.10 and 6.11.

3.4 Discussion

3.4.1 SPAs are not interictal spikes

Spontaneous population bursts were generated in neocortical slices derived from pharmacoresistant (ResEpi) and pharmacoresponsive (ContrEpi) epileptic patients as well as non-epileptic (NoEpi) patients (also see [13]). SPAs described in these patients showed remarkable similarities to population activity detected in epileptic human hippocampal [8, 10, 11] and neocortical [12, 14] slices. However, the epileptogenicity of the *in vitro* spontaneous network events was questioned by one research group who compared population bursts emerging in the human epileptic neocortex to the physiologically occurring sharp-wave ripple complexes [12, 63]. On the other hand, these bursts were called interictal-like activity in neocortical slices from tumour patients with and without preoperative seizures [14]. The patients included in the latter study suffered from gliomas known to be highly epileptogenic, and the authors related the emergence of these events to the epileptogenicity of the human peritumoural neocortex. In the study presented here, spontaneous population bursts could be detected in tumour patients without preoperative seizures (the NoEpi group), including not only glial tumours but metastasis of carcinomas, as well as other symptoms, such as meningioma or haematoma (see table 3.2).

Moreover, while SPAs detected in epileptic (ResEpi and ContrEpi) and non-epileptic (NoEpi) tissue were mainly similar, the presented results strongly suggest that SPAs considerably differ

from both *in vitro* IID and interictal spikes occurring in epileptic patients (figures 3.3 and 3.4 and table 3.4). The recurrence frequency of SPAs (1 Hz) was significantly higher than that of IIDs (0.05 Hz), with the latter being closer to 4-aminopyridine induced epileptiform activity (0.3 to 0.1 Hz) in the human neocortex *in vitro* [89] and to spiking activity in the subiculum (0.15 Hz) of epileptic patients [34]. The significantly higher LFPg and MUA amplitudes of IID suggest that a considerably larger set of neurons is involved in these hypersynchronous events than in the SPAs. Moreover, the intracortical emergence site was different: SPAs were mainly generated in the supragranular layers (figure 3.6 and table 3.5 as well as [12, 14]) and activity of supragranular as well as granular cells tended to precede the firing of infragranular cells (table 3.13), while *in vitro* spontaneous IIDs (presented here) and *in vivo* interictal spikes [32] emerged in the granular or infragranular layers (figure 3.6 and table 3.5). Furthermore, interictal-like activity induced by 4-aminopyridine in human neocortical slices also arose from the middle (possibly corresponding to the granular) layer [89].

3.4.2 The role of bursting behaviour in the generation of population activity

The firing of bursting neurons showed a close correlation with the emergence of interictal spikes in humans *in vivo* [60]. The analysis of burstiness of human neocortical neurons in our study indicates that the burstiness of neurons in the infragranular layers (which generate *in vivo* interictal spikes as discussed above [32]) was lower than that in the supragranular layers (table 3.9). This means that the generation mechanisms for SPAs differ from those of *in vivo* interictal spikes. However, there seems to be a relationship between burstiness and neuronal participation in SPAs, as cells that show more bursting behaviour increased their firing more intensely than non-bursting cells (table 3.13).

Surprisingly, the results presented here revealed that the burstiness of cells in ResEpi tissue was significantly lower than that in NoEpi or ContrEpi tissue (figure 3.8 and tables 3.8 and 3.9), indicating that burst firing is not essential for the initiation of SPAs or IIDs. An interesting aspect of this is that in contrast to ResEpi PCs, ContrEpi PCs were able to fire action potentials in bursts (as do NoEpi neurons). Moreover, ContrEpi INs were found to fire more irregularly than ResEpi and even NoEpi INs (figure 3.8 and tables 3.8 and 3.9). This raises the question whether the loss of neuronal burstiness in PCs and/or the firing irregularity of INs is causally linked to the success of pharmacological antiepileptic treatment. It would be interesting to study this relationship in an extended dataset including more patients with controlled epilepsy at the time of surgery. One of the questions that could be addressed is the relation between the mechanism of action of the antiepileptic drug and the consequences on the firing patterns such as burstiness for different cell types.

3.4.3 Simultaneous generation of SPAs and IIDs

The relatively low incidence of spontaneous IIDs in the study presented here (table 3.3) is in accordance with previous findings, i.e. overt epileptiform activity usually does not emerge spontaneously, but can be induced under appropriate pharmacological conditions [90]. Interestingly,

when epileptiform activity was induced in human subicular (via decreased extracellular Mg^{+} concentration or increased pH [91]) or mouse hippocampal slices (via decreased extracellular Mg^{+} or increased extracellular K^{+} concentrations, 4-aminopyridine, or gabazine [92]), the slices underwent a transition from a state in which spontaneous activity was generated to a state in which pharmacologically induced epileptiform activity was generated. Except for a short time period during the transition phase in the human subicular slices [91], the states in which the slice could generate these different types of events were mutually exclusive. In contrast, the IID presented here could occur simultaneously with SPAs (figure 3.5C) and were generated without pharmacological manipulations of the tissue slices. It can be speculated that the reason for the largely mutually exclusive physiological and epileptiform activities lies within the pharmacologically induced nature of the latter, i.e. the pharmacological alterations that enable the generation of the epileptiform type restrict the generation of the physiological type of activity. The data presented in this study suggest that physiological (SPA) and epileptiform (IID) events can occur simultaneously if none of them requires altered pharmacological conditions for their generation. These results demonstrate that SPA is a network phenomenon different from epileptic or epileptiform discharges. Since SPAs detected in NoEpi were nearly identical to those found in the epileptic neocortex (ResEpi and ContrEpi), it can be assumed that it is generated independently of epilepsy, and therefore cannot be considered as the *in vitro* correlate of interictal spikes.

3.4.4 SPAs and IIDs are mostly local events

As to the spatial extent, SPAs were usually local events in regard to neocortical layers, remaining within laminar borders. As it has been shown that interictal spikes are generated in layers IV and V [32], we considered the possibility that supragranular SPAs were initiated by the firing of infragranular cells. However, the findings that infragranular cells do not increase their firing more than supragranular or granular cells and tend to fire later during the SPAs than supragranular or granular cells (table 3.13), contradict this hypothesis. Moreover, neurons preferred to participate in the SPAs emerging close to the cell body and were mostly not responding to SPAs initiated in other layers (see results on local vs. distant neurons e.g. table 3.14 or figure 3.10E). Largely limited cortical synaptic connections – due to slice preparation procedures – also indicate a local generation for SPAs.

The laminar occurrence of SPAs properly reflects intra- and interlaminar connections in neocortical slices. SPAs were often observed within the same neocortical layer across a large portion of the neocortical slice. This suggests that the connectivity within the neocortical layers is stronger than within the neocortical columns (which run perpendicular to the neocortical layers). This fits to literature describing that local axonal arborisation is more extensive within each neocortical layer than interlaminar connections [93]. Moreover, supragranular connections have been shown to be stronger than infragranular ones [94], which fits to our finding that supragranular SPAs are more common than infragranular ones (table 3.5 and figure 3.6). Thus, the data presented here provide further evidence against the notion of the cortical column being a major functional unit of the brain [95]. This is in accordance with other studies that have questioned the functional relevance of the cortical columns [96].

The laminar restriction of the SPAs is not caused by a failure to generate SPAs in the other neocortical layers, as multiple simultaneous SPAs could occur in different layers independently (section 3.3.3). As mentioned in section 3.3.3, some crosstalk between the neuronal populations generating the different spatial types must be assumed, as the different types sometimes occurred at the exact same time, possibly triggering one another. Moreover, many neurons were involved in more than one or all SPAs (section 3.3.6). This concept was strikingly similar to the situation we observed in the rat hippocampus, where the findings also supported the notion of overlapping neuronal populations generating (or participating in) different types of population activity (section 2.4.3). However, in both the rat hippocampal SPWs (sections 2.3.8 and 2.3.9) and the human neocortical SPAs (section 3.3.6), neurons were shown to be able to differentiate between the different types of population activity and adjust their firing patterns accordingly.

3.4.5 Increased excitability in epilepsy modifies SPAs

SPAs found in epileptic and non-epileptic patients were basically similar regarding network and cellular characteristics (figures 3.3 and 3.4 and table 3.4). SPAs in the epileptic neocortex differed though in a few aspects from those in tumour tissue, which all point to the hyperexcitability of the epileptic neuronal network [97]. The LFPg amplitude of SPAs was higher and more neurons enhanced their firing rate during SPAs in the epileptic compared to non-epileptic neocortex (figures 3.4 and 3.10 and tables 3.4, 3.11 and 3.14). Moreover, it was found that NoEpi required a higher number of local PCs to be able to generate SPA compared to ResEpi (table 3.10). It can be speculated that a higher number of PCs was required to balance the inhibitory action of INs. According to this hypothesis, the amount of excitation is not sufficient for generating SPAs in areas where fewer PCs are present (in relation to INs). The finding that ResEpi is able to generate SPAs in areas with a lower ratio of active (and thus detectable and clusterable) PCs (than in NoEpi) gives reason to speculate that cells are more excitable overall in ResEpi, enabling a lower number of PCs to balance the inhibition present in ResEpi tissue. One mechanism for this might be the difference in mean firing frequency between ResEpi and NoEpi. While both PCs and INs displayed higher firing frequencies in ResEpi compared to NoEpi, it is worth noting that the difference was larger for PCs than for INs (table 3.8 and figure 3.8). This apparent difference in excitation might be caused by the synaptic reorganisation that takes place in epileptic tissue, which results in highly interconnected PCs [98].

The shift in balance between excitation and inhibition might also explain the tighter connection of the neuronal firing to the present SPAs, as the firing frequency of a cell was positively affecting features such as the reliability, dependency and whether or not a cell increased its firing during the SPA (though, to a smaller extent it negatively affected how much it increases its firing during the SPA). In summary, ResEpi cells show a tighter connection to SPAs, which can at least partially be explained by their differences in firing frequency.

3.4.6 The role of excitatory and inhibitory neuronal activity during SPAs

Despite its importance, excitatory action was not the sole contributor to SPA activity. In all patient groups both PCs and INs were found to participate in the generation of SPA (e.g. figure 3.10). However, INs showed a stronger involvement in the SPA than PCs (as indicated by their reliability, dependency and proportion of neurons showing increased firing, table 3.12 and figures 3.11 and 3.10).

Notably, in the ContrEpi group a larger number of INs was detected compared to the other two patient groups (table 3.7). Although this does not necessarily reflect a higher number of INs in ContrEpi patients, it is a consequence of a higher number of *active* INs in that group. It can be speculated that this higher number of active INs in ContrEpi tissue (compared to ResEpi tissue) might be the reason why an increase in GABA-mediated inhibition (a common strategy of antiepileptic drugs, for review see [99]) resulted in the successful antiepileptic treatment in this group of patients.

In terms of firing sequences, Pallud and colleagues [14] suggested that interneurons initiate synchronous population events while pyramidal cells follow. In contrast to this, in our dataset both cell types were observed to display diverse temporal firing patterns (figure 3.9) and that there were no significant differences in their time of maximal firing in all three patient groups (tables 3.12 and 3.13). The variable firing patterns of the observed cells recall the situation observed during interictal discharges *in vivo* [60], where a large diversity of neuronal firing pattern has been described in the human epileptic neocortex. This suggests that multiple distinct neuronal groups interact to generate hypersynchronous discharges. Furthermore, an earlier *in vitro* study investigated the complex connectivity of human neocortical microcircuits [100]. They reported complex event sequences initiated by single pyramidal cell action potentials in non-epileptic human neocortical slices. Thus, the active participation of both PCs and INs, the presented heterogeneous firing patterns of the involved cells as well as the occurrence of multiple SPAs and simultaneous SPAs-IIDs in the same slice indicate the presence of an exceptionally complex neuronal network able to induce complex synchronies.

4. Conclusion and Thesis statements

Many valuable insights into the neuronal mechanisms behind cortical synchronous population activities could be gained by studying the *in vitro* slice models of *in vivo* population activities.

It could be shown that the rat hippocampus is able to generate two different types of sharp-waves (SPWs) *in vitro*. Different neuronal populations, with different proportions of pyramidal cells and distinct subsets of interneurons, were activated during the two types of SPWs. The activation of specific inhibitory cell subsets, with the possible leading role of perisomatic INs seems to be crucial to synchronise distinct ensembles of CA3 pyramidal cells, resulting in the expression of different SPW activities. The fact that both types of SPWs could occur simultaneously in the same slice suggests that the hippocampus can generate dynamic changes in its activity stemming from the same excitatory and inhibitory circuits, even *in vitro*.

Similarly, human neocortical slices from epileptic as well as non-epileptic patients were able to generate multiple different types of synchronous population activity (SPA), which differed in their spatial distribution across the neocortical layers. These spatial subtypes sometimes interacted and triggered each other, which indicates cross-talk between the neuronal populations involved in their generation. However, cells could differentiate between different spatial subtypes of SPAs, many of them participating in some but not all spatial subtypes of SPAs. Together with the finding that both excitatory and inhibitory neuronal populations participate, this demonstrates that SPAs are complex events at the neuronal network level. Although SPAs are similar across tissue from patients with different epilepsy statuses, some differences could be observed, mostly in the behaviour of neurons during SPAs, which point to an increased amount of excitation in the epileptic tissue.

In addition to those spatial subtypes of SPAs, tissue slices from epileptic patients were able to generate a qualitatively different type of synchronous activity (IIDs) which resembled interictal activity observed *in vivo*. The finding that SPAs, but not IIDs could be observed in non-epileptic patients shows that SPAs cannot be related to epileptic processes. Moreover, differences between epileptic patients whose epilepsy could be controlled or not controlled pharmacologically were discovered in the process, potentially guiding the way for future studies investigating why and how antiepileptic treatment does not work in all patients.

These results suggest that the rat hippocampal CA3 region and the human neocortical neuronal networks can generate complex patterns of population activity *in vitro*. The findings constitute a substantial contribution to the current scientific knowledge on cortical synchronous events *in vitro* and, in case of the human neocortical events, provide valuable insight into the differences between physiological and pathological synchronies.

4.1 Thesis statements

4.1.1 Thesis group 1: Rat SPW study findings

- Ia** *This is the first time a multielectrode has been used to differentiate between different types of rat hippocampal SPWs. Due to the spatial information the multielectrode provides, the different LFPg and current source density patterns of the two SPW types could be discovered. SPWs with a negative LFPg peak in the str. pyramidale and a positive peak in the str. radiatum (apical dendritic layer) were called type 1. The CSD pattern of T1 SPWs consisted of a sink-source pair in the str. pyramidale. On the other hand, positive LFPg peaks in the str. pyramidale as well as in the str. lacunosum-moleculare (distal apical dendrites) combined with a negative LFPg peak in the str. radiatum (apical dendritic layer) were termed type 2. This type exhibited a sink-source triplet: a source in the str. pyramidale, adjoined by one sink each in the str. oriens and str. radiatum. They further differed in their amplitude and recurrence frequency. The two types of SPWs could not be distinguished on one-channel referential recordings.*
- Ib** *The two types of SPWs can occur simultaneously in the same recording. Two overlapping but distinct subpopulations seemed to have created the different synchronous population activities at the same time. Clustered neurons can differentiate between the two types of SPWs, with some of them adjusting their firing pattern accordingly.*
- Ic** *Both types of SPWs depend on both excitatory and inhibitory processes. This was apparent as both types were blocked during the application of either an AMPAR and KA receptor antagonist (NBQX) or a GABA_AR antagonist (bicuculline).*
- Id** *The two types of SPWs are generated by different mechanisms, involving different subpopulations of interneurons. This was revealed by the application of DAMGO, a μ -opioid receptor agonist, which reduces the activity of some interneuron subtypes (mostly PV-positive basket and somatostatin-positive O-LM cells), but not others.*

4.1.2 Thesis group 2: Human SPA study findings

- IIa** *The human epileptic as well as non-epileptic neocortex can generate synchronous population activity (SPA) in vitro. SPAs from epileptic and non-epileptic tissue appear to be very similar and only differ in their LFPg and CSD amplitudes. SPAs cannot directly be related to epilepsy, as they occur in tissue from non-epileptic as well as epileptic patients.*
- IIb** *Slices from epileptic human neocortex are able to generate two types of population activity: SPAs and interictal spikes (IIDs). They differ in their generation site, LFPg, CSD and MUA amplitudes as well as their recurrence frequency.*
- IIc** *Spatial subtypes of NSAs occurred across different neocortical layers (in the supragranular, granular and/or infragranular layers). Some NSAs are able to span across more than one cellular layer (sup+gran, gran+inf or entire).*

- II d** *The different spatial types can occur simultaneously.* They can occur independently from each other, but are also able to interact: Some sharing a common refractory period, some triggering each other. Two overlapping but distinct neuronal subpopulations are thought to create the different SPAs at the same time.
- II e** *Epilepsy modifies the SPAs as well as the cell behaviour during SPAs.* All discovered differences point to an increased excitability in the epileptic compared to the non-epileptic tissue. This was indicated by a larger LFPg amplitude and a larger proportion of actively participating neurons in epileptic tissue.
- II f** *Firing patterns of neurons during SPAs are very heterogeneous.* Together with the fact that PCs and INs do not seem to fire in a clear order, complex interactions between those two neuronal cell types must be assumed.
- II g** *SPA is a very local event in regard to neocortical layers.* Neurons mostly respond to the SPA that is located close to their own cell body and often did not respond to SPAs occurring in other neocortical layers.

4.1.3 Thesis group 3: Data processing and algorithm development

- III a** *I developed a novel algorithm for the purpose of analysing the firing behaviour of neurons during the population activity using a Monte Carlo approach.* Observed spike trains of cells and SPAs are analysed and compared to shuffled versions of themselves. If the observed firing pattern of the neuron was extremely increased or decreased compared to the shuffled versions, it was regarded a significant firing change.
- III b** *I developed a MatLab program with a user interface for the unbiased categorisation of neurons.* Using this program, the user can sort the displayed neurons into categories judging their autocorrelogram and action potential shape, while being blind to factors that should not be taken into account. This ensures an unbiased categorisation in respect to the tissue of origin of the cells.
- III c** *I wrote custom software in C++ for analysing the size and shape of the averaged LFPg and MUA traces of NSAs.*

5. References

- [1] G. Buzsáki, L.-W. S. Leung, and C. H. Vanderwolf, *Cellular bases of hippocampal EEG in the behaving rat*, 1983. DOI: [10.1016/0165-0173\(83\)90037-1](https://doi.org/10.1016/0165-0173(83)90037-1).
- [2] G. Buzsáki, “Two-stage model of memory formation,” *Neuroscience*, vol. 31, no. 3, pp. 551–570, 1989.
- [3] D. Kubota, L. L. Colgin, M. Casale, F. A. Brucher, and G. Lynch, “Endogenous Waves in Hippocampal Slices,” *J Neurophysiol*, vol. 89, pp. 81–89, 2003, ISSN: 0022-3077. DOI: [10.1152/jn.00542.2002](https://doi.org/10.1152/jn.00542.2002).
- [4] C. J. Behrens, L. P. van den Boom, L. de Hoz, A. Friedman, and U. Heinemann, “Induction of sharp wave-ripple complexes in vitro and reorganization of hippocampal networks.,” *Nature neuroscience*, vol. 8, no. 11, pp. 1560–1567, 2005, ISSN: 1097-6256. DOI: [10.1038/nn1571](https://doi.org/10.1038/nn1571).
- [5] K. T. Hofer, Á. Kandrás, I. Ulbert, I. Pál, C. Szabó, L. Héja, and L. Wittner, “The hippocampal CA3 region can generate two distinct types of sharp wave-ripple complexes, in vitro,” *Hippocampus*, vol. 25, no. 2, pp. 169–186, 2015, ISSN: 10981063. DOI: [10.1002/hipo.22361](https://doi.org/10.1002/hipo.22361).
- [6] N. Maier, V. Nimmrich, and A. Draguhn, “Cellular and network mechanisms underlying spontaneous sharp wave-ripple complexes in mouse hippocampal slices,” *The Journal of physiology*, vol. 550, no. 3, pp. 873–887, 2003, ISSN: 0022-3751. DOI: [10.1113/jphysiol.2003.044602](https://doi.org/10.1113/jphysiol.2003.044602).
- [7] C. Wu, M. N. Asl, J. Gillis, F. K. Skinner, and L. Zhang, “An in vitro model of hippocampal sharp waves: regional initiation and intracellular correlates.,” *Journal of neurophysiology*, vol. 94, no. March 2005, pp. 741–753, 2005.
- [8] I. Cohen, V. Navarro, S. Clemenceau, M. Baulac, and R. Miles, “On the Origin of Interictal Activity in Human Temporal Lobe Epilepsy in Vitro,” *Science*, vol. 298, no. 5597, pp. 1418–1421, 2002, ISSN: 1095-9203. DOI: [10.1126/science.1076510](https://doi.org/10.1126/science.1076510).
- [9] C. Wozny, A. Knopp, T.-N. Lehmann, U. Heinemann, and J. Behr, “The subiculum: a potential site of ictogenesis in human temporal lobe epilepsy.,” *Epilepsia*, vol. 46 Suppl 5, no. s5, pp. 17–21, Jul. 2005, ISSN: 0013-9580. DOI: [10.1111/j.1528-1167.2005.01066.x](https://doi.org/10.1111/j.1528-1167.2005.01066.x).

- [10] G. Huberfeld, L. Wittner, S. Clemenceau, M. Baulac, K. Kaila, R. Miles, and C. Rivera, “Perturbed chloride homeostasis and GABAergic signaling in human temporal lobe epilepsy.,” *The Journal of Neuroscience*, vol. 27, no. 37, pp. 9866–9873, 2007, ISSN: 0270-6474. DOI: [10.1523/JNEUROSCI.2761-07.2007](https://doi.org/10.1523/JNEUROSCI.2761-07.2007).
- [11] L. Wittner, G. Huberfeld, S. Clémenceau, L. Eróss, E. Dezamis, L. Entz, I. Ulbert, M. Baulac, T. F. Freund, Z. Maglóczy, and R. Miles, “The epileptic human hippocampal cornu ammonis 2 region generates spontaneous interictal-like activity in vitro,” *Brain*, vol. 132, no. 11, pp. 3032–3046, 2009, ISSN: 00068950. DOI: [10.1093/brain/awp238](https://doi.org/10.1093/brain/awp238).
- [12] R. Köhling, A. Lücke, H. Straub, E. J. Speckmann, I. Tuxhorn, P. Wolf, H. Pannek, and F. Ooppel, “Spontaneous sharp waves in human neocortical slices excised from epileptic patients,” *Brain*, vol. 121, no. 6, pp. 1073–1087, 1998, ISSN: 00068950. DOI: [10.1093/brain/121.6.1073](https://doi.org/10.1093/brain/121.6.1073).
- [13] B. P. Kerekes, K. Tóth, A. Kaszás, B. Chiovini, Z. Szadai, G. Szalay, D. Pálfi, A. Bagó, K. Spitzer, B. Rózsa, I. Ulbert, and L. Wittner, “Combined two-photon imaging, electrophysiological, and anatomical investigation of the human neocortex in vitro,” *Neurophotonics*, vol. 1, no. 1, p. 11 013, 2014, ISSN: 2329-423X. DOI: [10.1117/1.NPh.1.1.011013](https://doi.org/10.1117/1.NPh.1.1.011013).
- [14] J. Pallud, M. Le Van Quyen, F. Bielle, C. Pellegrino, P. Varlet, M. Labussiere, N. Cresto, M.-J. Dieme, M. Baulac, C. Duyckaerts, N. Kourdougli, G. Chazal, B. Devaux, C. Rivera, R. Miles, L. Capelle, and G. Huberfeld, “Cortical GABAergic excitation contributes to epileptic activities around human glioma,” *Science translational medicine*, vol. 6, no. 244, 244ra89, 2014, ISSN: 1946-6242. DOI: [10.1126/scitranslmed.3008065](https://doi.org/10.1126/scitranslmed.3008065).
- [15] C. Wu, W. P. Luk, J. Gillis, F. Skinner, and L. Zhang, “Size does matter: generation of intrinsic network rhythms in thick mouse hippocampal slices.,” *Journal of neurophysiology*, vol. 93, no. 4, pp. 2302–2317, 2005.
- [16] C. Wu, H. L. Huang, M. Nassiri Asl, J. W. He, J. Gillis, F. K. Skinner, and L. Zhang, “Spontaneous rhythmic field potentials of isolated mouse hippocampal-subicular-entorhinal cortices in vitro.,” *The Journal of physiology*, vol. 576, no. Pt 2, pp. 457–476, 2006, ISSN: 0022-3751. DOI: [10.1113/jphysiol.2006.114918](https://doi.org/10.1113/jphysiol.2006.114918).
- [17] G. Buzsáki, Z. Horváth, R. Urioste, J. Hetke, and K. Wise, “High-frequency network oscillation in the hippocampus.,” *Science (New York, N.Y.)*, vol. 256, no. 5059, pp. 1025–1027, 1992, ISSN: 0036-8075. DOI: [10.1126/science.1589772](https://doi.org/10.1126/science.1589772).
- [18] A. Ylinen, A. Bragin, Z. Nádasdy, G. Jandó, I. Szabó, A. Sik, and G. Buzsáki, “Sharp wave-associated high-frequency oscillation (200 Hz) in the intact hippocampus: network and intracellular mechanisms.,” *The Journal of neuroscience : The official journal of the Society for Neuroscience*, vol. 15, no. 1 Pt 1, pp. 30–46, 1995, ISSN: 0270-6474.
- [19] J. Csicsvári, H. Hirase, A. Mamiya, and G. Buzsáki, “Ensemble patterns of hippocampal CA3-CA1 neurons during sharp wave-associated population events.,” *Neuron*, vol. 28, no. 2, pp. 585–594, 2000, ISSN: 08966273. DOI: [10.1016/S0896-6273\(00\)00135-5](https://doi.org/10.1016/S0896-6273(00)00135-5).

- [20] C. Papatheodoropoulos and G. Kostopoulos, “Spontaneous, low frequency (approximately 2-3 Hz) field activity generated in rat ventral hippocampal slices perfused with normal medium.,” *Brain research bulletin*, vol. 57, no. 2, pp. 187–93, Jan. 2002, ISSN: 0361-9230.
- [21] T. Kano, Y. Inaba, and M. Avoli, “Periodic oscillatory activity in parahippocampal slices maintained in vitro,” *Neuroscience*, vol. 130, no. 4, pp. 1041–1053, 2005, ISSN: 03064522. DOI: [10.1016/j.neuroscience.2004.10.012](https://doi.org/10.1016/j.neuroscience.2004.10.012).
- [22] V. Nimmrich, N. Maier, D. Schmitz, and A. Draguhn, “Induced sharp wave-ripple complexes in the absence of synaptic inhibition in mouse hippocampal slices,” *The Journal of physiology*, vol. 563, no. Pt 3, pp. 663–70, 2005, ISSN: 0022-3751. DOI: [10.1113/jphysiol.2004.079558](https://doi.org/10.1113/jphysiol.2004.079558).
- [23] T. J. Ellender, W. Nissen, L. L. Colgin, E. O. Mann, and O. Paulsen, “Priming of hippocampal population bursts by individual perisomatic-targeting interneurons.,” *The Journal of neuroscience : The official journal of the Society for Neuroscience*, vol. 30, no. 17, pp. 5979–5991, 2010, ISSN: 0270-6474. DOI: [10.1523/JNEUROSCI.3962-09.2010](https://doi.org/10.1523/JNEUROSCI.3962-09.2010).
- [24] L. L. Colgin, D. Kubota, Y. Jia, C. S. Rex, and G. Lynch, “Long-term potentiation is impaired in rat hippocampal slices that produce spontaneous sharp waves.,” *The Journal of physiology*, vol. 558, no. Pt 3, pp. 953–961, 2004, ISSN: 0022-3751. DOI: [10.1113/jphysiol.2004.068080](https://doi.org/10.1113/jphysiol.2004.068080).
- [25] N. Hájos, M. R. Karlócai, B. Németh, I. Ulbert, H. Monyer, G. G. Szabó, F. Erdélyi, T. F. Freund, and A. I. Gulyás, “Input-Output Features of Anatomically Identified CA3 Neurons during Hippocampal Sharp Wave/Ripple Oscillation In Vitro,” *Journal of Neuroscience*, vol. 33, no. 28, pp. 11 677–11 691, 2013, ISSN: 0270-6474. DOI: [10.1523/JNEUROSCI.5729-12.2013](https://doi.org/10.1523/JNEUROSCI.5729-12.2013).
- [26] T. F. Freund and G. Buzsáki, “Interneurons of the hippocampus.,” *Hippocampus*, vol. 6, no. 4, pp. 347–470, 1996, ISSN: 1050-9631. DOI: [10.1002/\(SICI\)1098-1063\(1996\)6:4<347::AID-HIP01>3.0.CO;2-I](https://doi.org/10.1002/(SICI)1098-1063(1996)6:4<347::AID-HIP01>3.0.CO;2-I).
- [27] R. Miles, K. Tóth, A. I. Gulyás, N. Hájos, and T. F. Freund, “Differences between somatic and dendritic inhibition in the hippocampus.,” *Neuron*, vol. 16, no. 4, pp. 815–23, Apr. 1996, ISSN: 0896-6273.
- [28] T. F. Freund and I. Katona, “Perisomatic Inhibition,” *Neuron*, vol. 56, no. 1, pp. 33–42, Oct. 2007, ISSN: 08966273. DOI: [10.1016/j.neuron.2007.09.012](https://doi.org/10.1016/j.neuron.2007.09.012).
- [29] D. Schlingloff, S. Káli, T. F. Freund, N. Hájos, and A. I. Gulyás, “Mechanisms of Sharp Wave Initiation and Ripple Generation,” *Journal of Neuroscience*, vol. 34, no. 34, pp. 11 385–11 398, 2014, ISSN: 0270-6474. DOI: [10.1523/JNEUROSCI.0867-14.2014](https://doi.org/10.1523/JNEUROSCI.0867-14.2014).
- [30] M. Bazelot, M. T. Tele, and R. Miles, “Single CA3 pyramidal cells trigger sharp waves in vitro by exciting interneurons.,” *Journal of Physiology*, no. January, pp. 1–13, 2016, ISSN: 00223751. DOI: [10.1113/JP271644](https://doi.org/10.1113/JP271644).
- [31] I. Ulbert, E. Halgren, G. Heit, and G. Karmos, “Multiple microelectrode-recording system for human intracortical applications,” *Journal of Neuroscience Methods*, vol. 106, no. 1, pp. 69–79, 2001.

- [32] I. Ulbert, G. Heit, J. R. Madsen, G. Karmos, and E. Halgren, “Laminar analysis of human neocortical interictal spike generation and propagation: current source density and multiunit analysis in vivo,” *Epilepsia*, vol. 45 Suppl 4, pp. 48–56, 2004, ISSN: 0013-9580. DOI: [10.1111/j.0013-9580.2004.04011.x](https://doi.org/10.1111/j.0013-9580.2004.04011.x).
- [33] I. Ulbert, Z. Maglóczy, L. Eröss, S. Czirják, J. Vajda, L. Bognár, S. Tóth, Z. Szabó, P. Halász, D. Fabó, E. Halgren, T. F. Freund, and G. Karmos, “In vivo laminar electrophysiology co-registered with histology in the hippocampus of patients with temporal lobe epilepsy,” *Experimental Neurology*, vol. 187, no. 2, pp. 310–318, 2004, ISSN: 00144886. DOI: [10.1016/j.expneurol.2003.12.003](https://doi.org/10.1016/j.expneurol.2003.12.003).
- [34] D. Fabó, Z. Maglóczy, L. Wittner, Á. Pék, L. Eröss, S. Czirják, J. Vajda, A. Sólyom, G. Rásonyi, A. Szűcs, A. Kelemen, V. Juhos, L. Grand, B. Dombóvári, P. Halász, T. F. Freund, E. Halgren, G. Karmos, and I. Ulbert, “Properties of in vivo interictal spike generation in the human subiculum,” *Brain*, vol. 131, no. 2, pp. 485–499, 2008, ISSN: 00068950. DOI: [10.1093/brain/awm297](https://doi.org/10.1093/brain/awm297).
- [35] N. Hájos and O. Paulsen, “Network mechanisms of gamma oscillations in the CA3 region of the hippocampus,” *Neural Networks*, vol. 22, no. 8, pp. 1113–1119, 2009, ISSN: 08936080. DOI: [10.1016/j.neunet.2009.07.024](https://doi.org/10.1016/j.neunet.2009.07.024).
- [36] G. G. Szabó, N. Holderith, A. I. Gulyás, T. F. Freund, and N. Hájos, “Distinct synaptic properties of perisomatic inhibitory cell types and their different modulation by cholinergic receptor activation in the CA3 region of the mouse hippocampus,” *European Journal of Neuroscience*, vol. 31, no. 12, pp. 2234–2246, Jun. 2010, ISSN: 0953816X. DOI: [10.1111/j.1460-9568.2010.07292.x](https://doi.org/10.1111/j.1460-9568.2010.07292.x).
- [37] C. T. Drake and T. A. Milner, “Mu opioid receptors are in discrete hippocampal interneuron subpopulations,” *Hippocampus*, vol. 12, no. 2, pp. 119–136, 2002, ISSN: 1050-9631. DOI: [10.1002/hipo.1107](https://doi.org/10.1002/hipo.1107).
- [38] A. I. Gulyás, N. Hájos, I. Katona, and T. F. Freund, “Interneurons are the local targets of hippocampal inhibitory cells which project to the medial septum,” *The European journal of neuroscience*, vol. 17, no. 9, pp. 1861–72, May 2003, ISSN: 0953-816X.
- [39] A. I. Gulyás, G. G. Szabó, I. Ulbert, N. Holderith, H. Monyer, F. Erdélyi, G. G. Szabó, T. F. Freund, and N. Hájos, “Parvalbumin-containing fast-spiking basket cells generate the field potential oscillations induced by cholinergic receptor activation in the hippocampus,” *The Journal of neuroscience : The official journal of the Society for Neuroscience*, vol. 30, no. 45, pp. 15 134–45, 2010, ISSN: 1529-2401. DOI: [10.1523/JNEUROSCI.4104-10.2010](https://doi.org/10.1523/JNEUROSCI.4104-10.2010).
- [40] H. Kamiya, H. Shinozaki, and C. Yamamoto, “Activation of metabotropic glutamate receptor type 2/3 suppresses transmission at rat hippocampal mossy fibre synapses,” *The Journal of physiology*, vol. 493 (Pt 2, pp. 447–55, Jun. 1996, ISSN: 0022-3751.
- [41] L. Hazan, M. Zugaro, and G. Buzsáki, “Klusters, NeuroScope, NDManager: a free software suite for neurophysiological data processing and visualization,” *Journal of neuroscience methods*, vol. 155, no. 2, pp. 207–16, Sep. 2006, ISSN: 0165-0270. DOI: [10.1016/j.jneumeth.2006.01.017](https://doi.org/10.1016/j.jneumeth.2006.01.017).

- [42] G. Paxinos and C. Watson, *The Rat Brain in Stereotaxic Coordinates Fourth Edition*. 1998, p. 237, ISBN: 9780125476195. DOI: [0125476191](https://doi.org/10.1254/76191).
- [43] G. Buzsáki, “Hippocampal sharp waves: Their origin and significance,” *Brain Research*, vol. 398, no. 2, pp. 242–252, 1986, ISSN: 00068993. DOI: [10.1016/0006-8993\(86\)91483-6](https://doi.org/10.1016/0006-8993(86)91483-6).
- [44] G. Foffani, Y. G. Uzcategui, B. Gal, and L. Menendez de la Prida, “Reduced Spike-Timing Reliability Correlates with the Emergence of Fast Ripples in the Rat Epileptic Hippocampus,” *Neuron*, vol. 55, no. 6, pp. 930–941, Sep. 2007, ISSN: 08966273. DOI: [10.1016/j.neuron.2007.07.040](https://doi.org/10.1016/j.neuron.2007.07.040).
- [45] C. Nicholson and J. A. Freeman, “Theory of current source-density analysis and determination of conductivity tensor for anuran cerebellum.,” *Journal of neurophysiology*, vol. 38, no. 2, pp. 356–68, Mar. 1975, ISSN: 0022-3077.
- [46] J. A. Freeman and C. Nicholson, “Experimental optimization of current source-density technique for anuran cerebellum.,” *Journal of neurophysiology*, vol. 38, no. 2, pp. 369–82, Mar. 1975, ISSN: 0022-3077.
- [47] C. Papatheodoropoulos and G. Kostopoulos, “Spontaneous GABA(A)-dependent synchronous periodic activity in adult rat ventral hippocampal slices.,” *Neuroscience letters*, vol. 319, no. 1, pp. 17–20, Feb. 2002, ISSN: 0304-3940.
- [48] L. L. Colgin, Y. Jia, J. M. Sabatier, and G. Lynch, “Blockade of NMDA receptors enhances spontaneous sharp waves in rat hippocampal slices,” *Neuroscience Letters*, vol. 385, no. 1, pp. 46–51, 2005, ISSN: 03043940. DOI: [10.1016/j.neulet.2005.05.005](https://doi.org/10.1016/j.neulet.2005.05.005).
- [49] C. S. Rex, L. L. Colgin, Y. Jia, M. Casale, T. K. Yanagihara, M. DeBenedetti, C. M. Gall, E. A. Kramar, and G. Lynch, “Origins of an intrinsic hippocampal EEG pattern,” *PLoS ONE*, vol. 4, no. 11, pp. 1–13, 2009, ISSN: 19326203. DOI: [10.1371/journal.pone.0007761](https://doi.org/10.1371/journal.pone.0007761).
- [50] P. Giannopoulos and C. Papatheodoropoulos, “Effects of μ -opioid receptor modulation on the hippocampal network activity of sharp wave and ripples,” *British Journal of Pharmacology*, vol. 168, no. 5, pp. 1146–1164, 2013, ISSN: 00071188. DOI: [10.1111/j.1476-5381.2012.02240.x](https://doi.org/10.1111/j.1476-5381.2012.02240.x).
- [51] I. Katona, B. Sperlagh, A. Sik, A. Kafalvi, E. S. Vizi, K. Mackie, and T. F. Freund, “Presynaptically located CB1 cannabinoid receptors regulate GABA release from axon terminals of specific hippocampal interneurons.,” *The Journal of neuroscience : The official journal of the Society for Neuroscience*, vol. 19, no. 11, pp. 4544–58, Jun. 1999, ISSN: 1529-2401.
- [52] S. Reichinnek, T. Kunsting, A. Draguhn, and M. Both, “Field potential signature of distinct multicellular activity patterns in the mouse hippocampus.,” *The Journal of neuroscience : The official journal of the Society for Neuroscience*, vol. 30, no. 46, pp. 15 441–15 449, 2010, ISSN: 0270-6474. DOI: [10.1523/JNEUROSCI.2535-10.2010](https://doi.org/10.1523/JNEUROSCI.2535-10.2010).

- [53] J. F. Ramirez-Villegas, N. K. Logothetis, and M. Besserve, “Diversity of sharp-wave–ripple LFP signatures reveals differentiated brain-wide dynamical events,” *Proceedings of the National Academy of Sciences*, E6379–E6387, 2015, ISSN: 0027-8424. DOI: [10.1073/pnas.1518257112](https://doi.org/10.1073/pnas.1518257112).
- [54] T. Klausberger, P. J. Magill, L. F. Márton, J. D. B. Roberts, P. M. Cobden, G. Buzsáki, and P. Somogyi, “Brain-state- and cell-type-specific firing of hippocampal interneurons in vivo.,” *Nature*, vol. 421, no. February, pp. 844–848, 2003, ISSN: 0028-0836. DOI: [10.1038/nature04910](https://doi.org/10.1038/nature04910).
- [55] J. Csicsvári, H. Hirase, A. Czurkó, and G. Buzsáki, “Reliability and state dependence of pyramidal cell-interneuron synapses in the hippocampus: An ensemble approach in the behaving rat,” *Neuron*, vol. 21, no. 1, pp. 179–189, 1998, ISSN: 08966273. DOI: [10.1016/S0896-6273\(00\)80525-5](https://doi.org/10.1016/S0896-6273(00)80525-5).
- [56] K. Hartwich, T. Pollak, and T. Klausberger, “Distinct Firing Patterns of Identified Basket and Dendrite-Targeting Interneurons in the Prefrontal Cortex during Hippocampal Theta and Local Spindle Oscillations,” *Journal of Neuroscience*, vol. 29, no. 30, pp. 9563–9574, Jul. 2009, ISSN: 0270-6474. DOI: [10.1523/JNEUROSCI.1397-09.2009](https://doi.org/10.1523/JNEUROSCI.1397-09.2009).
- [57] G. Buzsáki and F. L. da Silva, “High frequency oscillations in the intact brain,” *Progress in Neurobiology*, vol. 98, no. 3, pp. 241–249, Sep. 2012, ISSN: 03010082. DOI: [10.1016/j.pneurobio.2012.02.004](https://doi.org/10.1016/j.pneurobio.2012.02.004).
- [58] L. Wittner and R. Miles, “Factors defining a pacemaker region for synchrony in the hippocampus.,” *The Journal of physiology*, vol. 584, no. Pt 3, pp. 867–83, 2007, ISSN: 0022-3751. DOI: [10.1113/jphysiol.2007.138131](https://doi.org/10.1113/jphysiol.2007.138131).
- [59] M. de Curtis and G. Avanzini, “Interictal spikes in focal epileptogenesis.,” *Progress in neurobiology*, vol. 63, no. 5, pp. 541–67, Apr. 2001, ISSN: 0301-0082.
- [60] C. J. Keller, W. Truccolo, J. T. Gale, E. Eskandar, T. Thesen, C. Carlson, O. Devinsky, R. Kuzniecky, W. K. Doyle, J. R. Madsen, D. L. Schomer, A. D. Mehta, E. N. Brown, L. R. Hochberg, I. Ulbert, E. Halgren, and S. S. Cash, “Heterogeneous neuronal firing patterns during interictal epileptiform discharges in the human cortex,” *Brain*, vol. 133, no. 6, pp. 1668–1681, 2010, ISSN: 00068950. DOI: [10.1093/brain/awq112](https://doi.org/10.1093/brain/awq112).
- [61] D. A. McCormick, “GABA as an inhibitory neurotransmitter in human cerebral cortex.,” *Journal of neurophysiology*, vol. 62, no. 5, pp. 1018–27, Nov. 1989, ISSN: 0022-3077.
- [62] A. Simon, R. D. Traub, N. Vladimirov, A. Jenkins, C. Nicholson, R. G. Whittaker, I. Schofield, G. J. Clowry, M. O. Cunningham, and M. A. Whittington, “Gap junction networks can generate both ripple-like and fast ripple-like oscillations.,” *The European journal of neuroscience*, vol. 39, no. 1, pp. 46–60, Jan. 2014, ISSN: 1460-9568. DOI: [10.1111/ejn.12386](https://doi.org/10.1111/ejn.12386).
- [63] R. Köhling, M. Qü, K. Zilles, and E. J. Speckmann, “Current-source-density profiles associated with sharp waves in human epileptic neocortical tissue,” *Neuroscience*, vol. 94, no. 4, pp. 1039–1050, 1999, ISSN: 03064522. DOI: [10.1016/S0306-4522\(99\)00327-9](https://doi.org/10.1016/S0306-4522(99)00327-9).

- [64] A. K. Roopun, J. D. Simonotto, M. L. Pierce, A. Jenkins, C. Nicholson, I. S. Schofield, R. G. Whittaker, M. Kaiser, M. A. Whittington, R. D. Traub, and M. O. Cunningham, “A nonsynaptic mechanism underlying interictal discharges in human epileptic neocortex,” *Proceedings of the National Academy of Sciences of the United States of America*, vol. 107, no. 1, pp. 338–343, 2010, ISSN: 0027-8424. DOI: [10.1073/pnas.0912652107](https://doi.org/10.1073/pnas.0912652107).
- [65] M. R. Karlócai, L. Wittner, K. Tóth, Z. Maglóczy, Z. Katarova, G. Rásonyi, L. Eröss, S. Czirják, P. Halász, G. G. Szabó, J. A. Payne, K. Kaila, and T. F. Freund, “Enhanced expression of potassium-chloride cotransporter KCC2 in human temporal lobe epilepsy,” *Brain structure & function*, vol. 221, no. 7, pp. 3601–15, Sep. 2016, ISSN: 1863-2661. DOI: [10.1007/s00429-015-1122-8](https://doi.org/10.1007/s00429-015-1122-8).
- [66] K. Tóth, L. Eross, J. Vajda, P. Halász, T. F. Freund, and Z. Maglóczy, “Loss and reorganization of calretinin-containing interneurons in the epileptic human hippocampus,” *Brain : A journal of neurology*, vol. 133, no. 9, pp. 2763–77, Sep. 2010, ISSN: 1460-2156. DOI: [10.1093/brain/awq149](https://doi.org/10.1093/brain/awq149).
- [67] Z. Maglóczy, L. Wittner, Z. Borhegyi, P. Halász, J. Vajda, S. Czirják, and T. F. Freund, “Changes in the distribution and connectivity of interneurons in the epileptic human dentate gyrus,” *Neuroscience*, vol. 96, no. 1, pp. 7–25, 2000, ISSN: 0306-4522.
- [68] T. L. Babb, J. K. Pretorius, W. R. Kupfer, and P. H. Crandall, “Glutamate decarboxylase-immunoreactive neurons are preserved in human epileptic hippocampus,” *The Journal of neuroscience : The official journal of the Society for Neuroscience*, vol. 9, no. 7, pp. 2562–74, Jul. 1989, ISSN: 0270-6474.
- [69] U. Heinemann, S. Gabriel, R. Jauch, K. Schulze, A. Kivi, A. Eilers, R. Kovacs, and T. N. Lehmann, “Alterations of glial cell function in temporal lobe epilepsy,” *Epilepsia*, vol. 41 Suppl 6, S185–9, 2000, ISSN: 0013-9580.
- [70] T. N. Lehmann, S. Gabriel, R. Kovacs, A. Eilers, A. Kivi, K. Schulze, W. R. Lanksch, H. J. Meencke, and U. Heinemann, “Alterations of neuronal connectivity in area CA1 of hippocampal slices from temporal lobe epilepsy patients and from pilocarpine-treated epileptic rats,” *Epilepsia*, vol. 41 Suppl 6, S190–4, 2000, ISSN: 0013-9580.
- [71] A. Williamson, “Correlations between granule cell physiology and bioenergetics in human temporal lobe epilepsy,” *Brain*, vol. 128, no. 5, pp. 1199–1208, Mar. 2005, ISSN: 1460-2156. DOI: [10.1093/brain/awh444](https://doi.org/10.1093/brain/awh444).
- [72] A. Kivi, T. N. Lehmann, R. Kovács, A. Eilers, R. Jauch, H. J. Meencke, A. von Deimling, U. Heinemann, and S. Gabriel, “Effects of barium on stimulus-induced rises of [K⁺]_o in human epileptic non-sclerotic and sclerotic hippocampal area CA1,” *The European journal of neuroscience*, vol. 12, no. 6, pp. 2039–48, Jun. 2000, ISSN: 0953-816X.
- [73] S. Gabriel, “Stimulus and Potassium-Induced Epileptiform Activity in the Human Dentate Gyrus from Patients with and without Hippocampal Sclerosis,” *Journal of Neuroscience*, vol. 24, no. 46, pp. 10 416–10 430, Nov. 2004, ISSN: 0270-6474. DOI: [10.1523/JNEUROSCI.2074-04.2004](https://doi.org/10.1523/JNEUROSCI.2074-04.2004).

- [74] M. Isokawa and I. Fried, “Extracellular slow negative transient in the dentate gyrus of human epileptic hippocampus in vitro,” *Neuroscience*, vol. 72, no. 1, pp. 31–37, May 1996, ISSN: 03064522. DOI: [10.1016/0306-4522\(95\)00544-7](https://doi.org/10.1016/0306-4522(95)00544-7).
- [75] M. Thom, L. Martinian, A. Sen, J. H. Cross, B. N. Harding, and S. M. Sisodiya, “Cortical neuronal densities and lamination in focal cortical dysplasia,” *Acta neuropathologica*, vol. 110, no. 4, pp. 383–92, Oct. 2005, ISSN: 0001-6322. DOI: [10.1007/s00401-005-1062-0](https://doi.org/10.1007/s00401-005-1062-0).
- [76] L. Alonso-Nanclares, R. Garbelli, R. G. Sola, J. Pastor, L. Tassi, R. Spreafico, and J. DeFelipe, “Microanatomy of the dysplastic neocortex from epileptic patients,” *Brain*, vol. 128, no. 1, 158 LP–173, Dec. 2004.
- [77] O. Kargiotis, S. Markoula, and A. P. Kyritsis, “Epilepsy in the cancer patient,” *Cancer chemotherapy and pharmacology*, vol. 67, no. 3, pp. 489–501, Mar. 2011, ISSN: 1432-0843. DOI: [10.1007/s00280-011-1569-0](https://doi.org/10.1007/s00280-011-1569-0).
- [78] M. A. Wilson and B. L. McNaughton, “Dynamics of the hippocampal ensemble code for space,” *Science (New York, N.Y.)*, vol. 261, no. 5124, pp. 1055–8, Aug. 1993, ISSN: 0036-8075.
- [79] J. Csicsvári, H. Hirase, A. Czurkó, A. Mamiya, and G. Buzsáki, “Oscillatory coupling of hippocampal pyramidal cells and interneurons in the behaving Rat,” *The Journal of neuroscience : The official journal of the Society for Neuroscience*, vol. 19, no. 1, pp. 274–287, 1999, ISSN: 0270-6474.
- [80] P. Barthó, H. Hirase, L. Monconduit, M. Zugaro, K. D. Harris, and G. Buzsáki, “Characterization of neocortical principal cells and interneurons by network interactions and extracellular features,” *Journal of Neurophysiology*, vol. 92, no. 1, pp. 600–608, 2004.
- [81] L. Kostal, P. Lansky, and J. P. Rospars, “Neuronal coding and spiking randomness,” *European Journal of Neuroscience*, vol. 26, no. 10, pp. 2693–2701, 2007, ISSN: 0953816X. DOI: [10.1111/j.1460-9568.2007.05880.x](https://doi.org/10.1111/j.1460-9568.2007.05880.x).
- [82] I. V. Viskontas, A. D. Ekstrom, C. L. Wilson, and I. Fried, “Characterizing Interneuron and Pyramidal Cells in the Human Medial Temporal Lobe In Vivo Using Extracellular Recordings,” *Hippocampus*, vol. 17, no. 1, pp. 49–57, 2007. DOI: [10.1002/hipo.20241](https://doi.org/10.1002/hipo.20241).
- [83] H. White, “A Heteroskedasticity-Consistent Covariance Matrix Estimator and a Direct Test for Heteroskedasticity,” *Econometrica*, vol. 48, no. 4, pp. 817–838, 1980, ISSN: 00129682, 14680262. DOI: [10.2307/1912934](https://doi.org/10.2307/1912934).
- [84] P. J. Huber, “The behavior of maximum likelihood estimates under nonstandard conditions,” in *Proceedings of the Fifth Berkeley Symposium on Mathematical Statistics and Probability, Volume 1: Statistics*, ser. Fifth Berkeley Symposium on Mathematical Statistics and Probability, Berkeley, Calif.: University of California Press, 1967, pp. 221–233, ISBN: 0097-0433.
- [85] F. Eicker, “Limit theorems for regressions with unequal and dependent errors,” in *Proceedings of the Fifth Berkeley Symposium on Mathematical Statistics and Probability, Volume 1: Statistics*, ser. Fifth Berkeley Symposium on Mathematical Statistics and Probability, Berkeley, Calif.: University of California Press, 1967, pp. 59–82, ISBN: 0097-0433.

- [86] J. M. Wooldridge, *Introductory Econometrics: A Modern Approach*, 6th ed. Boston, MA: Cengage Learning, 2016, p. 789, ISBN: 978-1-305-27010-7.
- [87] T. Breusch and A. Pagan, “A Simple Test for Heteroscedasticity and Random Coefficient Variation,” *Econometrica*, vol. 47, no. 5, pp. 1287–1294, 1979.
- [88] R. Koenker, *A note on studentizing a test for heteroscedasticity*, 1981. DOI: [10.1016/0304-4076\(81\)90062-2](https://doi.org/10.1016/0304-4076(81)90062-2).
- [89] M. Avoli, D. Mattia, A. Siniscalchi, P. Perreault, and F. Tomaiuolo, “Pharmacology and electrophysiology of a synchronous GABA-mediated potential in the human neocortex,” *eng, Neuroscience*, vol. 62, no. 3, pp. 655–666, Oct. 1994, ISSN: 0306-4522 (Print).
- [90] M. Avoli, J. Louvel, R. Pumain, and R. Köhling, “Cellular and molecular mechanisms of epilepsy in the human brain,” *Progress in Neurobiology*, vol. 77, no. 3, pp. 166–200, 2005, ISSN: 03010082. DOI: [10.1016/j.pneurobio.2005.09.006](https://doi.org/10.1016/j.pneurobio.2005.09.006).
- [91] G. Huberfeld, L. Menendez de la Prida, J. Pallud, I. Cohen, M. Le Van Quyen, C. Adam, S. Clemenceau, M. Baulac, and R. Miles, “Glutamatergic pre-ictal discharges emerge at the transition to seizure in human epilepsy,” *Nat Neurosci*, vol. 14, no. 5, pp. 627–634, May 2011, ISSN: 1097-6256.
- [92] M. R. Karlócai, Z. Kohus, S. Káli, I. Ulbert, G. G. Szabó, Z. Máté, T. F. Freund, and A. I. Gulyás, “Physiological sharp wave-ripples and interictal events in vitro: What’s the difference?” *Brain*, vol. 137, no. 2, pp. 463–485, 2014, ISSN: 14602156. DOI: [10.1093/brain/awt348](https://doi.org/10.1093/brain/awt348).
- [93] A. M. Thomson and A. P. Bannister, “Interlaminar connections in the neocortex,” *Cerebral cortex (New York, N.Y. : 1991)*, vol. 13, no. 1, pp. 5–14, 2003, ISSN: 1047-3211. DOI: [10.1093/cercor/13.1.5](https://doi.org/10.1093/cercor/13.1.5).
- [94] A. P. Bannister, “Inter- and intra-laminar connections of pyramidal cells in the neocortex,” *Neuroscience research*, vol. 53, no. 2, pp. 95–103, Oct. 2005, ISSN: 0168-0102. DOI: [10.1016/j.neures.2005.06.019](https://doi.org/10.1016/j.neures.2005.06.019).
- [95] V. B. Mountcastle, “Modality and topographic properties of single neurons of cat’s somatic sensory cortex,” *Journal of neurophysiology*, vol. 20, no. 4, pp. 408–34, Jul. 1957, ISSN: 0022-3077.
- [96] J. C. Horton and D. L. Adams, “The cortical column: a structure without a function,” *Philosophical Transactions of the Royal Society B: Biological Sciences*, vol. 360, no. 1456, pp. 837–862, Apr. 2005, ISSN: 0962-8436. DOI: [10.1098/rstb.2005.1623](https://doi.org/10.1098/rstb.2005.1623).
- [97] D. A. McCormick and D. Contreras, “On the cellular and network bases of epileptic seizures,” *Annual review of physiology*, vol. 63, pp. 815–46, 2001, ISSN: 0066-4278. DOI: [10.1146/annurev.physiol.63.1.815](https://doi.org/10.1146/annurev.physiol.63.1.815).
- [98] P. Marco and J. DeFelipe, “Altered synaptic circuitry in the human temporal neocortex removed from epileptic patients,” *Experimental brain research*, vol. 114, no. 1, pp. 1–10, Mar. 1997, ISSN: 0014-4819.
- [99] M. A. Rogawski and W. Loscher, “The neurobiology of antiepileptic drugs,” *Nat Rev Neurosci*, vol. 5, no. 7, pp. 553–564, Jul. 2004, ISSN: 1471-003X.

- [100] G. Molnár, S. Oláh, G. Komlósi, M. Füle, J. Szabadics, C. Varga, P. Barzó, and G. Tamás, “Complex events initiated by individual spikes in the human cerebral cortex.,” *PLoS biology*, vol. 6, no. 9, e222, Sep. 2008, issn: 1545-7885. DOI: [10.1371/journal.pbio.0060222](https://doi.org/10.1371/journal.pbio.0060222).

6. Appendices

6.1 NSA and AP waveform measurements

6.1.1 NSA waveform measurements

The following section uses averaged LFPg waveforms of SPAs as an example to illustrate how the amplitude as well as the width and asymmetry (at a defined height) of averaged NSA LFPg and MUA waveforms are measured for further analysis. The calculations for LFPg and MUA waveforms are analogous with the exception that only positive peaks are taken into account in case of the MUA (representing the point with the largest increase in cellular activity) while the peak search for LFPg waves accepts positive or negative peaks.

As action potentials of single units were sometimes visible on the waveform of the averaged LFPg of the NSA, the point of the largest amplitude was not always a good fit for the detection of the LFPg peak. Thus, the sum of all data points within a 2.5 ms shifting time window was used for finding the peak (figure 6.1B), which is equivalent to a filtering step before searching for the amplitude peak. In the time window from -100 to +100 ms, the first 50 consecutive data points (2.5 ms) were summed up. After the sum of the amplitudes for the points was calculated for a given window position, the window was shifted by one data point and the sum of points was calculated again. A maximum search for the absolute value was employed to find the channel, time point and amplitude of the largest LFPg peak (positive or negative) in the average file. The time point of the NSA LFPg peak was defined by the middle of the time window, whereas the amplitude was defined as the median amplitude of the data points in the time window.

The NSA width can be calculated at any arbitrary threshold height, expressed as percentages of the detected peak amplitude relative to the baseline. Moving from the peak outwards, each instance where the threshold height (horizontal orange line in figure 6.1A and C) is crossed by the LFPg trace is noted (black dots in figure 6.1C). For each side (left and right of the peak) this is done separately. It is possible that NSA events lie so closely together in time that they form secondary peaks in the average. To avoid that potential intersections far away from the peak influence the measured width, the search for intersections is limited. For this purpose, a termination threshold is defined at 33 % height of the measuring threshold. When the LFPg crosses the termination threshold for the first time, the search for further intersections is stopped (for that side). This method avoids overestimating the width of the NSA due to artefact intersections far away from the peak while at the same time allowing for very wide NSAs by not setting a fixed limit such as 50 ms or 100 ms. The number of intersections with the threshold is always odd (for each side), as the trace always lies above the threshold at the peak and below the threshold at the baseline.

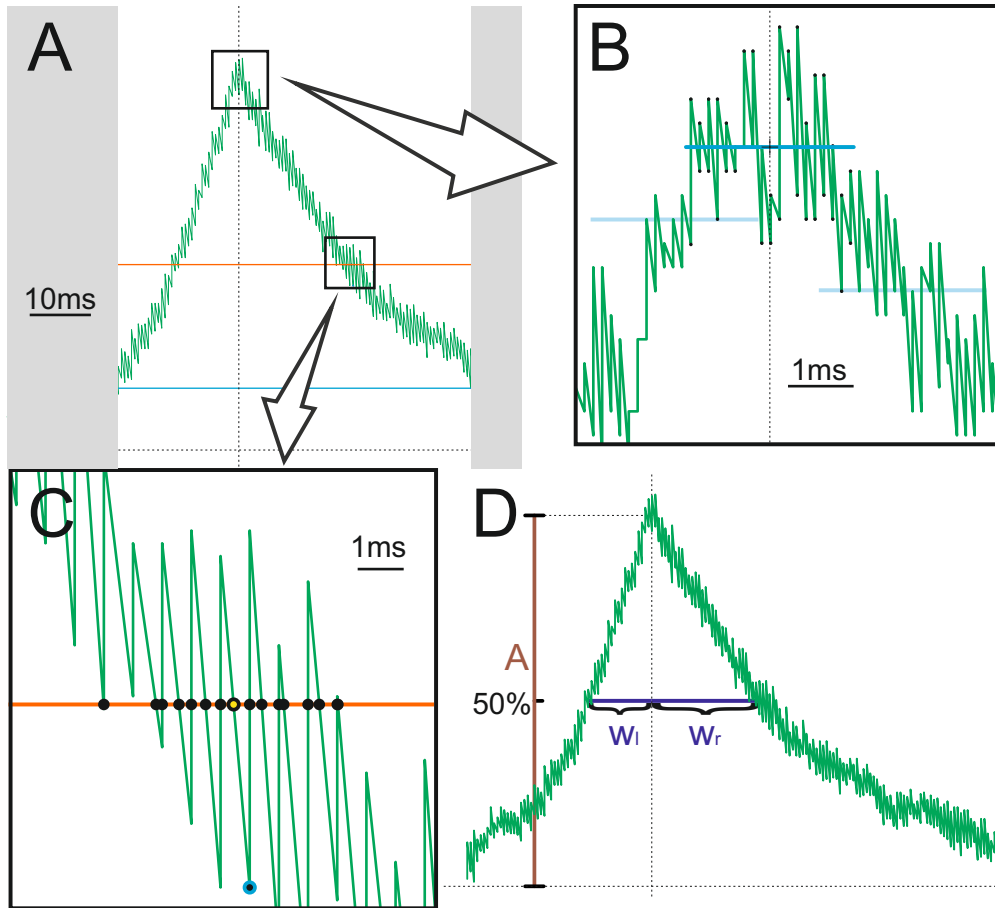


Figure 6.1: NSA and MUA waveform measurements Averaged LFPg traces from one channel of a representative NSA. Note that the number of data points was reduced for the purpose of this illustration in all panels. (A) The vertical dashed line indicates the peak, the orange and the horizontal blue lines indicate the measuring and termination thresholds, respectively. The horizontal dashed line indicates the baseline. (B) Time windows of 50 consecutive data points each are investigated. In the illustration three example time windows and their median amplitude are represented as horizontal blue lines. The window achieving the largest sum of amplitudes is shown in dark blue, with the resulting peak time point and amplitude indicated by a small black cross. (C) Visualisation of the NSA width measurement on the right side. Points where the averaged LFPg trace crosses the measuring threshold (horizontal orange line) are indicated by black dots. The median intersection is indicated by a yellow dot with a black outline. A black dot with blue outline indicates the point used for measuring the width after rounding up to the next data point (amplitude irrelevant). The search for intersections is continued until the LFPg trace crosses the termination threshold (horizontal blue line and grey background outside the search area in (A)). (D) Overview over the measured features: the amplitude (brown line) and the widths measured left and right of the peak at the defined height (dark purple lines).

The median intersection (black circle with yellow centre), rounded up to the next data point (blue circle with black centre, note that its amplitude is completely irrelevant) is used to measure the width for that side. From the two partial widths (w_l and w_r the total width $W_{total} = w_l + w_r$ and the asymmetry $Asym = w_r/w_l$ are calculated for the LFPg wave at that height (figure 6.1D)

6.1.2 Action potential waveform measurements

For each action potential the unfiltered average trace as well as the 300 – 3000 Hz filtered average trace were measured. As a first step, the largest amplitude (relative to the baseline defined as -4 ms to -1 ms before the peak) was searched across all channels. As the sign of the spike can be disregarded in case of the LFPg, negative as well as positive peaks were taken into account. For simplification, terms like maximum, minimum, positive and negative will always refer to cases with positive AP peaks from here on. While the baseline served as the main reference for measuring the amplitude in case of LFPg and MUA waves, it was just one of the references used for measuring the waveform of an action potential (figure 6.2). In addition to the baseline level, the minimum amplitudes left as well as right (figure 6.2 points L and R, the latter is the afterhyperpolarisation peak) of the action potential peak were also taken as a reference point. The AP widths were calculated at 10 % and 50 % height from the baseline to the peak (figure 6.2 a and b) and from the minimum amplitude left of the peak to the peak (figure 6.2C and D). It should be noted that many unfiltered AP traces did not have a negative peak (point L) before the main peak and/or an afterhyperpolarisation, but almost all traces filtered from 300 – 3000 Hz did (example in figure 6.2). To measure the width/duration of the AP at higher precision than 0.05 ms (the delay between 2 consecutive measuring points due to the 20 kHz acquiring frequency) the intersections interpolated between the neighbouring data points. Again, the width was calculated separately for the left and right side of the peak and used to calculate the AP width as well as the asymmetry at the respective height. Moreover, the delay of the afterhyperpolarisation peak (also called peak-to-peak delay) was determined. Its amplitude (to the baseline) was calculated as the percentage to the amplitude of the main AP peak.

The AP measurements performed in reference to the baseline are discussed in the thesis and helped to distinguish between the two major cell types in the neocortex: principal cells and interneurons. This permitted conclusions about the interactions between excitation and inhibition within the neuronal network, which is a major interest in the study of epileptic processes.

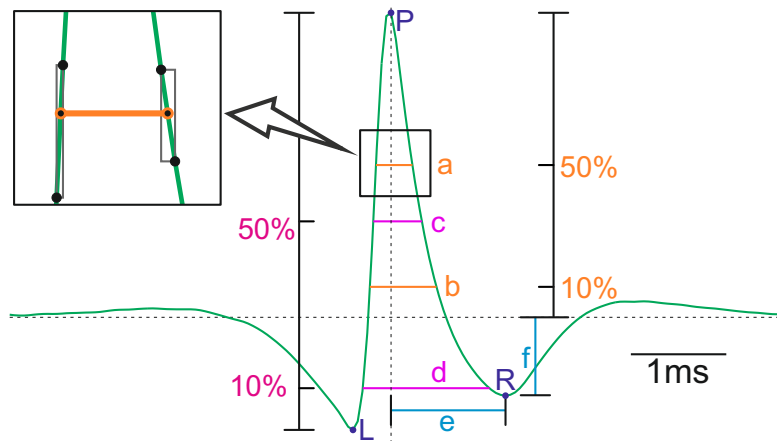


Figure 6.2: AP waveform measurements One channel of a 300 – 3000 Hz filtered average AP trace with indicated measurements. P: peak, the largest amplitude (positive or negative) across all channels, defining the AP amplitude relative to the baseline; L: the minimum amplitude left of the action potential peak; R: the minimum amplitude right of the action potential peak, the peak of the afterhyperpolarisation; It should be noted that many unfiltered AP traces didn't have a negative peak before the main peak (point L) and/or an afterhyperpolarisation (point R), but almost all traces filtered from 300 – 3000 Hz did. The delay of the afterhyperpolarisation peak (blue line e, also called peak-to-peak delay) was measured as the time from point P to point R. Moreover, amplitude of the afterhyperpolarisation (blue line f: baseline to point R) was calculated as a percentage to the AP amplitude (baseline to point P). The AP widths were calculated at 10% and 50% height from the baseline to the peak (orange lines a and b) and from point L to the peak (pink lines c and d). Inset: As the delay of 0.05 ms between 2 consecutive measuring points is a relevant difference for the widths of APs, each intersection (black dots with orange surrounding) of the action potential trace with the defined height was interpolated between the two closest data points (pairs of black dots). As for the LFPg and MUA waveforms, the width was assessed for the left and right side of the peak and combined to calculate the AP width as well as the asymmetry at the respective height.

6.2 Explanatory notes on multiple regression analysis

Each measured and/or calculated property of NSAs, cells or cell-SPA interactions is potentially influenced by (and correlated with) multiple known (independent) variables such as age, patient group, gender, neocortical lobe of origin and others. Checking correlations and differences for each of these independent variables separately is likely to lead to false conclusions. A better approach is to analyse the relationship of the (dependent) variable to all of these independent variables simultaneously using multiple linear regression. In short, linear regression analysis tries estimate how the dependent variable is expected to change when the value of any of the independent variables is changed. This allows making conclusions of how useful the information of each independent variable is when trying to predict the dependent variable. This "usefulness" is reflected by two numbers for each independent variable: the beta-coefficient, which reflects how large the change in the dependent variable is when the independent variable is changed, and a p-value, which describes how significant the relationship between the two variables is. More accurately, the beta-coefficient describes by how much the dependent variable changes if the independent variable is increased by one unit (or if it is shifted to another category in case of categorical independent variables). If the dependent and/or the independent variables were transformed using the natural logarithm (ln), the properties of the exponential function allow an interpretation of the beta-coefficient as x -fold change. E.g. if the dependent variable was ln transformed and the independent variable was not, a beta-coefficient of x can be (approximately)

interpreted as an x -fold change in the dependent variable with every one unit increase of the independent variable.

Moreover, the R^2 and/or the adjusted R^2 are measures for how well all the independent variables together describe the variation within the dependent variable. R^2 values describe the proportion of the variation in the dependent variable that could be explained by the regression. The adjusted R^2 (adj. R^2) values take the number of independent variables into account and correct for the increase in R^2 that is expected by chance due to the inclusion of additional independent variables.

In order to include categorical independent variables (patient group, cell location, etc.), they were encoded by multiple dummy variables (one less than the number of categories). To obtain a single p-value for the beta-coefficient of each categorical variable (instead of one for each of the dummy variables), non-heteroskedasticity-robust and heteroskedasticity-robust LM statistics were calculated as described in [86, Chapters 5-2a and 8-2a]. Note that ideally, another categorical independent variable would have been included to differentiate each patient from the others (resulting in $number\ of\ patients - 1$ additional dummy variables). However, due to the high number of patients this overparameterised the model and lead to problems with overfitting and was thus not included.

Contrary to widespread belief, for regression analysis neither the dependent nor the independent variables are required to be normally distributed. However, a range of other assumptions have to be fulfilled to be able to interpret the results. One of the most important ones are asymptotically normally distributed residuals. Despite multiple attempts using variable transformations (ln transforms, roots, etc.), the assumptions could not always be fulfilled, which means that the results for the regressions on some dependent variables cannot be interpreted and are thus not presented.

For limited dependent variables and/or dichotomous variables (such as the quantile, stability and other dependent variables), a binomial regression (logit / probit model) would be appropriate. One of the advantages of these models are that the predicted values can never fall below zero or exceed one (or 0% and 100%), however, the predicted values are not of interest in this study and will not be interpreted. Another advantage is, that a binomial model (correctly) considers the difference from 0.5-0.55 as less important than the difference between 0.9 and 0.95. However, in cases of heteroskedasticity (unequal variance) of residuals across different values of an independent variable, the assumptions of the model are violated and the p-values cannot be relied upon (though the beta coefficients are still consistent). Linear regressions make the same assumptions, but in this case heteroskedasticity-robust p-values can be calculated (White heteroskedasticity-robust t-statistic [83–85]). Thus, whenever homoskedasticity assumptions about the residuals were violated (Breusch-Pagan heteroskedasticity test, modified by Koenker [87, 88]), a linear regression was performed and interpreted using White heteroskedasticity-robust p-values, even if a logit/probit model would have been more appropriate in terms of the dependent variable.

It should be emphasised that regression analyses correlations, which do not automatically imply causation. Any interpretation and discussion of the results obtained by regression analysis (and most other types of statistical analysis for that matter) should be viewed with that in mind. Any interpretations based on these results are not meant to be understood as necessarily causal relationships.

6.3 Additional findings

6.3.1 Multiple spots of NSAs within one slice

Overall, 17.7% (13/76) of slices contained multiple spots generating different population activity patterns. There was no significant difference between the patient groups, though the percentage tended to be higher in the NoEpi group than in the ContrEpi group (NoEpi: 30.4%, ContrEpi: 0.0%, ResEpi: 14.6%, $0.05 < p < 0.1$, non-significant trend, Fisher's exact test). Comparing the number of spots generating different population activities within one slice resulted in a similar finding (medians are all 1, mean \pm SD: NoEpi: 1.43 ± 0.73 , ContrEpi: 1.00 ± 0.00 , ResEpi: 1.20 ± 0.51 , not significantly different, $0.05 < p < 0.1$, Kruskal Wallis).

6.3.2 Regression on SPA recurrence properties

Comparing the first two rows in table 3.6, it can be seen that the beta coefficients as well as the R^2 values are very similar, with opposite signs in case of the former. Moreover, if the recurrence frequency is included as an independent variable (row 3), the predictability (R^2) of the ISI median rises from a very low 0.122 to a very high 0.972 (97.2% of the variance are explained). Combined with the negative sign of the beta coefficient, this is a reflection of the fact that the recurrence frequency and the ISI median are inversely proportional. While this might seem trivial, it is not at all obvious and although this does not necessarily imply a normal or even symmetric distribution of ISIs, it points to the existence of a structured relationship between the recurrence frequency and the ISI median. Accordingly, the different measures of ISI variability as well as the stability can be predicted moderately to well (rows 4, 5 and 6).

Interestingly, age was a significant predictor of the recurrence frequency and the ISI median (rows 1 and 2). In this dataset, older patients seemed to have a higher recurrence frequency (and shorter SPA ISI) than younger patients. However, the overall predictability of the recurrence frequency and the ISI median were very low (R^2 : 0.115 and 0.122, respectively). Thus, although significant, the effect age has on the SPA recurrence frequency is not very large (0.15 and/or 0.13 fold change over 10 years). Nonetheless, the effect is interesting as the ages of patients are not equal across patient groups. ResEpi patients are significantly younger than NoEpi patients (medians: NoEpi: 67.63 years, ContrEpi: 43.50 years, ResEpi: 34.25 years, $p < 0.05$, Kruskal-Wallis test, also see patient table 3.2). This is related to the fact that epilepsy patients are in general younger at the time of surgery than brain tumour patients. Thus, in short, NoEpi patients are significantly older than ResEpi patients and older patients have significantly higher SPA recurrence frequencies. However, interestingly, the results of the regression analysis imply that when age and other factors are taken into account and patients of equal ages are compared, NoEpi patients non-significantly tended to have a lower SPA recurrence frequency and longer SPA ISI than ResEpi patients ($0.05 < p < 0.1$ for both the recurrence frequency and the ISI median, for medians and significant differences between the groups see table 3.6).

6.3.3 AP shapes across patient groups and cell types

As the AP width was a major criterion for differentiating the cell types, it is little surprising that PCs were wider than UCs, which were wider than INs in each of the patient groups (all: $p < 1E-09$ except for: ContrEpi: PC<UC: $p < 0.05$, IN<UC: $p < 1E-04$). Similarly, the peak-to-peak delay, which has also been used to differentiate PCs from INs in the literature [80], showed the same pattern of INs<UCs<PCs. These differences were highly significant within the NoEpi and the ResEpi groups (all $p < 1E-08$ or $p < 1E-09$). In the ContrEpi group, however, probably due to the lower case numbers, the p-values were larger and the difference between PC and UC was not significant (IN<PC: $p < 1E-06$, PC<UC: $p > 0.1$, IN<UC: $p < 0.01$).

In terms of AP amplitudes, the picture was less clear. INs tended to have smaller amplitudes than PCs or UCs, but this was not consistent across all patient groups (see table 3.8 for details). On the other hand, the APs of PCs had a more pronounced right/left asymmetry at 50 % amplitude than INs coherently across all patient groups (NoEpi: $p < 0.001$, ContrEpi: $p < 0.05$, ResEpi: $p < 1E-09$, all Kruskal Wallis). The amplitude of the afterhyperpolarisation (AHP, in percent to the amplitude of the main peak) was identified as a further difference between cell types: In the NoEpi and ResEpi groups, INs had larger AHPs than PCs (NoEpi: $p < 1E-08$, ContrEpi: $p > 0.1$, ResEpi: $p < 1E-09$). Surprisingly, PCs in the ResEpi group had smaller AHPs than their counterparts in the NoEpi and ContrEpi groups ($p < 0.05$ and $p < 0.01$, respectively).

6.4 Significant differences

The following section contains lists of significant p-values and graphically illustrates all resulting p-values for the given statistical test. As mentioned in the main text of the thesis, properties of cells and cell-SPA interactions are exclusively compared across cell types within each patient group and across patient groups within each cell type. Accordingly, SPAs and IIDs were compared within the ResEpi group, properties of SPAs were compared across patient groups.

For each p-value (whether significant or not) one edge/line was drawn. The thickness of the line was determined from the p-value: the lower the p-value, the thicker the line. If two vertices are not connected by an edge, it means that no test was performed to compare these two groups (as for ResEpi IIDs vs NoEpi or ContrEpi SPAs in table 6.1). In case of significant differences ($p < 0.05$), red < and/or > signs indicate the direction of the difference. Non-significant trends ($0.05 < p < 0.1$) are listed in the tables (as $p < 0.1$), but are not indicated by red < or > signs in the visual representations (see figure 6.3) for the explanation of a specific example. In case of regression, all significant differences between groups are shown (e.g. PC<IN), even if the overall (LM statistics) p-value was not significant. In case of Kruskal-Wallis and Mann-Whitney U-tests, group differences are shown non-significant if the overall test statistic was non-significant.

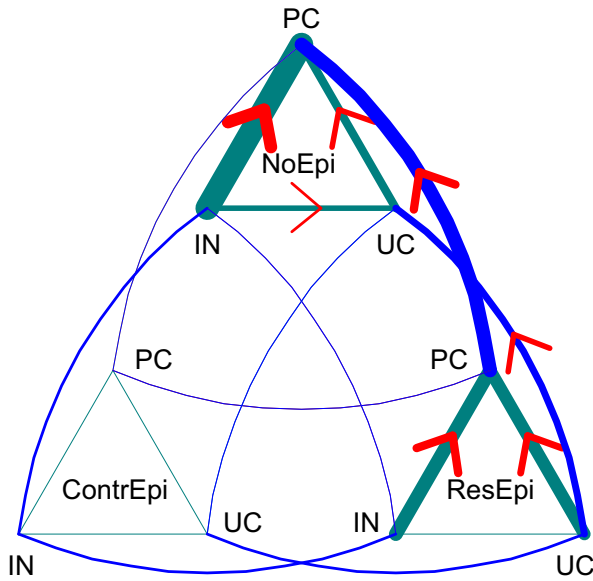


Figure 6.3: Example graphical representation of p-values The cell ISI median is used here to illustrate how p-values are represented. Smaller teal triangles comparisons between cell types within a patient group. It can be seen, that in NoEpi PC<UC, PC<IN and UC<IN, while in ResEpi only PC<UC and PC<IN was significant, as indicated by the red < and/or > signs on the respective lines. Larger, curved, blue triangles represent comparisons between patient groups within a cell type. In this example, NoEpi<ResEpi was significant for PCs and UCs, but not for INs. No significant differences to the ContrEpi group or within the ContrEpi group were found, although the tests were performed as indicated by the drawn lines.

NSA property	between patient groups (within SPAs)	between SPA and IID (within ResEpi)	graphical representation
recurrence frequency		ResEpi: IID<SPA p<1E-04	
ISI median		ResEpi: SPA<IID p<1E-04	
ISI QCD		ResEpi: SPA<IID p<0.05	
ISI varcoeff		ResEpi: SPA<IID p<0.01	

NSA property	between patient groups (within SPAs)	between SPA and IID (within ResEpi)	graphical representation
stability		ResEpi: IID<SPA p<0.01	
LFPg amp	SPA: NoEpi<ResEpi p<0.01	ResEpi: SPA<IID p<1E-04	
LFPg width			
LFPg asym			
CSD amp	SPA: NoEpi<ResEpi p<0.05	ResEpi: SPA<IID p<1E-05	
MUA amp		ResEpi: SPA<IID p<0.001	
MUA width			

Table 6.1: Significant differences regarding NSA properties. For medians and their CIs see table 3.4, for box plot visualisations see figure 3.4.

NSA property	group differences		graphical representations		
mean freq (ln)	inf<ent p<0.05 sup<ent p<0.05	o<f p<0.05 p<f p<0.1 ContrEpi<ResEpi p<0.1 NoEpi<ResEpi p<0.05			
ISI median (ln)1	ent<inf p<0.05 sup<inf p<0.1 f<o p<0.05	ResEpi<ContrEpi p<0.1 ResEpi<NoEpi p<0.05			
ISI median (ln)2	sup<ent p<0.01 sup<inf p<0.01	p<t p<0.05			
ISI QCD	ent<sup p<0.01 inf<sup p<0.01	f<o p<0.01 t<o p<0.05 f<p p<0.05 t<p p<0.1 ResEpi<ContrEpi p<0.1			
ISI varcoeff (ln)	ent<inf p<0.05 ent<sup p<0.001	f<t p<0.05 f<o p<0.05 f<p p<0.05			
stability (ln)	ent<inf p<0.1 ent<sup p<0.01	f<t p<0.05 f<o p<0.05 f<p p<0.01 t<p p<0.1			
LFPg largest amp	inf<ent p<0.1	o<f p<0.1 p<f p<0.05 NoEpi<ResEpi p<0.01			
LFPg width50	inf<ent p<0.05 inf<sup p<0.05	o<f p<0.05 o<p p<0.001 f<p p<0.1 t<p p<0.01 NoEpi<ContrEpi p<0.1 NoEpi<ResEpi p<0.1			
CSD largest amp	inf<ent p<0.1 o<f p<0.1	NoEpi<ResEpi p<0.01			
MUA largest amp	f<o p<0.1	t<o p<0.05 t<p p<0.1			
MUA width50					

Table 6.2: Significant differences regarding the regression on SPA properties. All significant differences for categorical variables with more than two groups, in respect to table 3.6. Abbreviations (going counter-clockwise, starting at the top of each triangle/square): SPA location: sup: SPA in supragranular and granular layers; ent: entire SPA (across all layers); inf: SPA in infragranular layers; lobe: fr, frontal lobe; pa, parietal lobe; oc, occipital lobe; te, temporal lobe; patient group: NoEpi; ContrEpi; ResEpi;

Cell property	between patient groups (within each cell type)	between cell types (within each patient group)	graphical representation
recurrence frequency	PC: NoEpi<ResEpi $p < 1E-04$ IN: NoEpi<ResEpi $p < 0.01$ UC: NoEpi<ResEpi $p < 0.01$	NoEpi: UC<IN $p < 0.05$ ResEpi: UC<PC $p < 0.01$ ResEpi: UC<IN $p < 0.001$	
ISI median	PC: NoEpi<ResEpi $p < 0.001$ UC: NoEpi<ResEpi $p < 0.05$	NoEpi: PC<IN $p < 1e-06$ NoEpi: PC<UC $p < 0.01$ NoEpi: UC<IN $p < 0.05$ ResEpi: PC<IN $p < 0.001$ ResEpi: PC<UC $p < 0.001$	
ISI QCD		ResEpi: IN<UC $p < 0.01$	
ISI varcoeff	IN: NoEpi<ContrEpi $p < 0.05$ IN: ResEpi<ContrEpi $p < 0.01$	NoEpi: IN<PC $p < 1e-07$ NoEpi: UC<PC $p < 0.01$ NoEpi: IN<UC $p < 0.01$ ResEpi: IN<PC $p < 1e-06$ ResEpi: UC<PC $p < 0.05$ ResEpi: IN<UC $p < 0.01$	
stability	PC: NoEpi<ResEpi $p < 1e-06$ UC: NoEpi<ResEpi $p < 0.001$	NoEpi: PC<IN $p < 1e-08$ NoEpi: UC<IN $p < 1E-04$ ResEpi: PC<IN $p < 1e-05$ ResEpi: UC<IN $p < 0.01$	
burstiness	PC: ResEpi<NoEpi $p < 1e-05$ PC: ResEpi<ContrEpi $p < 0.001$ UC: ResEpi<NoEpi $p < 0.001$	NoEpi: IN<PC $p < 0.001$ NoEpi: IN<UC $p < 0.05$ ContrEpi: IN<PC $p < 0.01$	

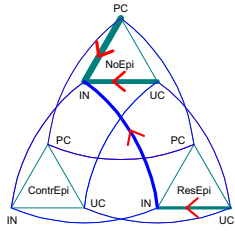
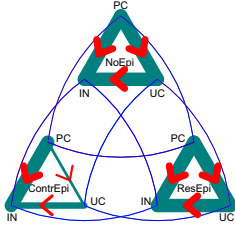
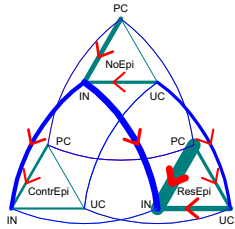
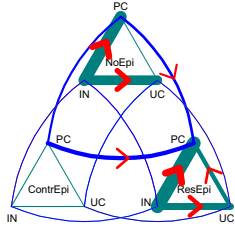
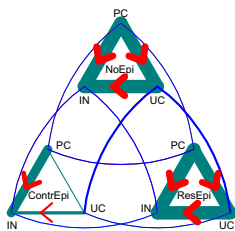
Cell property	between patient groups (within each cell type)	between cell types (within each patient group)	graphical representation
AP amp	IN: NoEpi<ResEpi p<0.01	NoEpi: IN<PC p<1E-04 NoEpi: IN<UC p<0.001 ResEpi: IN<UC p<0.01	
AP width		NoEpi: IN<PC p<1e-09 NoEpi: UC<PC p<1e-09 NoEpi: IN<UC p<1e-09 ContrEpi: IN<PC p<1e-09 ContrEpi: UC<PC p<0.05 ContrEpi: IN<UC p<1E-04 ResEpi: IN<PC p<1e-09 ResEpi: UC<PC p<1e-09 ResEpi: IN<UC p<1e-09	
AP asym	IN: ContrEpi<NoEpi p<0.01 IN: ResEpi<NoEpi p<1E-04 UC: ResEpi<NoEpi p<0.01	NoEpi: IN<PC p<0.001 NoEpi: IN<UC p<0.01 ContrEpi: IN<PC p<0.05 ContrEpi: IN<UC p<0.1 ResEpi: IN<PC p<1e-09 ResEpi: UC<PC p<0.01 ResEpi: IN<UC p<0.001	
AHP amp	PC: NoEpi<ContrEpi p<0.1 PC: ResEpi<NoEpi p<0.05 PC: ResEpi<ContrEpi p<0.01	NoEpi: PC<IN p<1e-08 NoEpi: UC<IN p<1e-06 ResEpi: PC<IN p<1e-09 ResEpi: PC<UC p<0.01 ResEpi: UC<IN p<1E-04	
peak to peak delay	UC: ContrEpi<NoEpi p<0.1 UC: ResEpi<NoEpi p<0.1	NoEpi: IN<PC p<1e-09 NoEpi: UC<PC p<1e-08 NoEpi: IN<UC p<1e-09 ContrEpi: IN<PC p<1e-06 ContrEpi: IN<UC p<0.01 ResEpi: IN<PC p<1e-09 ResEpi: UC<PC p<1e-08 ResEpi: IN<UC p<1e-09	

Table 6.3: Significant differences regarding cell properties. For medians and their CIs see table 3.8, for box plot visualisations see figure 3.8.

Cell property	group differences	graphical representations	
mean freq (ln)	<p>PC<IN p<0.1 UC<IN p<1e-05 UC<PC p<0.01</p>	<p>g<i p<0.001 g<s p<0.05 p<o p<0.05 p<f p<0.05 ContrEpi<ResEpi p<0.001 NoEpi<ResEpi p<1e-05</p>	
ISI median (ln)1	<p>PC<IN p<1e-11 UC<IN p<0.1 PC<UC p<1e-07</p>	<p>g<s p<0.01 i<s p<1E-04 t<f p<0.001 o<f p<1e-05 o<p p<0.001 o<t p<0.1 t<p p<0.05</p>	
ISI median (ln)2	<p>PC<IN p<1e-15 UC<IN p<0.001 PC<UC p<1e-05 g<s p<0.001 i<s p<1E-04</p>	<p>t<f p<1e-05 o<f p<1e-06 o<p p<0.01 p<f p<0.05 t<p p<0.1 ContrEpi<ResEpi p<0.05 NoEpi<ResEpi p<0.001</p>	
ISI QCD1	<p>PC<UC p<0.1 i<g p<0.05 i<s p<0.1</p>	<p>p<o p<0.001 p<f p<0.05 p<t p<0.001</p>	
ISI QCD2	<p>PC<UC p<0.1 i<g p<0.05 i<s p<0.1</p>	<p>p<o p<0.001 p<f p<0.05 p<t p<0.001</p>	
ISI varcoeff (ln)1	<p>IN<PC p<1e-12 IN<UC p<0.001 UC<PC p<1E-04 i<g p<0.1 s<g p<1e-05 s<i p<0.01</p>	<p>f<t p<0.05 f<o p<0.001 p<o p<0.01 p<t p<0.05 ResEpi<ContrEpi p<0.1 ResEpi<NoEpi p<0.05</p>	

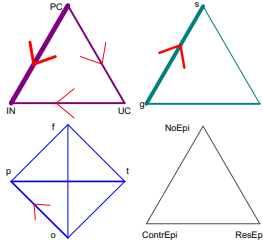
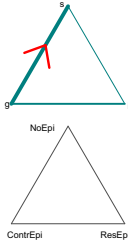
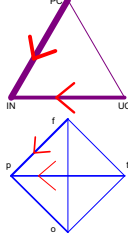
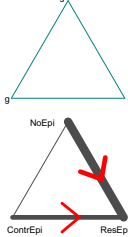
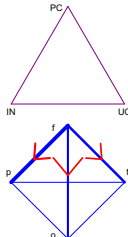
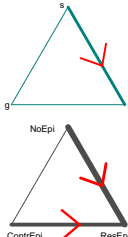
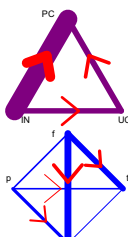
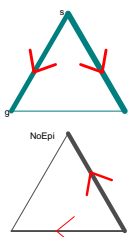
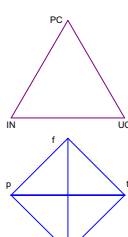
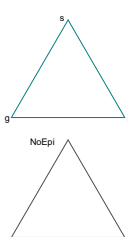
Cell property	group differences			graphical representations	
ISI varcoeff (ln)2	IN<PC p<0.001 IN<UC p<0.05 UC<PC p<0.05	i<g p<0.1 p<o p<0.05	s<g p<0.01 p<t p<0.1		
burstiness fried (sqrt)1	IN<PC p<1E-04 IN<UC p<0.01	p<o p<0.1 p<t p<0.05	p<f p<0.05		
burstiness fried (sqrt)2	i<s p<0.01 t<f p<0.01 o<f p<0.05 p<f p<0.001	ResEpi<ContrEpi p<0.001 ResEpi<NoEpi p<1e-06	ResEpi<ContrEpi p<0.01 ResEpi<NoEpi p<1E-04		
stability (ln)1	PC<IN p<1e-15 UC<IN p<1E-04 PC<UC p<1E-04 g<s p<0.001 i<s p<1E-04	t<f p<1e-05 o<p p<0.01	o<f p<1e-06 p<f p<0.1 t<p p<0.05		
stability (ln)2	t<p p<0.1				

Table 6.4: Significant differences regarding the regression on cell properties. All significant differences for categorical variables with more than two groups, in respect to table 3.9. Abbreviations (going counter-clockwise, starting at the top of each triangle/square): cell type: PC; IN; UC; cell location: s, supra; g, gran; i, infra; lobe: fr, frontal lobe; pa, parietal lobe; oc, occipital lobe; te, temporal lobe; patient group: NoEpi; ContrEpi; ResEpi;

Cell-SPA interaction	between patient groups (within each cell type)	between cell types (within each patient group)	graphical representation
reliability	PC: NoEpi<ResEpi $p<1e-09$ IN: NoEpi<ResEpi $p<1e-05$ IN: ContrEpi<ResEpi $p<0.05$ UC: NoEpi<ResEpi $p<1e-06$	NoEpi: PC<IN $p<0.05$ NoEpi: UC<IN $p<0.05$ ResEpi: PC<IN $p<0.01$ ResEpi: UC<IN $p<1E-04$	
dependency	PC: NoEpi<ResEpi $p<0.01$ IN: NoEpi<ResEpi $p<0.01$ IN: ContrEpi<ResEpi $p<0.1$ UC: NoEpi<ResEpi $p<0.01$	ResEpi: PC<IN $p<0.1$	
quantiles	PC: NoEpi<ContrEpi $p<0.05$ PC: NoEpi<ResEpi $p<0.01$ IN: NoEpi<ResEpi $p<0.001$ IN: ContrEpi<ResEpi $p<0.05$ UC: NoEpi<ResEpi $p<0.05$	NoEpi: PC<IN $p<0.05$ NoEpi: PC<UC $p<0.1$ ResEpi: PC<IN $p<0.001$ ResEpi: UC<IN $p<0.05$	
firing increase*	PC: NoEpi<ContrEpi $p<0.1$ PC: ResEpi<ContrEpi $p<0.1$		
fano factor*	PC: ResEpi<NoEpi $p<0.05$	NoEpi: IN<PC $p<0.01$	
max firing*			

Cell-SPA interaction	between patient groups (within each cell type)	between cell types (within each patient group)	graphical representation
rel max firing*			

Table 6.5: Significant differences regarding cell-SPA interactions. For medians and their CIs see table 3.12, for box plot visualisations see figure 3.11.

Cell-SPA interaction	group differences	graphical representations	
reliability cuberoot	<p>PC<IN p<0.001</p> <p>PC<UC p<0.001</p> <p>inf<ent p<0.1</p> <p>sup<ent p<0.05</p> <p>sup<inf p<0.05</p>	<p>o<f p<0.05 o<p p<1e-08</p> <p>o<t p<0.05 f<p p<0.001</p> <p>t<p p<1e-09</p> <p>NoEpi<ContrEpi p<0.1</p>	
dependency cuberoot	<p>PC<IN p<0.01</p> <p>PC<UC p<0.001</p>	<p>o<p p<0.01 f<p p<0.05</p> <p>t<p p<0.05</p>	
whether increased	<p>PC<IN p<1e-05</p> <p>UC<IN p<0.1</p> <p>PC<UC p<0.001</p> <p>i<s p<0.1</p>	<p>inf<ent p<0.1</p> <p>sup<ent p<0.1</p> <p>o<p p<0.01 f<p p<0.05</p> <p>t<p p<0.001</p>	
firing increase*	<p>PC<IN p<0.01</p> <p>PC<UC p<0.1</p> <p>inf<ent p<0.01</p> <p>sup<ent p<0.05</p>	<p>o<f p<0.05 o<p p<0.05</p> <p>o<t p<0.001 p<t p<0.1</p> <p>NoEpi<ContrEpi p<0.05</p> <p>ResEpi<ContrEpi p<0.01</p>	

Cell-SPA interaction	group differences	graphical representations	
fano factor*	$ent <_{inf} p < 0.1$ $ent <_{sup} p < 0.1$	$f <_o p < 0.001$ $p <_o p < 0.001$ $t <_o p < 0.01$ $ContrEpi < NoEpi p < 0.1$	
abs max firing* cuberoot	$g <_i p < 0.05$ $s <_i p < 0.05$	$p <_o p < 0.1$ $p <_f p < 0.1$ $p <_t p < 0.05$	
rel max firing*	$g <_i p < 0.01$ $s <_i p < 0.1$	$ent <_{inf} p < 0.05$	

Table 6.6: Significant differences regarding the regression on cell-SPA interactions. All significant differences for categorical variables with more than two groups, in respect to table 3.13. Abbreviations (going counter-clockwise, starting at the top of each triangle/square): cell type: PC; IN; UC; cell location: s, supra; g, gran; i, infra; SPA location: sup: SPA in supragranular and granular layers; ent: entire SPA (across all layers); inf: SPA in infragranular layers; lobe: fr, frontal lobe; pa, parietal lobe; oc, occipital lobe; te, temporal lobe; patient group: NoEpi; ContrEpi; ResEpi;

		incr.	unch.	decr.	n =		
(p<1e-8)	NoEpi	⇓	⇑		603		
	ContrEpi				74		
	ResEpi	⇑	⇓	⇑	392		
Colour legend		p<1E-10	p<0.001	p<0.05	p<0.1	p>0.1	p≥0.2

Table 6.7: Significances for the number of in- and decreased cells across patient groups Post-hoc significances for the totals in tables 3.11 and 3.14. The overall p-value for each test is displayed in parentheses in the first column. Double arrows (⇑⇓) indicate significantly more or fewer cases than expected. Simple arrows (⇑⇓) and empty cells indicate non-significant changes.

		incr.	unch.	decr.	n =		
NoEpi (p<0.01)	PC	⇓			217		
	IN	⇑		⇓	144		
	UC				242		
ContrEpi (p>0.5)	PC				18		
	IN				35		
	UC				21		
ResEpi (p<0.001)	PC	⇓	⇑		134		
	IN	⇑	⇓		114		
	UC				144		
Colour legend		p<1E-10	p<0.001	p<0.05	p<0.1	p>0.1	p≥0.2

Table 6.8: Significances for the number of in- and decreased PCs, INs and UCs Post-hoc significances for table 3.11. The overall p-value for each test is displayed in parentheses in the first column. Double arrows (⇑⇓) indicate significantly more or fewer cases than expected. Simple arrows (⇑⇓) and empty cells indicate non-significant changes.

		incr.	unch.	decr.	n =		
NoEpi (p<0.01)	local	⇑	⇓		261		
	distant	⇓	⇑		342		
ContrEpi (p>0.5)	local	⇑	⇓		34		
	distant	⇓	⇑		40		
ResEpi (p<0.001)	local	⇑	⇓		206		
	distant	⇓	⇑		186		
Colour legend		p<1E-10	p<0.001	p<0.05	p<0.1	p>0.1	p≥0.2

Table 6.9: Significances for the number of in- and decreased local and distant cells. Post-hoc significances for table 3.14. The overall p-value for each test is displayed in parentheses in the first column. Double arrows (⇑⇓) indicate significantly more or fewer cases than expected. Simple arrows (⇑⇓) and empty cells indicate non-significant changes.

		none	differen- tial	uniform	n =	
(p<0.01)	NoEpi			↓	160	
	ResEpi	↓		↑	59	
Colour legend	p<1E-10	p<0.001	p<0.05	p<0.1	p>0.1	p≥0.2

Table 6.10: Significances for the cell responses during multiple SPAs across patient groups Post-hoc significances for the direct comparison of the number of "none", "differential" and "all" responses between the ResEpi and NoEpi group (numbers shown in table 3.15). The overall p-value for the test is displayed in parentheses in the first column. Double arrows (↑↓) indicate significantly more or fewer cases than expected. Simple arrows (↑↓) and empty cells indicate non-significant changes.

		none	differen- tial	uniform	n =	
NoEpi	PC (p<0.1)			↑	72	
	IN (p>0.8)				27	
	UC (p>0.9)				61	
	total (p>0.1)			↑	160	
ResEpi	PC (p>0.8)				17	
	IN (p<0.05)	↑	↓	↑	18	
	UC (p>0.8)				24	
	total (p<0.1)	↑	↓		59	
Colour legend	p<1E-10	p<0.001	p<0.05	p<0.1	p>0.1	p≥0.2

Table 6.11: Significances for the cell responses during multiple SPAs within patient groups. Post-hoc significances for the number of "none", "differential" and "all" responses compared to what would be expected from the number of increased, unchanged and decreased responses, for each of the cell types in each of the patient groups (i.e. each row represents a separate test; case numbers are shown in table 3.15). The overall p-value for each test is displayed in parentheses in the second column. Double arrows (↑↓) indicate significantly more or fewer cases than expected. Simple arrows (↑↓) and empty cells indicate non-significant changes.

The project was supported by the European Union, co-financed by the European Social Fund (EFOP-3.6.3-VEKOP-16-2017-00002).